UNIVERSITA' DEGLI STUDI DI PADOVA

DIPARTIMENTO DI SCIENZE DEL FARMACO

CORSO DI LAUREA MAGISTRALE IN FARMACIA

TESI DI LAUREA

At the Heart of Chemotherapy: Unveiling the Impact of Proteasome Inhibitors on Vascular Function, Arterial Stiffness and Cardiovascular risk

RELATORE CHIAR.MA PROF.SSA: Sara de Martin

CO RELATORE CHIAR.MO PROF: Nicola Ferri
Wim Martinet
Pieter-Jan Guns
Callan Wesley

LAUREANDA: Annarita Sansonetti

ANNO ACCADEMICO 2025-2026

To all those who weren't lucky enough to be born on the right side of the world.
My privilege will be used in your service.
My knowledge will work to reduce health inequalities.
My life will stand at the forefront of change.
My voice will be a weapon for those whose tongues were cut off.

Table of Contents

Chapter 4: Results

Chapter 5: Discussion

Chapter 1

Introduction

Proteasomes are essential proteolytic complexes that maintain cellular homeostasis by degrading damaged, misfolded, or unnecessary proteins. Their function is critical in processes such as cell cycle regulation, DNA repair, and cell survival. A tightly regulated proteasomal degradation of cyclin-dependent kinase (CDK) activators and inhibitors enables orderly cell cycle progression, from DNA replication to mitosis **(1).** In addition to these roles, proteasomes help eliminate abnormal proteins that could otherwise lead to cellular stress or dysfunction.

Given their crucial functions, one might assume that proteasome inhibition would have devastating effects on normal tissues. Surprisingly, **proteasome inhibitors (PIs)** are generally well tolerated in clinical settings, with a relatively favorable side-effect profile. PIs have shown significant efficacy in hematologic malignancies, particularly in **multiple myeloma (MM)** and **mantle cell lymphoma (MCL)**, improving both progression-free survival (PFS) and overall survival (OS).

Multiple myeloma serves as an ideal model for proteasome inhibitor therapy due to the high volume of immunoglobulin production by malignant plasma cells. The increased protein synthesis in these cells leads to a heavy reliance on proteasomal degradation, thereby creating a therapeutic window where cancer cells are preferentially targeted over normal cells. In 2003, the U.S. Food and Drug Administration (FDA) approved **bortezomib (Velcade®)**, the first-in-class PI, for the treatment of relapsed/refractory MM. Since then, two additional agents—**carfilzomib (Kyprolis®)** and **ixazomib (Ninlaro®)**—have been approved for the treatment of MM, with bortezomib's indications later extended to include MCL. (2)

The expanding role of PIs in hematologic malignancies has led to the development of next-generation agents, such as **marizomib**, which may have utility in solid tumors like **glioblastoma**.

1.1 Mechanism of Action of Proteasome Inhibitors

The Ubiquitin-Proteasome Pathway

The **ubiquitin-proteasome pathway (UPP)** orchestrates the degradation of proteins marked for destruction by ubiquitination. Ubiquitination involves a three-step enzymatic cascade: activation by **E1 (ubiquitin-activating enzyme)**, conjugation by **E2 (ubiquitin-conjugating enzyme)**, and ligation by **E3 (ubiquitin-protein ligase)**. This cascade results in polyubiquitinated proteins that are recognized and processed by the **26S proteasome** (1, 2).

The 26S proteasome is composed of a **20S catalytic core** and one or two **19S regulatory particles**. The 19S caps recognize ubiquitinated proteins, cleave off ubiquitin chains, and unfold proteins to feed them into the 20S core. The 20S structure resembles a barrel formed by four stacked rings: two outer **α-rings** and two inner **β-rings**. Each β-ring contains three catalytically active sites: **chymotrypsin-like (β5)**, **trypsin-like (β2)**, and **caspase-like (β1)**. Among these, the **β5 site is the primary target** of clinically approved PIs (3). At higher concentrations, PIs can also inhibit the β1 and β2 sites.

1.2 Mechanisms of action on cancer

PIs exert anti-cancer activity through **multiple mechanisms**, including suppression of survival pathways, induction of pro-apoptotic proteins, and disruption of protein homeostasis.

1. Inhibition of NF-κB Pathway

The transcription factor **NF-κB** promotes cell proliferation, angiogenesis, and survival, particularly in hematopoietic malignancies. Under normal conditions, NF-κB is held inactive in the cytoplasm by **IκBα**, an inhibitory protein that is degraded via the proteasome upon cellular activation (4). Proteasome inhibition prevents IκBα degradation, thus sequestering NF-κB in the cytoplasm and suppressing its pro-survival signaling. Although initially considered the main mechanism of PI cytotoxicity, subsequent studies, including those with the IκB kinase inhibitor PS-1145, have shown that NF-κB inhibition alone does not recapitulate the full cytotoxic effects of PIs **(5).**

2. Activation of Apoptotic Pathways

PIs promote apoptosis through activation of the **JNK (c-Jun N-terminal kinase)** pathway and stabilization of **p53**, a tumor suppressor involved in DNA damage responses. JNK activation by PIs leads to activation of **caspases 8 and 3**, key executors of apoptosis. PIs can also induce **p53** accumulation, even in cells with mutant p53, suggesting p53-dependent and independent mechanisms of cell death **(6, 7).**

3. Stabilization of Pro-apoptotic Proteins

Proteins such as **Bim, Bid, and Bik**, which promote apoptosis, are usually short-lived due to rapid proteasomal degradation. PIs prevent this degradation, allowing these proteins to accumulate and trigger **caspase-mediated cell death** (**8–10**). **NOXA**, another pro-apoptotic protein regulated by p53, also accumulates with proteasome inhibition and activates **caspase-9**, pushing the cell toward apoptosis even in p53-independent contexts **(11–14).**

4. Endoplasmic Reticulum (ER) Stress and Unfolded Protein Response (UPR)

Cells like myeloma plasma cells, which produce high levels of immunoglobulin, rely heavily on the **ER's protein-folding capacity**. Misfolded proteins are usually exported from the ER and degraded via the proteasome. PI-mediated blockade of this process leads to **accumulation of misfolded proteins**, triggering **ER stress** and activation of the **UPR (15).** If ER stress becomes excessive, the UPR can shift from an adaptive to an apoptotic response, leading to **cell cycle arrest and apoptosis (16, 17).**

1.3 Clinical Development of Novel Proteasome Inhibitors

Bortezomib (Velcade®)

Bortezomib was the first PI to gain FDA approval in 2003 for relapsed/refractory MM. It is a **slowly reversible boronate inhibitor** that selectively targets β5 > β1 > β2. Administered intravenously or subcutaneously, bortezomib's side effects include **peripheral neuropathy, gastrointestinal symptoms, cytopenias, and infections**. Clinical trials have demonstrated significant efficacy: a phase II trial reported a 35% response rate, while a subsequent randomized trial showed a 38% response compared to 18% for dexamethasone, with significantly longer overall survival (18, 19).

Carfilzomib (Kyprolis®)

Approved in 2012, **carfilzomib** is an **irreversible epoxyketone inhibitor** targeting β5 > β2/β1. Unlike bortezomib, it has **less neurotoxicity** but can cause **dyspnea, cytopenias, fatigue, and rare cardiac events**. Administered intravenously, carfilzomib showed a 23.7% response rate and a median OS of 15.6 months in a phase II trial for relapsed/refractory MM (20). It is used in combination with dexamethasone or immunomodulatory agents such as lenalidomide or pomalidomide.

Ixazomib (Ninlaro®)

Ixazomib is the **first oral PI**, approved in 2015. It is a **reversible boronate inhibitor** with β5 > β1 selectivity. Used in combination with lenalidomide and dexamethasone, ixazomib has improved PFS in relapsed/refractory MM. In a large randomized trial, patients receiving ixazomib had a median PFS of **20.6 months vs. 14.7 months** with placebo (21). Its toxicity profile includes **gastrointestinal effects, cytopenias, peripheral neuropathy, and back pain**.

Emerging Agents: Marizomib and Beyond

Newer PIs, such as **marizomib**, are in clinical trials for both hematologic and solid tumors. Marizomib, a **broad-spectrum irreversible PI**, inhibits all three proteolytic activities (β1, β2, β5) of the proteasome and has demonstrated **central nervous system (CNS) penetration**, making it a potential candidate for **glioblastoma** treatment.

However in 2025 studies for their potential covalent bond with upregulated proteins Proteasome inhibitors are opening the doors to off label use, reinforcing novel clinical trials for **Lupus erythematosus.**

Bortezomib and the selective immunoproteasome inhibitors, ONX-0914 and zetomipzomib, ameliorate renal disease in murine lupus models. While clinically effective in refractory multiple myeloma. (28)
The use of bortezomib has since been extended to the treatment **of NSCLC and pancreatic cancer** in clinical trials
However, its application is limited by off-target effects and adverse reactions such as thrombocytopenia, peripheral neuropathy and gastrointestinal symptoms.

Proteasome inhibition is a very active area of research; there are over 10 structurally-distinct classes of proteasome inhibitors in development, with new agents expected to enter clinical testing in the hopes of finding drugs with optimal potency, reduced toxicity and oral bioavailability.

1.4 Multiple Myeloma

Multiple myeloma is a hematologic malignancy characterized by abnormal plasma cells in bone marrow inducing destructive bone lesions. This disease causes overpopulation of abnormal clonal plasma B cells in bone marrow, bringing downregulation of osteoblasts and activation of osteoclasts, which induce malignant bone lesions, kidney injury, anemia, hypercalcemia, and painful fractures (29) Bone deterioration, hematopoietic dysfunction, and end-organ failure are the most prevalent signs of excessive monoclonal protein synthesis (30). Multiple Myeloma (MM) is the second most common hematologic cancer. It involves abnormal proteins and increased plasma B cells in the bone marrow. MM is influenced by demographics, physiology, clinical risk factors, and various treatment approaches (31); MM contributes to up to 10 % of hematologic neoplasms. Less than two-thirds of people under 40 seem to experience it more regularly than people over 40, and the median age of diagnosis is 65 years. (32).

Epidemiology of Multiple Myeloma

The current information on MM is alarming; patients in stage III of the disease have an average life expectancy of 29 months, as opposed to those in stages I and II, who have average survival periods of 5 and 4 years, respectively. The progression of MM without treatment could eventually end with organ damage. Since the emergence of cutting-edge medicines, survival rates for MM have significantly increased. As MM is a curable cancer, several novel treatments that have the potential to be developed are accomplished for the medication (33) Targeted drugs like PIs and IMiDs, combined with autologous stem cell transplantation and high-dose Melphalan, have significantly improved outcomes for MM patients in the past two decades.
Novel therapeutic drugs have considerably increased patient survivability in the past 20 years, but the disease is still incurable, and the average overall life probability of patients with a new diagnosis is only about 6 years. The median overall survival for MM patients over 70 is around 5 years. On average, MM patients have a duration of persistence of nearly 6 years with current therapy (34)

1.5 Mechanism of action of Bortezomib and Carfilzomib on Multiple Myeloma

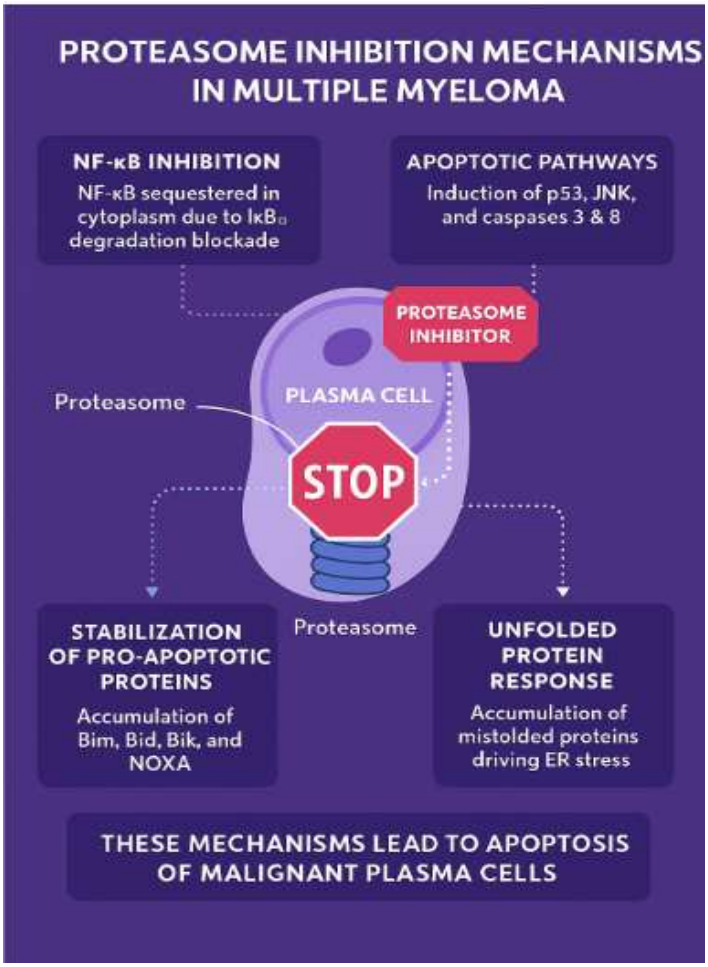

One central mechanism by which bortezomib functions in myeloma is via the inhibition of the breakdown of inhibitory kappa B (IκB) and consequently stabilization of the nuclear factor kappa B (NFκB) complex. This prevents NFκB translocation to the nucleus with consequent inactivation of multiple downstream pathways known to be important in myeloma cell signaling. It also decreases the adhesion of the myeloma plasma cell to stromal cells which increases sensitivity to apoptosis, as well as interrupting prosurvival paracrine and autocrine cytokine loops in the bone marrow microenvironment mediated by interleukin-6 (IL-6), insulin-like growth factor 1 (IGF-1), vascular endothelial growth factor (VEGF) and tumor necrosis factor-α(TNF). Other effects in myeloma include inhibition of angiogenesis, inhibition of DNA repair and impairment of osteoclast activity. Tumor cells appear to be more sensitive to the effects of proteasome inhibition than normal cells due to a loss of checkpoint mechanisms occurring during tumorigenesis; this means that normal cells can usually recover as the inhibition is transient and reversible.

Novel Updated Guidelines for Multiple Myeloma Treatment 2025

In recent years, clinical guidelines for Multiple Myeloma (MM) have evolved significantly to incorporate both novel immunotherapies and foundational agents such as proteasome inhibitors (PIs). PIs—most notably bortezomib, carfilzomib, and ixazomib—have remained central to MM therapy since their FDA approvals in 2003, 2012, and 2015 respectively. These agents are integrated at multiple stages of MM treatment, including induction, consolidation, maintenance, and relapse, and serve as the backbone of most frontline regimens. The 2025 NCCN Guidelines now recommend quadruplet regimens incorporating PIs and anti-CD38 monoclonal antibodies—such as daratumumab or isatuximab—paired with lenalidomide and dexamethasone (e.g., D-RVd or Isa-VRd) as preferred first-line therapy for both transplant-eligible and -ineligible patients. Phase 3 trials like ADVANCE have demonstrated that adding daratumumab to PI-based regimens significantly enhance minimal residual disease negativity compared to traditional triplets in the relapsed/refractory setting, PIs continue to play vital roles within regimens recommended by NCCN, alongside emerging options such as CAR-T therapies and bispecific antibodies. (35)

Treatment Phase	Regimen	Proteasome Inhibitor (PI)	Dosing Schedule	Notes
Induction (Transplant-Eligible)	D-RVd (Daratumumab + Lenalidomide + Bortezomib + Dex)	Bortezomib (Velcade)	1.3 mg/m² SC/IV Days 1, 4, 8, 11 of 21-day cycle	First-line for transplant-eligible patients
	KRd (Carfilzomib + Lenalidomide + Dex)	Carfilzomib (Kyprolis)	20/36–56 mg/m² IV on Days 1, 2, 8, 9, 15, 16 of 28-day cycle	Preferred in high-risk patients
Induction (Transplant-Ineligible)	VRd-lite (dose-adjusted Bortezomib + Rd)	Bortezomib	1.3 mg/m² SC weekly × 3 weeks every 28 days	Weekly dosing better tolerated in elderly/frail patients
Consolidation	Repeat induction regimen or PI-based triplet	Bortezomib or Carfilzomib	Same as induction	Often 2–4 cycles post-ASCT
Maintenance	Rd or PI + IMiD (in high-risk)	Ixazomib (Ninlaro)	4 mg PO Days 1, 8, 15 of 28-day cycle	Oral maintenance option, especially after ASCT
		Bortezomib	1.3 mg/m² SC every 2 weeks	Used in high-risk or PI-sensitive cases
Relapsed / Refractory	KRd, Dara-Kd, Isa-Kd	Carfilzomib	56 mg/m² IV Days 1, 2, 8, 9, 15, 16 (or 70 mg/m² once weekly Days 1, 8, 15)	High potency, cardiac monitoring advised
	IRd (Ixazomib + Lenalidomide + Dex)	Ixazomib	4 mg PO Days 1, 8, 15 of 28-day cycle	Fully oral triplet, convenient for outpatients
Emerging / Investigational	Combined with CAR-T or bispecifics	Varies	Per trial protocol	Combination approaches for PI-resistant disease

Table 1. Updated Clinical guidlines of Proteasome Inhibitors

Carfilzomib Vs Bortezomib in tackling Relapsed Multiple Myeloma

In one of the biggest clinical evaluation of efficacy on Proteasome inhibitors in overall survival of patients with MM it's specifically a was a phase III, randomized, open-label study of adult patients with RRMM who had received 1 to 3 previous lines of therapy, ENDEVOR, the aim was to evaluate the extended overall survival of patients with Relapsed Multiple Myeloma.
As of July 19, 2017, median follow-up was 44.3 months for Carfilzomib and dexamethasone and 43.7 months for Bortezomib and dexamethasone. Median Overall survival was 47.8 months Carfilzomib versus 38.8 months Bortezomib (hazard ratio, 0.76; 95% confidence interval, 0.633-0.915). OS was longer with Carfilzomib versus Bortezomib within age and cytogenetic subgroups, and according to number of previous lines of therapy, previous bortezomib exposure, previous lenalidomide exposure, and lenalidomide-refractory status.
With median follow-up of approximately 44 months, clinically meaningful improvements in OS were observed with Carfilzomib versus Bortezomib including in all subgroups examined. (45)

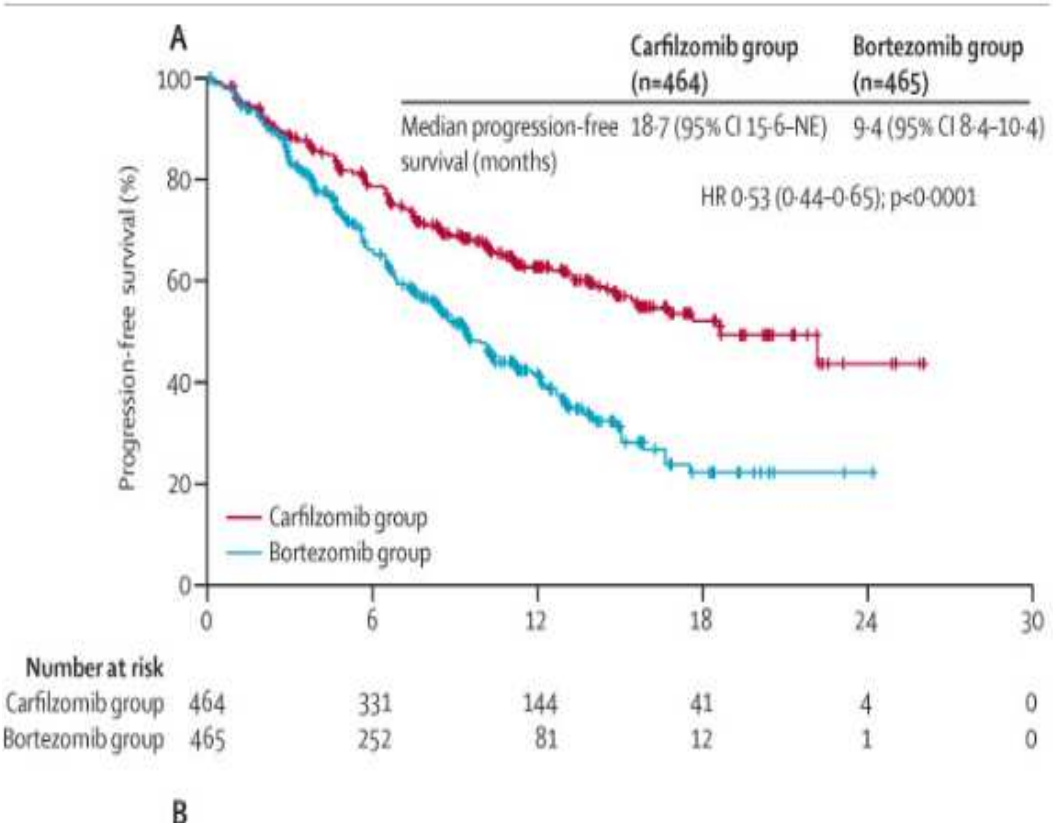

Figure1 *Progression-Free Survival in Relapsed/Refractory Multiple Myeloma: Carfilzomib vs. Bortezomib (ENDEAVOR Trial)*
This Kaplan–Meier curve compares progression-free survival (PFS) between patients treated with carfilzomib plus dexamethasone (Kd; red line) and those with bortezomib plus dexamethasone (Vd; blue line).All indicating a 47% reduction in the risk of disease progression or death with carfilzomib treatment

1.6 Clinically relevant data on PI induced cardiovascular complication

While the use of anti-myeloma therapies has allowed for improvements in overall survival (OS), the post-treatment course of the disease is frequently complicated by cardiovascular adverse events (CVAEs) which in turn contribute to treatment-associated morbidity and mortality. The concept of cardiotoxicity refers to the effect of antineoplastic intervention on accelerating the onset of cardiovascular (CV) disease. It also relates to its direct effect on the structure or function of the heart and vasculature, including systemic hypertension, myocardial dysfunction and congestive heart failure (CHF), coronary heart disease, arrhythmias, thromboembolic disease, pulmonary hypertension, valvular disease, pericardial complications, or other vascular diseases including stroke and peripheral vascular disease. The exact risk conferred by anti-myeloma agents, as shown in clinical trials, may vary depending on which endpoints were used to define cardiotoxicity. F

As stated in the **EMEA's Product information brochure Carfilzomib** The most serious side effects when used with lenalidomide and dexamethasone or with dexamethasone alone include harmful effects on the heart, lungs and liver, and hypertension (high blood pressure) that can be severe.
For **Bortezomib** the most serious side effects include heart failure, tumor lysis syndrome (complications due to sudden breakdown of cancer cells), pulmonary hypertension (high blood pressure in the arteries of the lungs).
It's not recommended in patients with acute diffuse infiltrative pulmonary disease or pericardial disease.

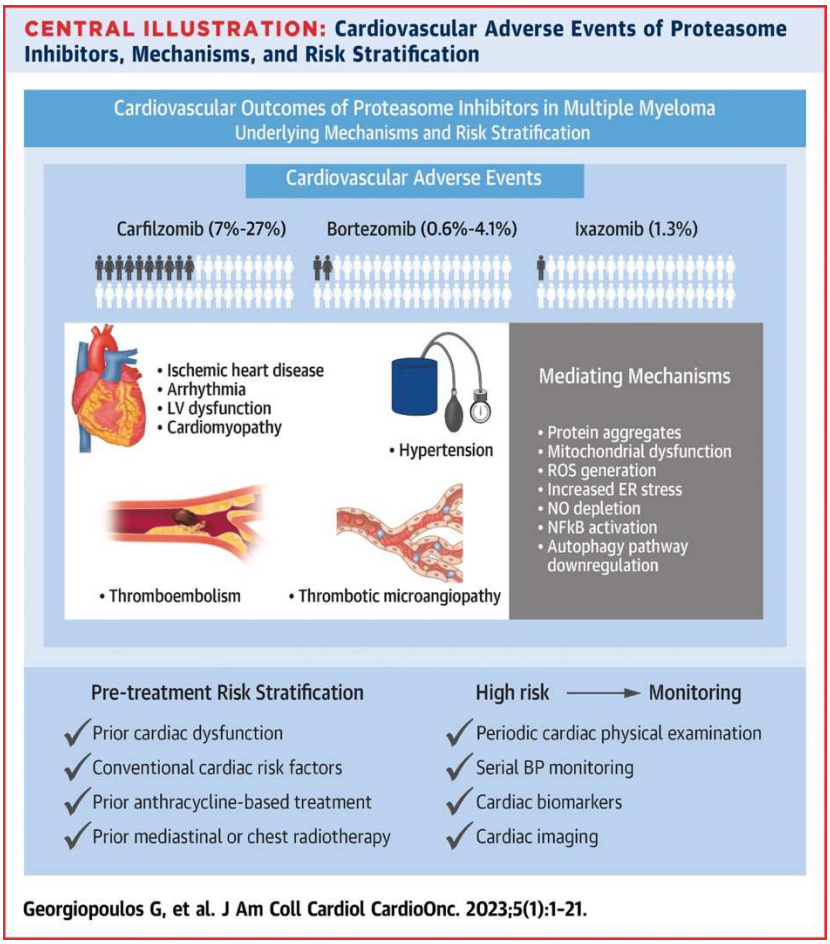

Carfilzomib with its irreversible proteasome inhibition properties is associated with an increased incidence of **hypertension** (9%-27%), (46) HF/left ventricular (LV) systolic dysfunction (4.1%-16.2%), IHD (1.8%-17.6%), and arrhythmias (2.4%-7%). Bortezomib is associated with cardiovascular toxicity as well, albeit not to the degree of carfilzomib. On the other hand, the oral PI ixazomib is generally not associated with a high risk for cardiovascular toxicity, apart from scarce evidence. All 3 PIs have been related to **thrombotic microangiopathy** (TMA) (46)
However, the population affected with Multiple Myeloma is elderly Median age at the time of diagnosis of MM is 66 years, with 54% above 65 years at

diagnosis. Old age is marked by reduced UPP activity and consequently increased proteome instability, and 2 conditions may predispose to cardiovascular toxicity related to PIs. First, there is higher prevalence of traditional cardiovascular risk factors in the elderly, and patients with MM often present a history of exposure to other potentially cardiotoxic therapies such as anthracyclines and/or chest radiotherapy, which can further increase the likelihood of cardiotoxicity. (47) Second, aging induces proteome instability across all human cell types and is associated with decreased activity of the ubiquitin conjugation pathway, as well as with down-regulated proteasome and transcription factor NRF1/NRF2 (transcriptional regulator of antioxidant/proteostatic genes) functionality. Consequently, AEs related to PIs would be expected to be enhanced in the elderly.

The higher cardiotoxicity of carfilzomib has been suggested to be caused by its irreversible proteasome inhibition and its distinctive molecular mechanism, which includes AMPKα inactivation and autophagy-related protein downregulation (48)

In a network meta-analysis of clinical trials, the risk of cardiovascular toxicity was over 2.5 times higher in patients treated with carfilzomib than in those who received control treatment (49) Most studies investigating the cardiovascular toxicity of proteasome inhibitors have focused on carfilzomib However some studies show that even Bortezomib has their implication.

In a Korean study of 2024, it has been shown that the incidence of CVAEs during bortezomib-based chemotherapy in patients with MM was 20.8% for any grade and 14.7% for grade 3 or higher. (50)

1.7 Pre-clinical Mechanisms of Proteasome Inhibitor-Induced Cardiotoxicity

Understanding the pre-clinical mechanisms underlying proteasome inhibitor (PI)–associated cardiotoxicity is crucial for the development of preventive and therapeutic strategies. Multiple studies in animal models and cell lines have elucidated several interconnected molecular pathways that contribute to this toxicity, ranging from proteomeostasis disruption maladaptive stress responses.

1. Proteasome Inhibition and Myocardial Protein Homeostasis

Cardiomyocytes exhibit higher basal proteasome activity compared to many other cell types due to their non-proliferative nature and constant requirement for sarcomeric protein turnover. Therefore, they are particularly susceptible to proteasome inhibition [15]. Pre-clinical studies in rats have demonstrated that carfilzomib, a selective PI, accumulates in cardiac tissue, leading to potent and sustained inhibition of the myocardial proteasome [14]. This results in the accumulation of ubiquitinated and misfolded proteins that cannot be adequately degraded. In cardiomyocytes, this proteotoxic stress impairs cellular homeostasis and may lead to the formation of toxic oligomers, aggresomes, and eventually insoluble inclusion bodies [17–19]. These aggregates interfere with essential cellular functions and may activate apoptotic pathways.

2. ER Stress and the Unfolded Protein Response

The inability to degrade misfolded proteins triggers endoplasmic reticulum (ER) stress and activates the unfolded protein response (UPR). While the UPR initially serves as a protective mechanism, prolonged or severe ER stress leads to apoptotic signaling via pathways involving PERK, CHOP, and caspase activation [16]. In myeloma cells, PIs induce ER stress by rapidly increasing the load of regulatory proteins. A similar mechanism occurs in cardiomyocytes, where the buildup of undegraded sarcomeric and cytoskeletal proteins exacerbates ER dysfunction, culminating in cell death and contractile impairment [16–19].

3. Altered NF-κB Signaling and Pro-inflammatory Responses

NF-κB signaling plays a dual role in both cancer pathogenesis and cardiovascular function. Bortezomib was initially developed for its ability to suppress NF-κB activity in multiple myeloma via inhibition of p100 to p52 processing in the non-canonical pathway [23–25]. However, in cardiomyocytes and other non-myeloma cell lines, PI treatment paradoxically results in increased canonical NF-κB signaling through IKKβ-dependent phosphorylation and degradation of IκBα [25]. In the cardiac context, prolonged NF-κB activation promotes maladaptive inflammatory responses, ER stress, and apoptosis. This is particularly evident in ischemia/reperfusion models where NF-κB activation downstream of MAPK pathways (ERK, JNK, and p38) contributes to pathological cardiac remodeling [29].

4. Mitochondrial Dysfunction and Oxidative Stress

Cardiac mitochondria are major targets of PI-induced toxicity. Animal studies have shown that bortezomib and MLN-273 cause mitochondrial swelling, vacuolization, and loss of membrane potential in cardiomyocytes, accompanied by fibrosis and left ventricular dysfunction [30–32]. These structural changes are associated with increased production of reactive oxygen species (ROS). In murine models, elevated ROS generation is a critical mediator of cardiomyopathy and fibrosis, especially in the context of comorbid conditions such as diabetes or in combination with anthracyclines [44, 45]. The synergistic cardiotoxicity observed when PIs are co-administered with anthracyclines is likely due to compounded oxidative stress and mitochondrial injury [45].

5. Autophagy Dysregulation and Off-target Toxicities

A recent pre-clinical study highlighted a novel mechanism of carfilzomib-induced cardiotoxicity involving off-target activation of protein phosphatase 2A (PP2A), leading to downstream autophagy inhibition [33••]. This finding was unique to carfilzomib and not observed with other PIs like bortezomib. Impaired autophagy hampers cellular clearance mechanisms and further contributes to the accumulation of cytotoxic protein aggregates, exacerbating proteotoxic stress and myocardial injury.

7. Cardiac Remodeling and Hypertrophy

PI-induced stress signaling cascades, including calcineurin-NFAT pathway activation, have been implicated in maladaptive cardiac hypertrophy. In murine models of desmin-related cardiomyopathy, high doses of bortezomib triggered hypertrophic remodeling, myocardial vacuolization, and eventual heart failure [30]. Similar findings have been reported with other PIs,

suggesting that interference with sarcomere homeostasis and cellular stress responses drives the remodeling phenotype.

8. Implications and Drug-Specific Toxicity

Importantly, not all proteasome inhibitors exhibit identical cardiotoxic profiles. The off-target effects observed with carfilzomib suggest that individual PIs may have unique toxicity mechanisms. Differences in dosing, pharmacokinetics, and animal models used in pre-clinical studies further complicate direct comparisons across agents [37]. These observations underscore the need for drug-specific cardiotoxicity

9. Impact of Proteasome Inhibitors on Cytoskeletal Integrity

Proteasome inhibitors disrupt cytoskeletal remodeling by blocking the maturation of nascent myofibrils, essential for proper myofibril assembly in muscle cells. In both human and avian cardiomyocytes, various UPS inhibitors—including Bortezomib and Carfilzomib—halted myofibril development at the early stage. While this effect was reversible with most inhibitors, Carfilzomib uniquely caused sustained arrest.

These drugs, used in multiple myeloma treatment, are associated with cardiotoxic effects in 3–6% of patients. The observed impairment in cytoskeletal remodeling may underlie these adverse outcomes. Treated cardiomyocytes showed a buildup of ubiquitinated myosin II, suggesting that UPS-mediated degradation is required to clear early, improperly assembled myosin for mature myofibril formation. This process is particularly critical in cardiac tissue, which has high proteasomal activity, making it more sensitive to UPS inhibition. Thus, interference with proteasomal function likely contributes to the off-target cardiac effects seen in patients undergoing proteasome inhibitor therapy. (51)

Preliminary Proteasome inhibitors effect on vasculature

- **Vascular smooth muscle cells**
  Proteasome inhibition blocks VSMC proliferation and migration in vitro and in vivo, which may suppress pathological vascular remodeling such as that induced by AngII or in pulmonary hypertension (52) While this might be beneficial in some contexts, chronic exposure can also disrupt vascular integrity.
- **Oxidative Stress & Anti-Inflammatory Effects**
  At low doses, PIs may upregulate protective antioxidative enzymes (e.g., HO-1, SOD1) and reduce superoxide production and inflammation—potentially aiding vascular function **(**53) Conversely, chronic PI exposure is linked to oxidative stress, reduced endothelium-dependent relaxation, and arterial thickening
- **Thrombosis & Microvascular Injury**
  Proteasome inhibition has been associated with thrombotic microangiopathy (TMA), endothelial injury, and impaired VEGF signaling (54). Interestingly, PIs can also reduce thromboembolic events by increasing endothelial thrombomodulin levels -

Following an extensive and in-depth literature review, I have summarized the currently available (as of 2025) data on the effects of proteasome inhibition on the vasculature. To date, no studies have specifically assessed arterial stiffness as a cardiovascular risk parameter in the

context of proteasome inhibitor treatment. Most vascular studies have been conducted either ex vivo or in vitro, primarily focusing on the direct effects of carfilzomib on vascular reactivity. Among these, one study stands out as the most comprehensive in evaluating the impact of the irreversible proteasome inhibitor carfilzomib on in vitro vascular models without underlying in vivo comorbidities. (*54)*

However, a detailed investigation into arterial stiffness—especially in relation to observed collagen data—is critically needed. This would help establish a clearer mechanistic link between proteasome inhibitor– vascular activity and the cardiovascular adverse events (CVAEs) frequently reported in clinical settings, and would allow a more accurate comparison between reversible and irreversible proteasome inhibitors in this context

Chapter 2

2.0 Arterial Stiffness as a Marker of Vascular Safety in Safety Pharmacology

One of the limitations of most pre-clinical and clinical studies within the cardiovascular realm is to not include arterial stiffness a parameter of evaluation of Cardiovascular risk associated with Pharmacological safety. Arterial stiffness is associated with a range of cardiovascular risk factors and is an independent predictor of cardiovascular mortality which is not included into most study or reports(38) Progressive large artery stiffening is the predominant cause of increased pulse pressure, a marker of cardiovascular (CV) risk in the general population and a predictor of CV events .Furthermore, it reduces myocardial perfusion efficiency, increases left ventricular afterload and elicits mechanical stress on capillaries, potentially damaging the capillary wall of strongly perfused organs such as the heart, brain and kidneys.

Risk factor identification is useful to stratify patients at risk for the development of CVD and. However, this has proven insufficient to limit CVD, and hence more precise stratification of CV risk is needed including this specific parameter.
Safety Pharmacology is an essential component of early drug development, aimed at identifying potential adverse effects of investigational compounds on key physiological systems—namely, the cardiovascular, central nervous, and respiratory systems. These studies help to forecast clinical safety concerns, guide the selection and optimization of drug candidates, and reduce the likelihood of failure in later development phases. Unlike toxicology, which investigates long-term systemic effects, safety pharmacology focuses on the acute impact of a compound on vital functions. It typically involves dedicated or integrated experimental designs that enable the detection of infrequent but potentially life-threatening side effects. Among the primary areas of focus is cardiovascular safety, with particular attention to QT interval prolongation and the risk of torsade de pointes—serious arrhythmias that can lead to sudden cardiac death. While existing screening protocols are effective in identifying these liabilities, ongoing efforts aim to enhance their predictive value and ensure comprehensive risk assessment. (55)

Arterial stiffness is one of the leading risk markers for hypertension moreover clinical evaluation of arterial stiffness was also shown to independently predict CV events and fatal stroke.
A meta-analysis of studies analyzing arterial stiffness including 17 longitudinal studies that evaluated 15,877 subjects over a mean period of 7.7 years showed similar results. Several populations such as patients with hypertension, diabetes, ESRD, coronary artery disease and subjects from the general population or ethnic minorities were included. Age, sex, and cardiovascular risk factors were controlled for in most of the studies. Results showed that the relative risk for the development of CV events was linearly related from the first to the third tercile of aortic pulse wave velocity (clinical measurement of arterial stiffness). (56)
Given the direct correlation in clinical setting a pre-clinical arterial stiffness evaluation during pre-clinical steps of drug development might lead to decease adverse effect incidence during the clinical Phase.
Although current safety pharmacology practices have adopted effective screening methods to identify cardiovascular risks, opportunities for refinement still exist. Regulatory frameworks, including ICH S7A, advocate for hemodynamic evaluations—such as monitoring heart rate and blood pressure—in conscious animals prior to the initiation of phase 1 human trials. These in vivo

telemetry studies tend to offer reliable predictions of human responses, yet they often fall short in revealing the underlying mechanisms. This lack of mechanistic detail can hinder the development of a thorough clinical risk analysis and a comprehensive strategy for risk mitigation [10]. In this light, arterial stiffness emerges as a promising biomarker for early detection of cardiovascular risk. Interestingly, while arterial stiffness is closely linked to blood pressure, it independently predicts cardiovascular outcomes regardless of actual blood pressure readings However, despite its potential, it remains underutilized in standard safety pharmacology protocols. Integrating this parameter into routine evaluations could significantly enhance our ability to assess cardiovascular safety in both existing and emerging drug candidates, marking a potential shift in how we approach preclinical cardiovascular risk evaluation. (55)

2.1 Anatomical and Functional Overview of the Aorta

The aorta is the largest and most critical artery in the human body, responsible for distributing oxygenated blood from the heart to the systemic circulation. Structurally complex and highly specialized, the aorta is designed to withstand high pressures and accommodate the dynamic nature of blood flow. Its design ensures both durability and elasticity, allowing it to fulfill its vital function efficiently.

Structural Organization of the Aortic Wall

The wall of the aorta is composed of three distinct layers, each contributing specific structural and functional roles:

- **Tunica i Intima:**
  This innermost layer comprises a single layer of endothelial cells supported by a thin layer of connective tissue. It provides a smooth, frictionless surface that facilitates uninterrupted blood flow and prevents turbulence. The endothelial lining also plays a role in vascular tone and homeostasis by releasing nitric oxide and other vasoactive substances.
- **Tunica Media:**
  Located between the intima and adventitia, this thick middle layer is predominantly made up of concentric layers of smooth muscle cells interwoven with elastic fibers and collagen. The tunica media is critical for maintaining vascular tone and elasticity, enabling the aorta to expand during systole (when the heart contracts) and recoil during diastole (when the heart relaxes), thereby ensuring a continuous flow of blood.
- **Tunica Adventitia:**
  The outermost layer is composed mainly of collagen-rich connective tissue, fibroblasts, and nerve fibers. It serves a supportive role by anchoring the aorta to surrounding tissues and providing structural integrity. In larger arteries like the aorta, the adventitia also contains its own microvasculature known as the vasa vasorum, which supplies nutrients to the outer layers of the vessel wall.

Anatomical Subdivisions of the Aorta

The aorta is subdivided into several anatomical regions, each serving different vascular territories:

- **Aortic Root:**
  Located at the base of the heart, this section originates from the left ventricle and includes the aortic valve and coronary artery openings.
- **Ascending Aorta:**
  This initial segment arises from the aortic root and travels upward, supplying blood to the upper body through its branches, including the coronary arteries.
- **Aortic Arch:**
  A curved continuation of the ascending aorta, the arch gives rise to major arteries supplying the head, neck, and upper limbs—namely, the brachiocephalic trunk, left common carotid artery, and left subclavian artery.
- **Descending Thoracic Aorta:**
  Continuing from the arch, this portion runs downward through the chest cavity, supplying oxygenated blood to the thoracic organs and body wall.
- **Abdominal Aorta:**
  As the descending aorta passes through the diaphragm, it becomes the abdominal aorta, delivering blood to abdominal organs, pelvic structures, and lower limbs. Ti eventually bifurcates into the common iliac arteries.

Functional Specializations of the Aorta

- **Elasticity and Compliance:**
  The abundance of elastic fibers in the tunica media provides the aorta with the ability to stretch during systole and recoil during diastole, which helps dampen the pulsatile output of the heart and maintain steady blood pressure throughout the arterial system.
- **Endothelial Functionality:**
  The tunica intima’s smooth endothelial lining minimizes friction and turbulence, promoting laminar flow and reducing the risk of thrombosis or atherosclerotic plaque formation.
- **Branching and Distribution:**
  The aorta's strategic branching ensures the even distribution of blood to essential organs and tissues throughout the body. Each subdivision supports a specific physiological territory, maintaining systemic perfusion.

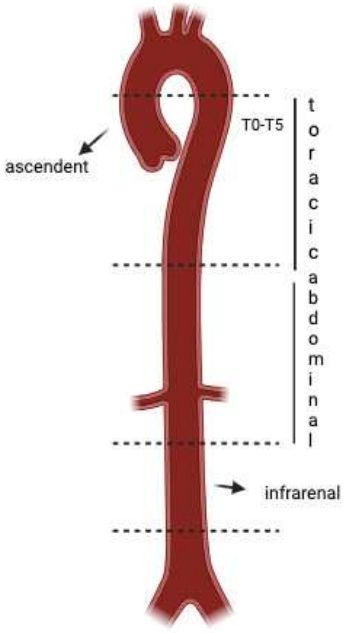

2.2Aortic Components

Aortic function is regulated by many cell components, including endothelial cells (ECs), vascular smooth muscle cells (VSMCs), and adventitial tissues with inflammatory cells, autonomic nervous system, and vasa vasorum. The interactions among these cells/tissues are substantially involved in the vascular health and disease.

1.Endothelial Cells

Endothelial cells line the interior surface of blood vessels and play a crucial role in preserving vessel architecture and regulating vascular function. Despite their importance, how mechanical forces—such as those from blood flow—influence intracellular signaling within endothelial cells remains only partially understood. Recent publications in *Arteriosclerosis, Thrombosis, and Vascular Biology (ATVB)* have explored the functional roles of endothelial cells and their contribution to vascular pathologies. For instance, Walshe et al. demonstrated that shear stress-induced signaling through transforming growth factor-beta (TGF-β) provides protective benefits to endothelial cells.

These cells are fundamental in initiating vascular diseases, yet studying their gene expression in arteries under in vivo conditions has proven challenging. Structurally, endothelial cells are polarized: their upper (luminal) surface interfaces directly with the bloodstream and circulating components, while the lower (basolateral) side is anchored to underlying tissues via a basement membrane, which the cells themselves produce. Their shape varies depending on their location in the vascular tree, though they typically appear thin and elongated. Dimensions range from approximately 30–50 micrometers in length, 10–30 micrometers in width, and a thickness of 0.1–10 micrometers. To minimize shear stress from blood flow, they align parallel to the direction of flow within the vessel.

Functionally, endothelial cells regulate various physiological processes, including vascular tone (by controlling vessel dilation and constriction), the movement of fluids, solutes, hormones, and macromolecules across the vascular wall, and the trafficking of platelets and blood cells. They also play a critical role in suppressing the migration and proliferation of vascular smooth muscle cells from the tunica media into the tunica intima, which is vital for maintaining vascular integrity and function.

Today, the endothelium is no longer viewed as a passive barrier. It is increasingly recognized as a dynamic organ capable of sensing environmental stimuli and actively responding through metabolic and endocrine activity. (57)

Due to their location, endothelial cells are highly sensitive to changes in blood flow and circulating biochemical signals. They respond by releasing vasoactive substances that modulate vascular tone. Under normal physiological conditions, a balance between vasodilators and vasoconstrictors is maintained, typically favoring dilation. Notably, nitric oxide (NO) release increases in response to heightened shear stress. This occurs through rapid activation of endothelial nitric oxide synthase (eNOS), followed by enhanced expression of the eNOS gene and activation of its promoter.

Endothelial cells are constantly exposed to various mechanical forces, including:

1. **Radial pressure** from within the vessel (blood pressure),
2. **Tangential forces** acting on the vessel wall due to cell-cell interactions and vasomotion, and
3. **Axial shear forces** generated by the friction of blood flow along the vessel lining.

Endothelial Cell Phenotypes

The vascular endothelium adapts to its environment by modifying its phenotype in response to mechanical and chemical signals. This adaptability is driven by changes in gene expression resulting from different forms of stress.

In the **aorta**, endothelial cells display both **activated** and **proliferative** behaviors. Activation is characterized by increased expression of surface adhesion molecules such as vascular cell adhesion molecule-1 (VCAM-1), intercellular adhesion molecule-1 (ICAM-1), and E-selectin. Meanwhile, proliferation of aortic endothelial cells can be stimulated by various growth factors, including vascular endothelial growth factor (VEGF), and is regulated by pathways like Hippo/VEGFR2.

Pathological Phenotypes in Disease

In certain disease states, endothelial cells exhibit abnormal behaviors. For example, in **idiopathic pulmonary arterial hypertension (IPAH),** researchers have identified a **hyperproliferative, apoptosis-resistant endothelial phenotype**. This dysfunctional state may stem from several possible origins

- An inherent cellular subset (such as resident progenitor cells),
- Environmental pressures driving epigenetic adaptations,
- Or acquired genetic mutations (e.g., in the TGF-β type II receptor).
  In many cases, it may result from a combination of these factors.

2. Vascular smooth muscle cells

Vascular smooth muscle cells (vSMCs) are the primary cell type located in the middle layer of the aortic wall, known as the **tunica media**. Their developmental origin varies depending on the region of the aorta: in the ascending aorta and aortic arch, vSMCs are derived from the neural crest, while in the descending aorta, they originate from the somatic mesoderm. These cells are essential for maintaining both the structural and functional integrity of the aortic wall and play a crucial role in synthesizing extracellular matrix (ECM) components.

Arterial remodeling involves structural and functional adaptations of the vessel wall in response to factors like aging, injury, or disease. VSMCs are central players in this remodeling process. A key feature of their function is **phenotypic switching**, where oxidative stress can trigger the release of extracellular vesicles, which promote calcification. The state of VSMCs influences the development, progression, and stability of vascular plaques. In the tunica media, VSMC phenotype is vital for preserving elasticity, regulating wall tension, and controlling arterial stiffness. Their inherent plasticity allows them to adapt to changing mechanical and environmental stimuli.

vSMCs Phenotype

In a healthy aorta, smooth muscle cells exhibit a **contractile phenotype**, marked by limited proliferation and high expression of specific contractile markers. Under stress or vascular injury, they can transition to a **synthetic phenotype**, which is characterized by enhanced proliferation, migration, and ECM production. This switch involves downregulation of contractile proteins and upregulation of molecules that promote cell division and movement. Synthetic VSMCs contribute to ECM remodeling by producing matrix metalloproteinases (MMPs), such as elastases and collagenases, which facilitate their migration to damaged areas. However, this remodeling can lead to **increased arterial stiffness**, a risk factor for systolic hypertension and dysfunction in target organs like the heart, kidneys, and brain.

Contractile apparatus of vSMCs

The **contractile machinery** of vSMCs consists of thin filaments made of **alpha-actin** (encoded by the *ACTA2* gene) and thick filaments composed of **myosin heavy chains** (encoded by *MYH11*), paired with two regulatory and two essential light chains. Contraction begins when calcium ions enter the cell and bind to calmodulin, forming a complex that activates myosin light chain kinase (MLCK, encoded by *MYLK*). MLCK then phosphorylates the regulatory light chains of myosin, initiating the contraction cycle through myosin ATPase activity, which drives the sliding of myosin heads along actin filaments. Relaxation follows when calcium levels drop, leading to the inactivation of MLCK and dephosphorylation of the regulatory light chain by myosin light chain phosphatase, a process regulated by cyclic GMP-dependent protein kinase type I.

This contractile system is anchored to the ECM via integrin-rich structures known as **dense plaques**. These integrin receptors connect to elastin through microfibrils, which are primarily composed of fibrillin-1, a large glycoprotein encoded by the *FBN1* gene. Mutations in *FBN1* result in **Marfan syndrome**, a connective tissue disorder characterized by tall stature, flexible joints, and serious complications in connective tissue-rich organs. Importantly, Marfan syndrome also compromises the structure of the aortic wall, significantly increasing the risk for **thoracic aortic aneurysms**.

Protein expression involvement into mVSMC phenotypic switching

During this phenotypic transition, VSMCs show reduced expression of **contractile proteins** including alpha smooth muscle actin (**α-SMA)** and smooth muscle 22 alpha (**SM22α).** For example In thoracic aortic aneurysms, additional proteins such as **smoothelin, calponin, vimentin,** and smooth muscle myosin heavy chain 2 are also decreased. Together with elastic components like collagen and elastin, vSMCs form a cohesive unit that is crucial for maintaining vascular structure and function. Their contractile ability is essential for sustaining the mechanical tension between cells and the ECM and plays a key role in **mechanotransduction**—the process by which mechanical forces are converted into cellular signals.

VSMCs also play an active role in immune responses within the vessel wall. They can recruit immune cells and foster a pro-inflammatory environment. Various cytokines, such as interleukins

IL-1β, IL-5, and IL-6, have been shown to influence VSMC function. For instance, IL-1β promotes matrix turnover by altering the expression of collagen and enzymes like collagenase in human VSMCs. In abdominal aortic aneurysms, immune cells such as mast cells accumulate and release cytokines including IL-6 and interferon gamma (IFN-γ), which may lead to VSMC apoptosis, upregulation of proteolytic enzymes, and further remodeling of the aortic wall

The extracellular matrix (ECM) plays a crucial role in regulating arterial stiffness. It is primarily composed of structural proteins such as collagen and elastin, which maintain the mechanical integrity and elasticity of blood vessels. Far from being a static scaffold, the ECM is a dynamic structure that undergoes continuous remodeling through processes such as chemical modification, crosslinking, and degradation.

3. ECM (Extra cellular matrix)

Beyond its structural role, the ECM serves as a reservoir for a variety of cytokines and growth factors and plays a key role in their regulation. Bioactive ECM components interact with numerous extracellular molecules as well as with receptors on the surface of vascular cells, including G protein-coupled receptors, enzyme-linked receptors, and ion channels. These interactions are critical in modulating intracellular signaling, cell communication (merocrine signaling), and cell behavior such as **proliferation, migration, differentiation, and apoptosis.**

Collagen

Collagen is primarily synthesized by vascular smooth muscle cells (VSMCs) in the intima and media layers of the vessel wall, while fibroblasts in the adventitia contribute to collagen deposition in that region. In their contractile state, VSMCs can migrate, proliferate, and produce collagen as part of ECM remodeling. A variety of chemical and mechanical stimuli can trigger phenotype switching in VSMCs, which promotes collagen synthesis. Moreover, VSMCs respond to existing collagen in their environment through post-translational mechanisms that help regulate further collagen production. (59)

Elastin

Elastin is the most abundant ECM protein in large arteries, which are regularly subjected to high pulsatile pressures from cardiac contractions. Produced initially as **proelastin,** elastin undergoes a crosslinking process that imparts its essential elastic properties, allowing arteries to stretch during systole and recoil during diastole. Elastin fibers are integrated with microfibrillar glycoproteins, such as **fibrillins**, and account for roughly 90% of the elastic fiber content. The crosslinking not only provides elasticity but also mechanical stability and resistance to ECM turnover, thereby preserving embedded cytokines and growth factors. Elastin also plays a regulatory role in controlling the proliferation of VSMCs.

Other ECM Components

The ECM also contains a variety of glycoproteins—including **fibronectin, vitronectin, laminin, entactin, tenascin, and thrombospondin**—which facilitate simultaneous interactions between cells and ECM components. Proteoglycans, another key group of ECM molecules, contribute to

tissue-specific properties such as hydration and filtration. They also influence cellular processes like adhesion, proliferation, differentiation, and migration.

Integrins, a family of transmembrane receptors, play a central role in sensing and transmitting mechanical signals. They are also involved in organizing ECM components into functional architectures. Recent studies suggest that integrins may help coordinate the structural arrangement of newly synthesized ECM proteins, optimizing their support function.

Matricellular proteins are a group of non-structural, non-collagenous ECM proteins that modulate cell-matrix interactions rather than providing mechanical strength. These proteins, such as **cartilage oligomeric matrix protein (COMP)**, contribute to maintaining the normal phenotype of endothelial and smooth muscle cells, suppressing inflammation, and preserving the physiological stiffness of the vessel wall. (60)

ECM in Pathological Conditions

In diseased large arteries**, ECM remodeling becomes maladaptive**. A hallmark of this pathological change is the fragmentation of elastin fibers, coupled with an increased collagen-to-elastin ratio. This shift in ECM composition contributes significantly to arterial stiffening, leading to impaired vascular function and promoting the progression of diseases such as hypertension and atherosclerosis.

From: Extracellular matrix in vascular homeostasis and disease

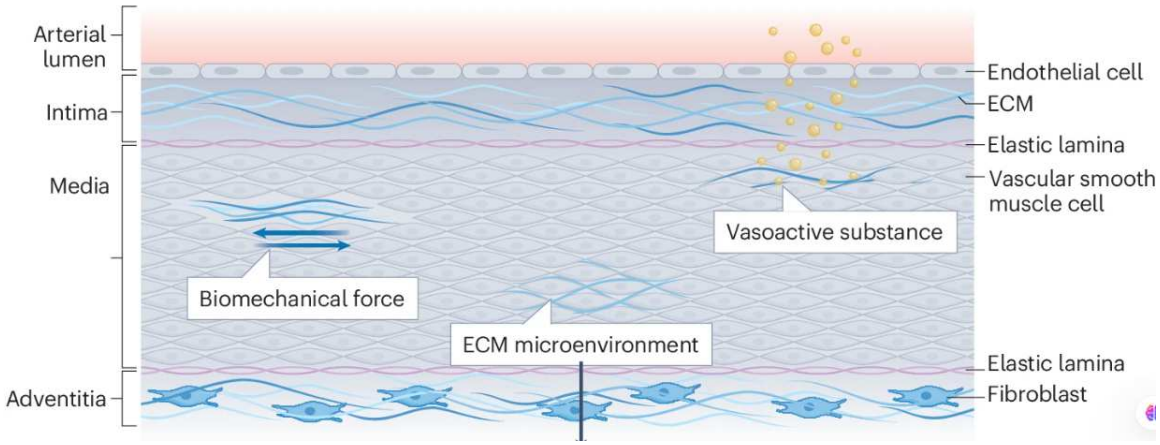

2.3 Underlying physiological mechanism in arterial stiffness

Arteries are structurally composed of three main layers: the innermost **tunica intima**, the muscular **tunica media**, and the outer **tunica adventitia** (With aging and the onset of arterial stiffening, the delicate elastic layer within the intima begins to degrade. Simultaneously, the intimal layer thickens due to the accumulation of extracellular matrix (ECM) components in the basement membrane.

In the tunica media (**active remodeling**) vascular smooth muscle cells (VSMCs) undergo a phenotypic transformation from a contractile to a proliferative state. This shift enhances the synthesis of ECM, particularly collagen types I and III, contributing to increased medial thickness and rigidity over time. Meanwhile, in the adventitia, healthy arteries contain a mix of fibrillar collagens and proteoglycans. However, during atherogenesis, these same molecules facilitate lipid entrapment within the arterial wall, promoting disease progression. Additionally, calcification of the intima and/or media—commonly seen in atherosclerotic lesions—further exacerbates vascular stiffening

The elastic and collagen fibers within arterial walls endow them with the ability to stretch and recoil under physiological pressures. In youthful, healthy arteries, this flexibility allows for effective expansion with each cardiac cycle. Yet, as pressure increases, the relationship between pressure and vessel diameter becomes nonlinear. Stiffness, measured by the change in pressure over the change in diameter, increases with rising pressure, while distensibility (the capacity to expand) diminishes. This behavior is primarily due to the gradual recruitment of collagen fibers at higher pressures, which have far less elasticity than elastin **(passive remodeling)**

Elastin, with a biological half-life of 40 to 50 years, naturally degrades with age. As elastin fibers deteriorate, the mechanical load shifts to the stiffer collagen fibers, making arteries less capable of stretching and accommodating blood flow during diastole.

A key driver in the early stages of this process is **endothelial dysfunction**, a condition influenced by nearly all major cardiovascular risk factors. This dysfunction is a critical initiator of arterial stiffening

Endothelial dysfunction is recognized as the earliest stage in the development of atherosclerosis and arterial stiffness. In the initial phases, various cardiovascular (CV) risk factors—particularly hypertension—gradually alter the structure and function of the vascular system.

Endothelial dysfunction plays a central role in the development and progression of arterial stiffness. Under normal physiological conditions, the endothelium maintains vascular homeostasis by balancing the release of endothelium-derived relaxing and contracting factors. Nitric oxide (NO), the most critical relaxing factor, is synthesized by endothelial nitric oxide synthase (eNOS) in response to stimuli such as shear stress. Once produced, NO diffuses into the vascular smooth muscle cells, activates guanylate cyclase, and promotes cyclic GMP-mediated vasodilation. This process not only regulates vascular tone but also inhibits platelet aggregation, leukocyte adhesion, and smooth muscle cell proliferation.

However, **when this balance is disrupted**—as seen in endothelial dysfunction—the production and bioavailability of **NO decrease**, while vasoconstrictive and pro-inflammatory mediators increase. This shift results in reduced vasodilatory capacity, heightened oxidative stress, and a pro-thrombotic, pro-inflammatory vascular environment. Such dysfunction contributes significantly to increased vascular tone and rigidity, promoting arterial stiffening. Over time, this condition predisposes individuals to hypertension, atherosclerosis, and other cardiovascular complications, often preceding visible morphological changes in the arterial wall. (61)

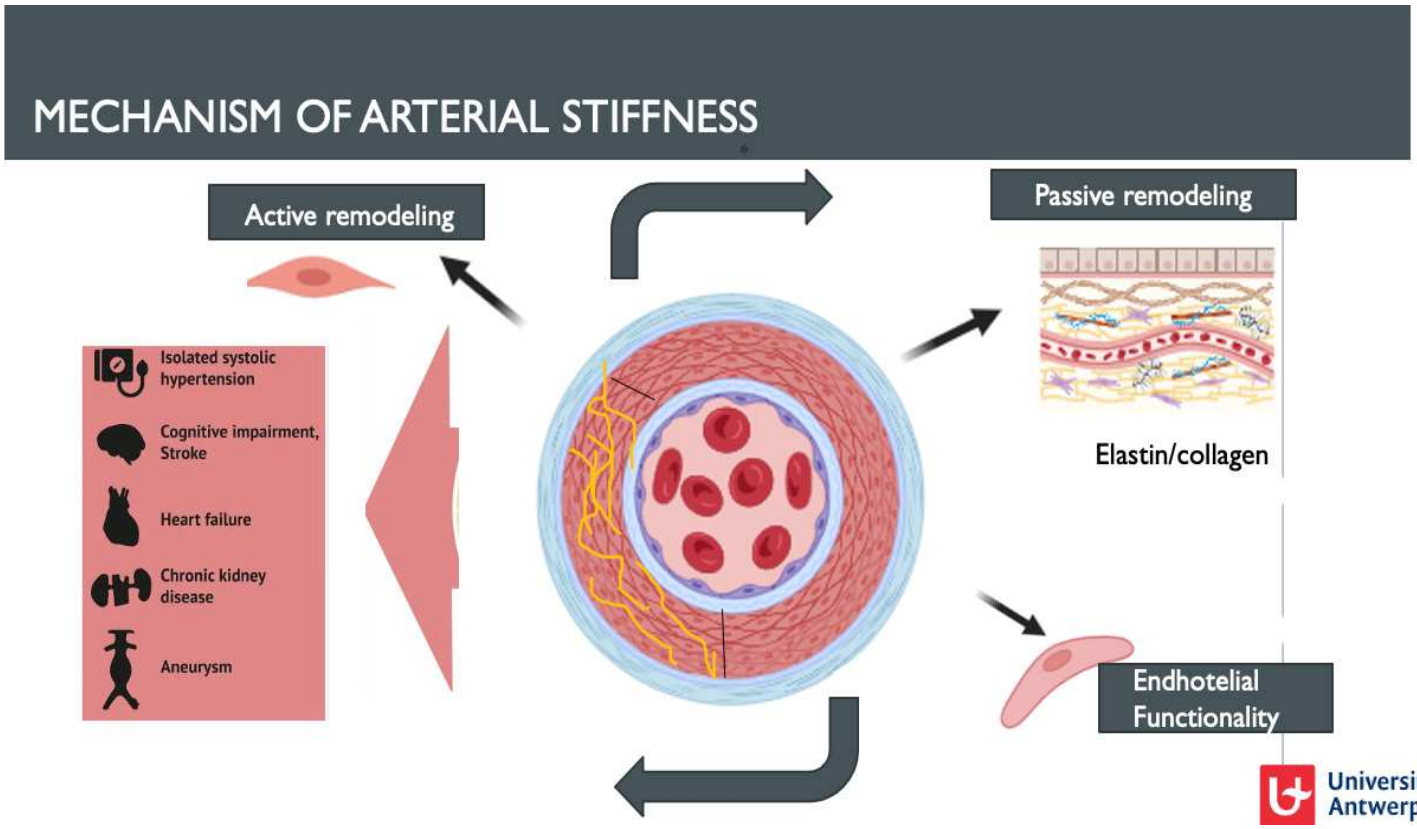

Figure A: The current figure provides a schematic overview of the three principal physiological mechanisms contributing to arterial stiffness: (1) endothelial dysfunction, which compromises vascular tone and homeostasis; (2) passive structural remodeling, including increased collagen deposition and degradation of elastin fibers; and (3) active remodeling processes involving phenotypic switching of vascular smooth muscle cells (VSMCs) from a contractile to a synthetic state."

2.4 Aortic regional variations in Arterial stiffness

Elastic and muscular arteries demonstrate distinct structural and functional characteristics that influence how they respond to mechanical stress. **Elastic arteries**, such as the aorta, are designed to stretch and recoil with each heartbeat, enabling them to buffer the pulsatile output of the heart and maintain stable arterial pressure. This elastic behavior is largely due to their high content of elastin fibers. On the other hand, **muscular arteries,** which are rich in layers of vascular smooth muscle cells, are more specialized for regulating blood flow and vascular tone, making them less reactive to pressure fluctuations. These anatomical and functional differences lead to regional variability in arterial stiffness across the vascular system. The aorta, in particular, displays unique mechanical properties that reflect regional differences in tissue architecture, blood flow patterns, and the surrounding microenvironment. Proximal elastic arteries tend to undergo structural alterations with aging and disease, such as changes in extracellular matrix composition, whereas distal muscular arteries are more prone to dysfunctions at the cellular level, especially involving smooth muscle cells. The distribution and proportion of structural proteins like collagen and elastin, along with age-associated changes in arterial wall composition and smooth muscle cell behavior, contribute significantly to these regional disparities. As a result, the mechanisms driving stiffness may vary depending on the location within the arterial tree.

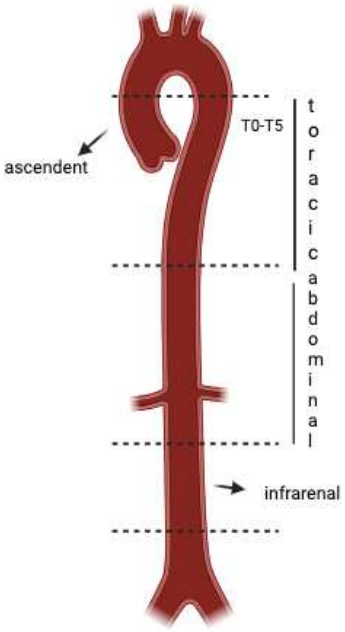

Parameter	Thoracic Ascending Aorta (TAA)	Thoracic Descending Aorta (TDA)	Abdominal Infrarenal Aorta (AIA)
Elasticity	High elasticity due to high elastin content	Moderate elasticity	Low elasticity; more stiffness
Collagen Content	Low	Moderate	Highest among regions
Collagen:Elastin Ratio	Lowest	Balanced	Highest
Arterial Stiffness (Passive)	Low	Moderate	High
Arterial Stiffness (Active)	Present, contributes to buffering	Moderate contribution	High vascular tone, low compliance
VSMC Contractility	Lower	Higher	Highest
Basal NO Index (EC function)	Highest	Moderate	Lowest
Endothelium-Dependent Relaxation (Ach, ATP)	Strong (Ach, ATP-induced NO)	Moderate	Impaired, especially with ATP
Endothelium-Independent Relaxation (DEANO)	No significant difference among regions	No significant difference among regions	No significant difference among regions
Age-Related Changes in Stiffness	Collagen increases; elastin fragmentation seen in TAA	Collagen increases; no elastin fragmentation	High stiffness with ageing
Age-Related VSMC Dysfunction	Present	Pronounced in ageing (TDA studied)	Most severe
Age-Related EC Dysfunction	Not pronounced at 24 months (TDA)	Mild	Significant in literature but not seen in this model
Hemodynamic Role	Main buffering zone	Transitional compliance zone	Less buffering, more resistant vessel
PWV Association	Low	Increases with age	Associated with high PWV in ageing

Table 1 This table summarizes the comprehensive research conducted by Callan Wesley, who has dedicated years to investigating the regional variations in vascular reactivity, cellular composition, and physiological characteristics across different segments of the aorta along the aortic tree. Showing how vascular research should showcase the intrinsic proprieties of different parts of vessels, physiologically structured differently to unravel underlying mechanism specifically in the realm of arterial stiffness and vascular reactivity cardiovascular research (62)

2.5 Clinical Measurement of arterial stiffness

Pulse Wave Velocity (PWV) is a widely accepted, non-invasive indicator of arterial stiffness and an important biomarker of cardiovascular health

PWV refers to the speed at which pressure waves, produced by the heart's systolic contraction, travel through the arterial tree. Measuring PWV offers additional insight into the elastic properties of the arterial system. whereby higher elasticity in younger, healthier vessels causes the pulse wave to travel more slowly. In comparison, increased arterial stiffness leads to faster pulse wave propagation, resulting in a higher PWV (63)
A higher PWV indicates reduced vessel distensibility and compliance, which is associated with greater arterial stiffness.

Since the mechanical characteristics of arterial walls differ throughout the vascular system—from central arteries to the peripheral ones—PWV is influenced by these changes. The pulse wave moves through the arteries, and its speed is determined by the specific properties of the vessel.

. Clinically, PWV can be assessed using various techniques and at different arterial sites, depending on the purpose of the evaluation and the available technology.

The **carotid-femoral PWV (cfPWV)** remains the reference standard for assessing aortic stiffness in clinical and research settings. This method evaluates the velocity of the pressure wave as it travels between the common carotid artery and the femoral artery. Guidelines recommend determining the pulse transit time by recording signals simultaneously at both sites. The distance traveled by the pulse wave is typically calculated as 80% of the direct surface distance between the two measurement points, a correction factor based on anatomical studies to account for vessel curvature and depth. The accuracy of tonometry is highly dependent on the proper placement of the sensor and the quality of the arterial signal obtained. Factors such as patient movement and external pressure on the artery strongly affect the measurement.
A range of **validated instruments** is available to measure cfPWV, utilizing different technologies:

- **Tonometry-based systems** employ pressure transducers to record arterial waveforms at the carotid and femoral sites, often requiring skilled operators for accurate placement and signal interpretation
- **Oscillometric devices**, using blood pressure cuffs placed on limbs and the neck, detect the time of arrival of the pulse wave through changes in cuff pressure, offering a more user-friendly and automated approach.
- **Doppler ultrasound** can track the velocity of blood flow to determine pulse arrival time, and is useful when tonometric access is limited or additional anatomical details are needed.
- **Magnetic Resonance Imaging (MRI)** provides highly accurate spatial and temporal resolution of blood flow and vessel structure, although its use is generally restricted to research settings due to cost and complexity. (65)

In addition to cfPWV, alternative indices such as **brachial-ankle PWV (baPWV)** and the **Cardio-Ankle Vascular Index (CAVI)** are widely used in Asia and some European countries. These indices, while not measuring aortic stiffness directly, provide practical and reproducible

estimates of systemic arterial stiffness using simpler equipment. CAVI, in particular, attempts to standardize PWV measurement by adjusting for blood pressure, making it less dependent on transient hemodynamic fluctuations (66).

Emerging technologies aim to simplify and broaden the accessibility of arterial stiffness measurements:

- **Arm cuff-based systems** offer integrated blood pressure and PWV estimation using waveform analysis algorithms
- **Photoplethysmographic fingertip sensors** use optical signals to detect pulse wave timing and morphology
- **Ballistocardiographic weighing scales** represent a novel approach, estimating PWV by detecting the mechanical effects of cardiac ejection through weight-displacement sensors

While these newer devices show promise for widespread screening and at-home monitoring, their clinical validity and reliability require further large-scale studies before they can be recommended for routine use.

Clinical Interpretation of PWV

According to the European Society of Hypertension, a cfPWV greater than 10 m/s is considered an indicator of subclinical target organ damage and increased cardiovascular risk (67). However, there is ongoing debate about applying a universal threshold value, as PWV is inherently pressure-dependent and influenced by acute hemodynamic changes. As such, context-specific interpretation is essential, especially in patients with variable blood pressure profiles Beyond cardiovascular risk, elevated PWV has been associated with diminished pulmonary function, highlighting its potential role as a systemic marker of vascular and respiratory health.

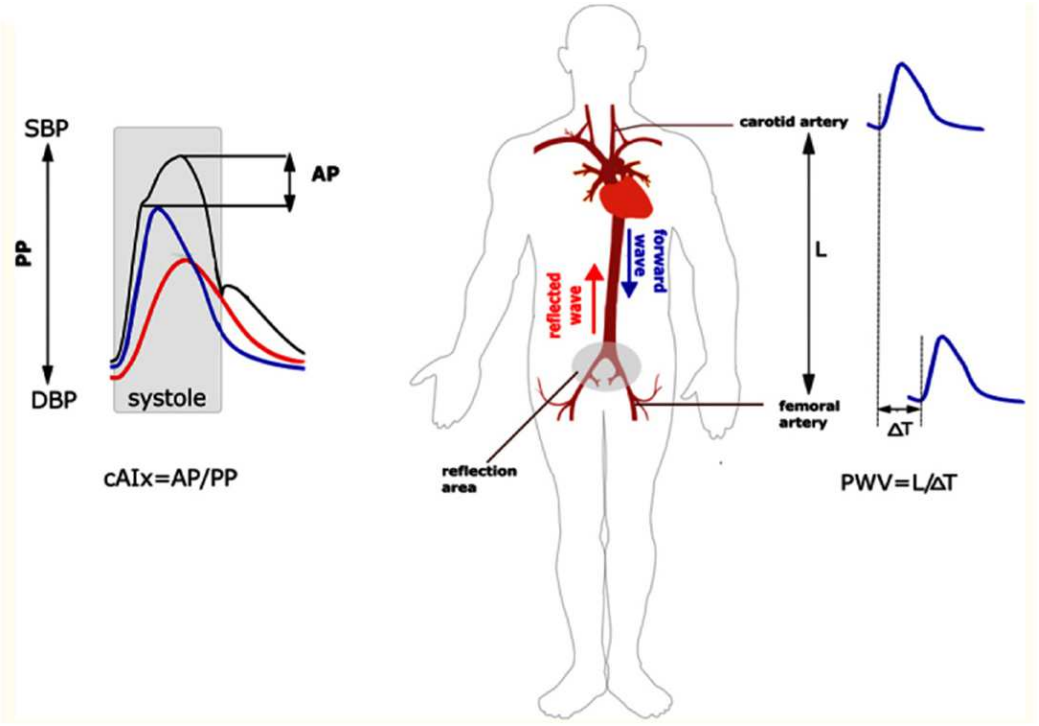

Figure 1 Evaluation of Central Arterial Function: Central Augmentation Index and Carotid-Femoral Pulse Wave Velocity

To determine the central augmentation index, the augmentation pressure is divided by the pulse pressure. This ratio reflects the extent to which pressure in the central arteries is increased due to wave reflections.

Carotid-femoral pulse wave velocity is assessed by capturing pressure waveforms at the common carotid artery and the femoral artery. The method used is called the foot-to-foot technique, which identifies the initial upstroke of the pressure wave at each site. The velocity of the pulse wave is calculated by dividing the physical distance between the two measurement sites by the time it takes for the pressure wave to travel from the carotid to the femoral artery. This combined assessment provides valuable information about arterial stiffness and central pressure dynamics.

2.6 ROTSAC Rodent Oscillatory Tension Set up to study Arterial Compliance: a novel preclinical tool that studies biomechanical vessel proprieties in safety Pharmacological setting

Most preclinical investigations within the field of Safety Pharmacology primarily focus on assessing hemodynamic parameters—such as heart rate and blood pressure—in conscious animals to evaluate cardiovascular safety prior to phase 1 clinical trials. These in vivo telemetry studies generally provide reliable translational insight into human physiology. However, arterial stiffness, an independent predictor of cardiovascular risk, is emerging as a promising parameter for inclusion in safety assessments of drug candidates.

While pulse wave velocity (PWV) is an established method for evaluating arterial stiffness in vivo, it presents certain limitations. An ex vivo approach that measures arterial elasticity under physiological stretch conditions could significantly enhance the assessment of vascular responses to drug candidates. This method allows for precise control over experimental conditions, enabling vessels to be subjected to different drug stimulations while capturing multiple physiological endpoints.

In current preclinical cardiovascular pharmacology studies, isolated mouse aortas are often evaluated under low-stretch frequencies or isometric conditions, which may not fully replicate physiological dynamics. **Yet, pacing studies in both rodents and humans have demonstrated that arterial compliance is dependent on stretch frequency.**

To address this, the Rodent Oscillatory Tension Set-up to study Arterial Compliance (ROTSAC), developed by the Physiopharmacology Lab at the University of Antwerp, offers a refined organ bath system. In this setup, aortic segments are connected to a force–length transducer that permits controlled clamping at various preloads. This system imposes oscillatory tension at physiological rates of up to 600 beats per minute, enabling a more accurate and dynamic evaluation of arterial compliance under near-physiological conditions.

Use and Functions
Aortic segments are mounted between two parallel wire hooks in 8 ml organ baths. The upper hook connects to a force–length transducer. This transducer consists of an aluminum lever linked to a coil suspended within the magnetic field of a permanent magnet. A controlled current source supplies current to the coil, generating a force. A photoelectric system continuously monitors the displacement of the lever.

Both force and displacement signals are acquired at 1 kHz using a PowerLab 8/30 data acquisition system and LabChart 7 software (ADInstruments, Oxford, UK).

To calculate the **transmural pressure** that corresponds to the vessel's wall stress and geometry, the **Laplace relationship** is applied:

P=F/ l*D

where F is the distension force, l is the length, and D is the diameter of the vessel. The transducer measures force directly, while diameter is derived from the displacement of the upper hook, which is directly proportional to the inner circumference.

Before each experiment, the length and diameter of the vessel segment are measured at three preload levels (20, 40, and 60 mN) using a stereomicroscope and calibrated image analysis software. Because the vessel length slightly decreases as the diameter increases, the average length over each cycle (100 ms) is calculated from the diameter–length relationship using linear regression.

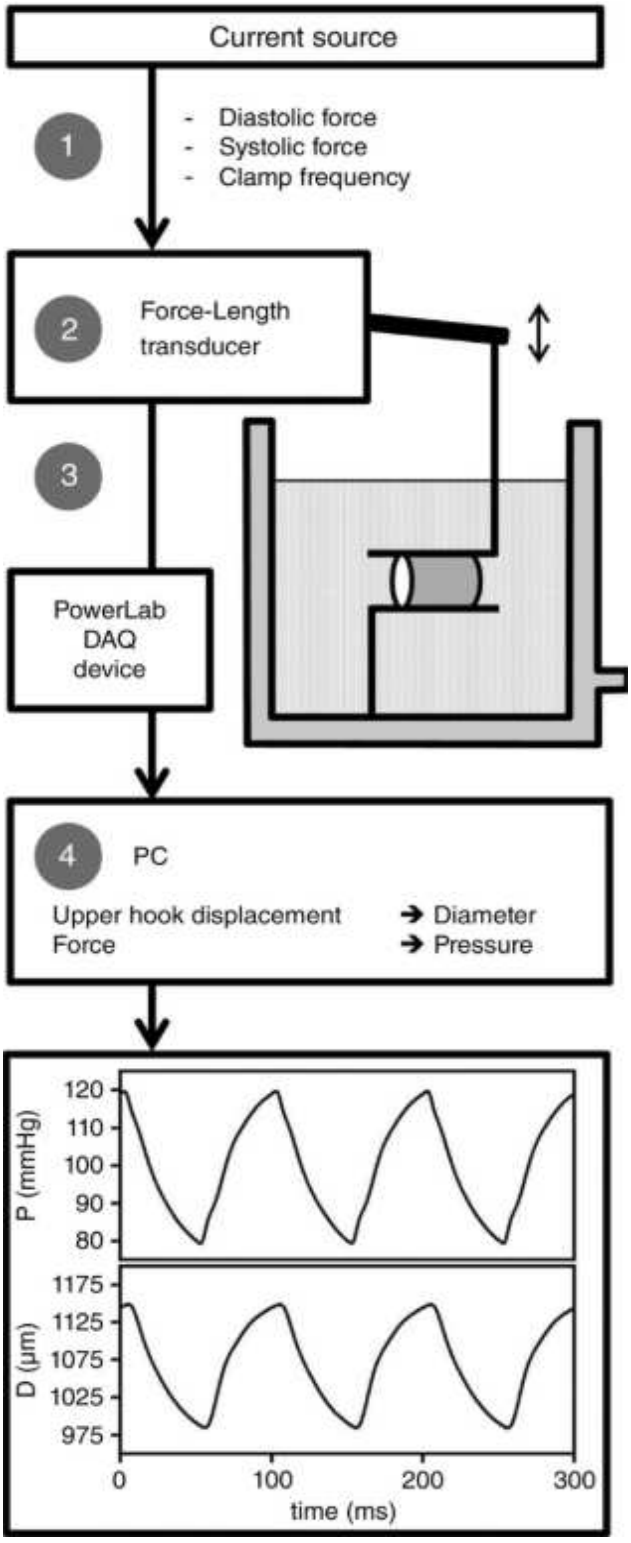

Fig.3 System Overview Validated and created by Psychopharmacology University of Antwerp Group

In the ROTSAC system, the aortic segment is suspended between two metal hooks inside an organ bath. A current source controls both the distension force and the oscillation frequency of the force–length transducer, which operates at 10 Hz to mimic the physiological heart rate of mice (~600 bpm). The transducer continuously measures force and displacement, and the signals are recorded via a Power Lab data acquisition system. These measurements, along with segment diameter and length, are used to compute transmural pressure. Preload is adjusted until the desired systolic and diastolic pressures are achieved.

Mechanical Analysis

Pressure–diameter loops are analyzed to assess the mechanical behavior of the vessel. Two key parameters are calculated:

- **Compliance (C):**

$C=\Delta D / \Delta PC$
where ΔD is the difference between systolic and diastolic diameters, and ΔPC is the pressure difference (±40 mmHg in this setup).

- **Peterson's modulus of elasticity (EP):**

The **Peterson's Elastic Modulus (Ep)** is calculated using the following formula:

$$\mathbf{Ep = \Delta P / (\Delta D / D_0)}$$

Where:

- **ΔP** = Change in pressure (systolic pressure − diastolic pressure)
- **ΔD** = Change in arterial diameter (systolic diameter − diastolic diameter)
- $\mathbf{D_0}$ = Diastolic diameter (68)

Pharmacological Modulation

This setup allows the application of diverse pharmacological protocols to activate vascular smooth muscle cells (VSMCs) and assess the vessel's elastic properties under various conditions, such as cyclic stretching, relaxation, and nitric oxide (NO) inhibition. By introducing different agents directly into the organ bath, the system serves as a validated and versatile experimental platform. It not only enables precise evaluation of vascular stiffness but also provides valuable insights into VSMC functionality, endothelial cell activation, and potential passive vascular remodeling. As such, it is a powerful tool for identifying early pathological changes and uncovering the underlying mechanisms driving vascular dysfunction.

2.7 Importance of studies on vasculature in Oncology

Advancements in cancer treatment have significantly improved patient outcomes across various malignancies, often enabling therapy with curative intent. As cancer survival rates rise, increasing attention is being directed toward the cardiovascular effects of chemotherapeutic agents. Beyond their acute vascular toxicity, the delayed onset of both direct and indirect cardiovascular complications is becoming more prominent, as patients now live long enough for these adverse effects to emerge as major clinical concerns. (69) Striking a practical balance between delivering effective anticancer therapy and minimizing cardiovascular risks has grown more challenging, contributing to the rapid development of cardio-oncology as a distinct subspecialty within cardiology.

While heart failure and myocardial toxicity—particularly from **anthracyclines and HER2-targeted therapies**—are now better recognized and supported by growing evidence to guide preventive strategies, the vascular complications of chemotherapy remain less well understood. Evidence and mechanistic insights into these vascular effects are still limited, highlighting a critical gap in current cardio-oncology research.

Investigating the biochemical pathways underlying chemotherapy-induced cardiovascular complications in vulnerable patients is crucial. Such research can expedite the identification of mechanisms contributing to these adverse effects and facilitate the use of existing pharmacological interventions to mitigate symptoms. This approach aims to enhance patient safety, enable prolonged exposure to chemotherapy and immunotherapy protocols, and ultimately improve long-term survival outcomes.

Preclinical models play a vital role in elucidating the mechanisms of chemotherapy-induced cardiotoxicity. These models, ranging from cellular assays to large animal studies, help identify potential biomarkers and cardioprotective therapies. By mimicking human disease conditions, they provide insights into the molecular pathways involved and facilitate the testing of therapeutic interventions before clinical application. (70)

In summary, advancing preclinical research to unravel the biochemical mechanisms of chemotherapy-induced cardiovascular toxicity also bi investigating specifically vasculature as well is essential. This knowledge can guide the development of personalized treatment strategies, improve patient safety, and enhance long-term survival rates.

Aim of the present study

Proteasome inhibitors, including bortezomib and carfilzomib, are integral to the treatment of relapsed or refractory multiple myeloma due to their ability to induce apoptosis. However, growing evidence links these agents to cancer therapy-related cardiovascular dysfunction (CTRCD), particularly hypertension, heart failure, and arrhythmias. Bortezomib is a reversible, first-generation inhibitor, while carfilzomib is a second-generation, irreversible inhibitor with a potentially higher cardiotoxicity profile.

This study explored the impact of these drugs on cardiac and vascular function, specifically left ventricular ejection fraction (LVEF), arterial stiffness, and vascular reactivity. Male C57BL/6J mice (12 weeks old, n = 8 per group) were randomly assigned to receive either vehicle, carfilzomib (8 mg/kg, I.P.), or bortezomib (0.5 mg/kg, I.P.). A subgroup received L-NAME (0.5 mg/kg) to induce hypertension and assess interactions with proteasome inhibition.

Cardiac performance was evaluated using echocardiography at baseline and after three days. By day six, the animals were euthanized for ex vivo vascular analysis.

Preceding the in vivo experiments, a pilot ex vivo study involved culturing mouse aortic segments to assess vascular smooth muscle and endothelial cell integrity under isometric tension. Complementary in vitro studies examined the cytotoxicity of bortezomib and carfilzomib across various concentrations and time points in different cell lines, including human and murine vascular smooth muscle cells (HAVSMCs and mVSMCs) and m Cardiac endothelial Cells. F-actin distribution was assessed at 24 hours to evaluate cytoskeletal integrity on mVSMC

To investigate the role of autophagy in drug-induced vascular changes, we used RFP-GFP-labeled MVSMCs to monitor autophagic flux in response to both drugs. This multiphase study—combining ex vivo, in vivo (across two models), and in vitro approaches—offers new insights into the safety profile and biological activity of bortezomib and carfilzomib, with a particular focus on their potential to induce arterial stiffness and cardiovascular dysfunction.

Chapter 3

Materials and Methods

3.1 Tissue Culturing

Experimental Protocol for Ex Vivo Aortic Segment Culture and Aorta Retrieval

Six wild-type C57BL/6 mice (n = 6) were euthanized via an overdose of pentobarbital. Following euthanasia, the thoracic cavity was opened, and the entire aorta—from the ascending aorta to the upper portion of the infrarenal—was carefully excised. To preserve the integrity of the vessel wall, perivascular adipose tissue was meticulously removed without damaging the adventitial layer.

The harvested aortas were immediately placed in Krebs–Ringer solution and pinned in place on a dissection plate. Under a stereomicroscope, each thoracic aorta was cut into five equal segments, 2 mm in length (designated T0–T5), generating five samples per mouse. The segments were then briefly rinsed in phosphate-buffered saline (PBS) and transferred to the cell culture facility.

To minimize positional bias, each segment was randomly labeled and placed into individual wells of a 6-well plate, each containing 2 mL of phenol red-free DMEM supplemented with 2% fetal bovine serum (FBS). One segment from each aorta served as a control and was cultured in medium only.

The remaining segments were treated with different concentrations of proteasome inhibitors:

- **Bortezomib**: 1 nM, 3 nM, 10 nM, 30 nM
- **Carfilzomib**: 300 nM, 1 μM

All samples were incubated at 37°C for 24 hours

3.2Functional Assessment of Vascular Reactivity in Thoracic Aortic Segments Ex Vivo Protocol

Thoracic aortic rings, each approximately 2 mm in length, were mounted on a wire myograph system and set to a passive tension of 20 mN, approximating a physiological intraluminal pressure of around 100 mmHg, representative of normal systemic arterial pressure. The tissues were allowed to equilibrate under these conditions to establish a stable baseline tension prior to pharmacological assessment. Vascular smooth muscle cell (VSMC) contractility was evaluated through cumulative administration of phenylephrine (PE), an α1-adrenergic receptor agonist, at concentrations ranging from 3 nM to 3 μM to generate a concentration–response curve for adrenergic-induced contraction. Subsequently, endothelial-dependent vasorelaxation was tested using increasing doses of acetylcholine (ACh), a muscarinic receptor agonist (3 nM–3 μM), which stimulates endothelial nitric oxide synthase (eNOS) to release nitric oxide (NO) and promote smooth muscle relaxation via cyclic GMP signaling. Between treatments, the rings were washed three times with Krebs–Ringer solution, pre-warmed to 37°C to avoid thermal shock and maintain

physiological conditions; this solution was continuously gassed with CO_2 to ensure optimal pH and contained glucose, sodium bicarbonate, and calcium bicarbonate. To investigate the NO-dependent component of ACh-induced relaxation, selected segments were pre-incubated with 300 µM Nω-Nitro-L-arginine methyl ester (L-NAME), a non-selective nitric oxide synthase (NOS) inhibitor, effectively blocking endogenous NO production. To directly assess VSMC responsiveness to NO independent of endothelial input, the NO donor 2-(N,N-diethylamino)-diazenolate-2-oxide sodium salt hydrate (DEANO) was applied in cumulative concentrations ranging from 0.3 nM to 10 µM, allowing the differentiation between endothelial dysfunction and impairments in smooth muscle NO sensitivity.

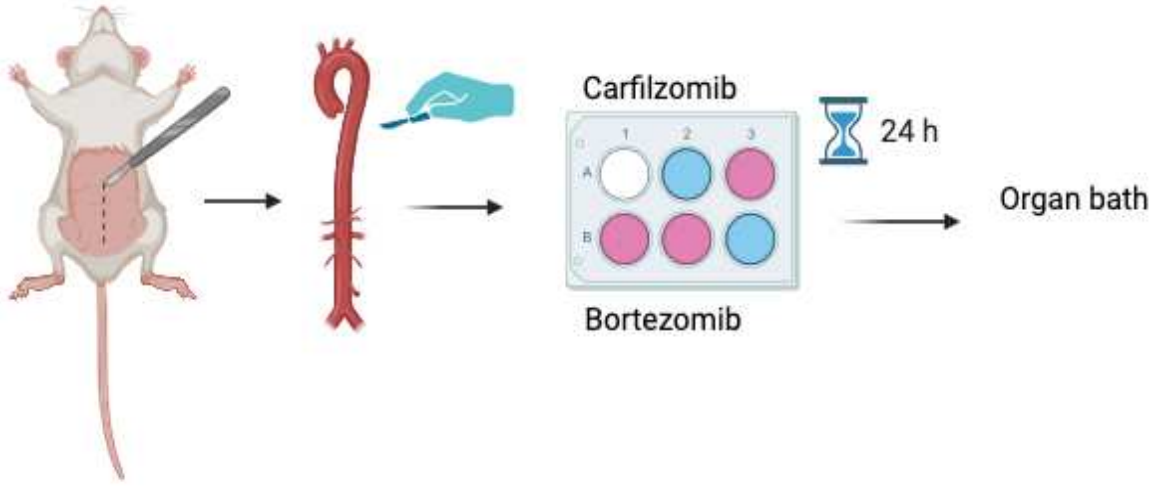

3.3 In Vivo Short-Term Protocol: 2 Injections

Objective: To evaluate in vivo parameters of arterial stiffness and vascular reactivity following short-term administration of proteasome inhibitors in mice.

Study Design:

Twelve black-six mice were randomly divided into three groups (n=4 per group) to assess the effects of two doses of intraperitoneal (IP) injections on arterial stiffness and vascular reactivity:

- **Control group:** Saline
- **Bortezomib group:** 8 mg/kg (dose translated from clinical use)
- **Carfilzomib group:** 0.5 mg/kg (dose translated from clinical use)

Protocol:

- **Day 1:** Each group received a single IP injection of their assigned treatment (saline, bortezomib, or carfilzomib).
- **Day 2 (24 hours later):** The same dose regimen was repeated for each group.
- **Day 3:** Mice were sacrificed for ex vivo evaluation of vascular reactivity and arterial stiffness.

Ex Vivo Evaluation:

- Two 2-mm segments of the thoracic aorta (from the TA3-TA4 region) were harvested from each mouse.
- Segments were mounted in an isometric organ bath containing Krebs-Ringer solution, following the previously described protocol.
- Initial stimulation with a 50 K mM solution was applied to induce polarization and vascular smooth muscle cell (VSMC) contraction to assess activity and integrity.
- Segments were washed three times with Krebs-Ringer solution and returned to basal tension (preload of 20 mN), simulating a mean arterial pressure of approximately 100 mmHg.

Vascular Reactivity Tests:

- **VSMC contractility:** Assessed by cumulative concentrations of phenylephrine (PE; 3 nM–3 μM), an α1-adrenergic agonist.
- **Endothelium-dependent relaxation:** Measured by increasing doses of acetylcholine (ACh; 3 nM–10 μM), which acts on muscarinic receptors.
- **NO inhibition:** Endogenous nitric oxide activity was blocked using L-NAME (300 μM), a non-selective NO synthase inhibitor.
- **NO sensitivity:** VSMC response to exogenous NO was tested with the NO donor DEANO (0.03 nM–10 μM), independent of endothelial influence.

This vascular reactivity protocol was performed for all groups and mice.

Arterial Stiffness Assessment:

- To mimic pulsatile blood pressure, aortic rings were subjected to cyclic mechanical stretching alternating between preload values corresponding to diastolic and systolic pressures at 10 Hz, simulating a mouse heart rate (~600 bpm).
- Transmural pressures on the vessel wall were calculated using the Laplace law, relating internal pressure, vessel radius, and wall tension.
- Cyclic expansion and recoil allowed assessment of arterial distensibility and elastic recoil capacity.
- The primary outcome was Peterson's pressure-strain elastic modulus (Ep), calculated from internal diastolic diameter, pressure differences, and vessel diameter changes.

All procedures utilized the previously described ROTSAC methodology.

Figure 1.A: shows the dose regimen followed in the short term 2 injections study

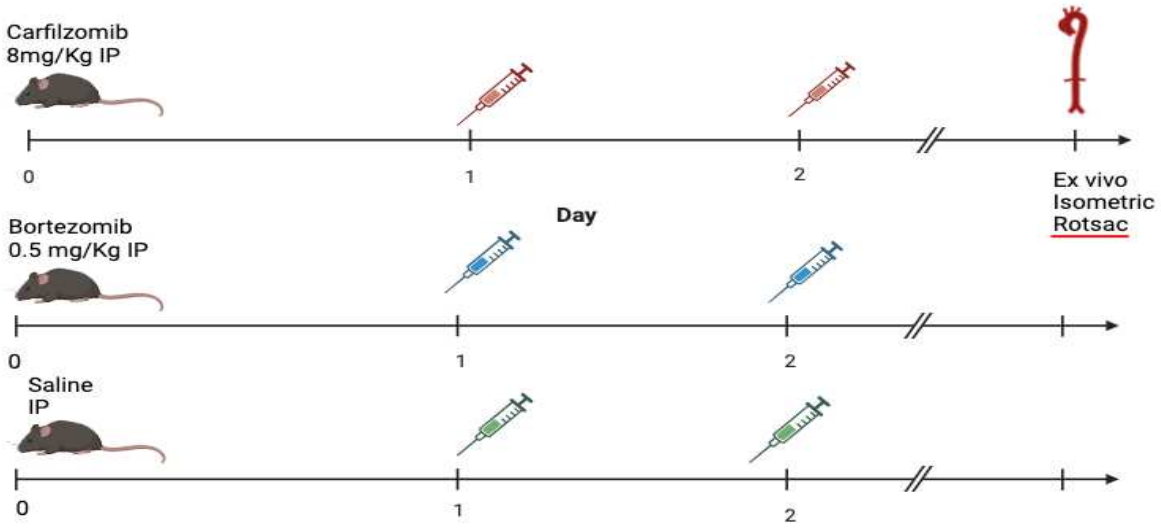

3.4 IN VIVO MAIN STUDY DESIGN

Animal Experimentation Protocol

Twelve-week-old male **C57BL/6J mice** (n = 8 per group) were obtained from **Charles River Laboratories** (Ecully, France) for in vivo experimentation. Upon arrival, all animals were acclimatized and housed in the accredited animal facility of the **University of Antwerp** under standard laboratory conditions: controlled temperature (20–24°C), stable humidity (45%), and a 12-hour light/dark cycle. Mice had unrestricted access to standard rodent chow and tap water. All procedures adhered strictly to the **ARRIVE guidelines** and complied with **Directive 2010/63/EU** of the European Parliament concerning the protection of animals used for scientific purposes. Experimental protocols were approved by the University of Antwerp's Animal Ethics Committee (**file number 2023-40**).

The study was designed to explore the acute vascular effects of proteasome inhibition under both normotensive and hypertensive conditions, mimicking clinical scenarios where **hypertension frequently coexists with cardiovascular complications** in cancer patients. To enhance the translational relevance of the findings, the study included both normotensive (Protocol A) and **L-NAME-induced hypertensive** (Protocol B) mouse models.

Hypertension Induction and Group Allocation

Hypertension was pharmacologically induced in the hypertensive cohort using **L-NG-Nitroarginine Methyl Ester (L-NAME)**, a non-selective nitric oxide synthase (NOS) inhibitor. L-NAME was administered via drinking water at a concentration of **2 mg/mL** for **7 days prior**

to the administration of any other treatment and was continued throughout the experimental timeline.

Following randomization, mice were divided into the following treatment groups:

1. **Vehicle control** (saline, intraperitoneally [I.P.])
2. **Bortezomib** (0.5 mg/kg I.P.)
3. **Carfilzomib** (8 mg/kg I.P.)
4. **L-NAME alone** (2 mg/mL in water + saline I.P.)
5. **L-NAME + Bortezomib** (2 mg/mL in water + 0.5 mg/kg I.P.)
6. **L-NAME + Carfilzomib** (2 mg/mL in water + 8 mg/kg I.P.)

All intraperitoneal injections were administered on **days 1, 2, 5, and 6**. These doses and timepoints were selected based on established protocols from prior studies, notably by Efentakis et al. [249, 250], ensuring consistency and relevance to preclinical oncology models.

Timeline of Experimental Procedures

Both **Protocol A (normotensive)** and **Protocol B (hypertensive)** followed an identical experimental timeline, with minor variation based on pre-treatment in the hypertensive group:

- **Day -7 to Day 0 (only in hypertensive group):** L-NAME administration began 7 days prior to treatment initiation.
- **Day 0:** Baseline **echocardiography** was performed to assess cardiac function.
- **Days 1, 2, 5, 6:** Intraperitoneal injections of either vehicle or proteasome inhibitors.
- **Day 3:** Intermediate echocardiographic analysis to evaluate acute cardiac changes post-treatment.
- **Day 6:** Endpoint measurements included animal sacrifice and **ex vivo** assessments of **arterial stiffness** and **vascular tone**.

Overview of Experimental Objectives

This study aimed to:

- Evaluate the **acute cardiovascular effects** of proteasome inhibitors (bortezomib and carfilzomib).
- Determine the **interplay between proteasome inhibition and pre-existing hypertension**.
- Investigate **vascular tone and stiffness alterations** through functional and mechanical analysis of excised arteries

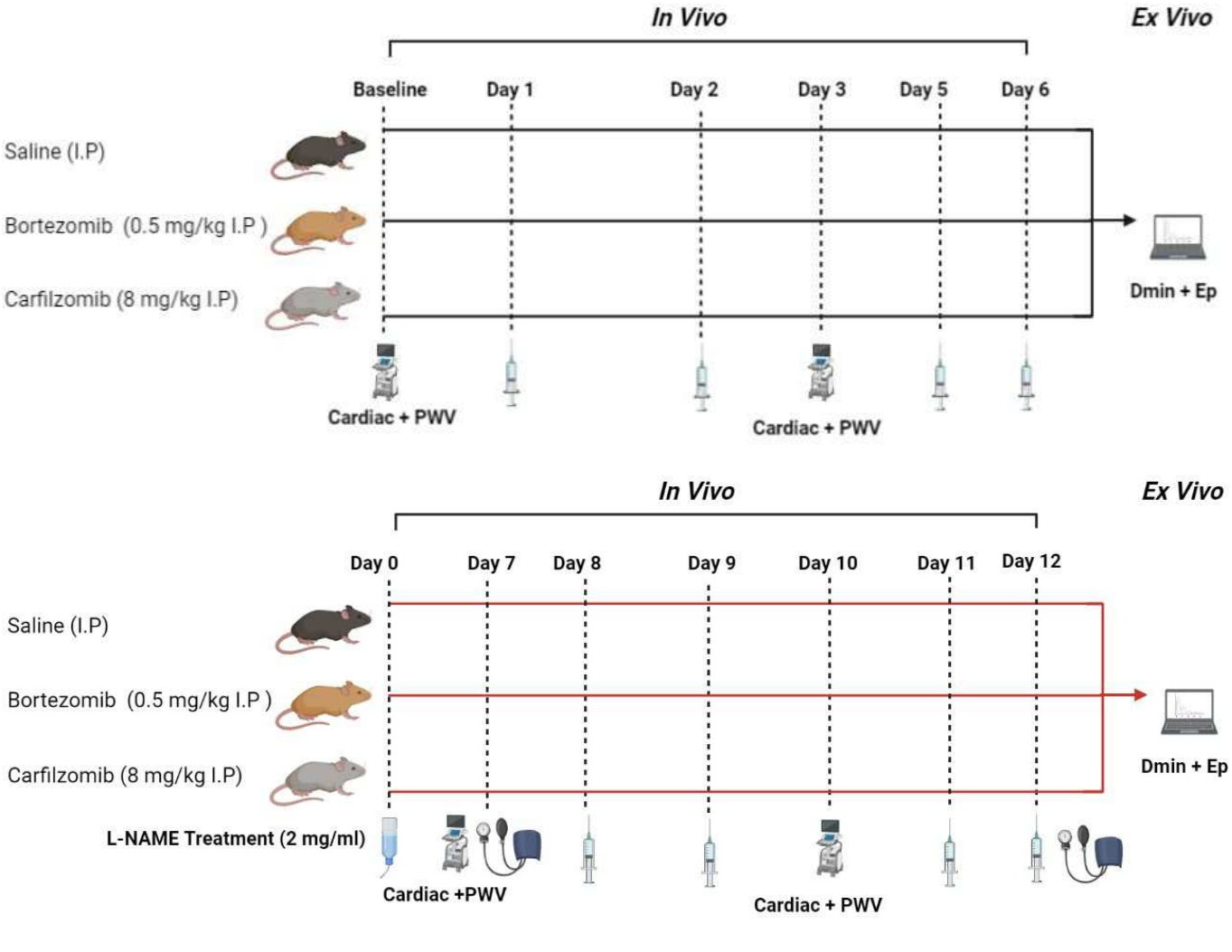

Figure-1.B the Upper figure shows the non hypertensive cohort the below figure (red) shows the Hypertensive L-Name induced cohort

Ultrasound Assessment of Cardiovascular Function

Cardiovascular function was evaluated using non-invasive high-resolution ultrasound imaging under light anesthesia to minimize animal stress and movement. Mice were anesthetized with 1.5–2.5% isoflurane (v/v) (Forene; Abbvie, Belgium), administered via a nose cone, and maintained on a heated platform to ensure physiological stability. Continuous monitoring ensured that both heart rate and core body temperature remained within the defined inclusion thresholds of 550 ± 50 beats per minute and 37°C, respectively, prior to image acquisition.

A Vevo2100 high-frequency ultrasound system (VisualSonics) equipped with a 24-MHz linear-array transducer was used to perform the imaging. M-mode echocardiography was employed to capture high-temporal-resolution cardiac cycles, allowing for the detailed assessment of left ventricular (LV) function. From the M-mode tracings, key parameters such as:

- **Left ventricular ejection fraction (LVEF)**
- **Fractional shortening (FS)**
- **Left ventricular internal diameter (LVID)**
- **Anterior wall thickness (LVAW)**
- **Posterior wall thickness (**LVPW)

were quantitatively analyzed using Vevo LAB software (Version 3.2.0). Measurements were derived from an average of three consecutive cardiac cycles to ensure accuracy and reduce variability.

In addition to cardiac structure and function, arterial stiffness was evaluated by measuring pulse wave velocity (PWV) in the abdominal aorta. This was performed using an electrocardiogram-gated kilohertz visualization (EKV) technique, which enables high-frame-rate imaging of vascular wall motion. PWV was calculated based on the time delay in the pulse wave propagation between two predefined sites along the abdominal aorta, offering a localized and sensitive readout of **aortic elasticity and stiffness**.

This multimodal ultrasound protocol enabled comprehensive, real-time insights into both **cardiac performance** and **vascular mechanics**, supporting the interpretation of systemic hemodynamic changes associated impedimental interventions.

Echocardiographic Parameters and Formulas

Parameter	Abbreviation	Definition	Formula	Units
Left Ventricular Ejection Fraction	LVEF	Percentage of blood ejected from LV during systole	LVEF = ((LVEDV - LVESV) / LVEDV) × 100 (Teichholz method estimates	%

			volumes from LVID)	
Fractional Shortening	FS	Relative change in LVID during systole	FS = ((LVIDd - LVIDs) / LVIDd) × 100	%
Left Ventricular Internal Diameter	LVID	Internal cavity diameter of the LV (diastole/systole)	Measured directly via M-mode or B-mode imaging	mm
Anterior Wall Thickness	LVAW	Thickness of the anterior LV wall (diastole or systole)	Measured directly via M-mode imaging	mm
Posterior Wall Thickness	LVPW	Thickness of the posterior LV wall (diastole or systole)	Measured directly via M-mode imaging	mm

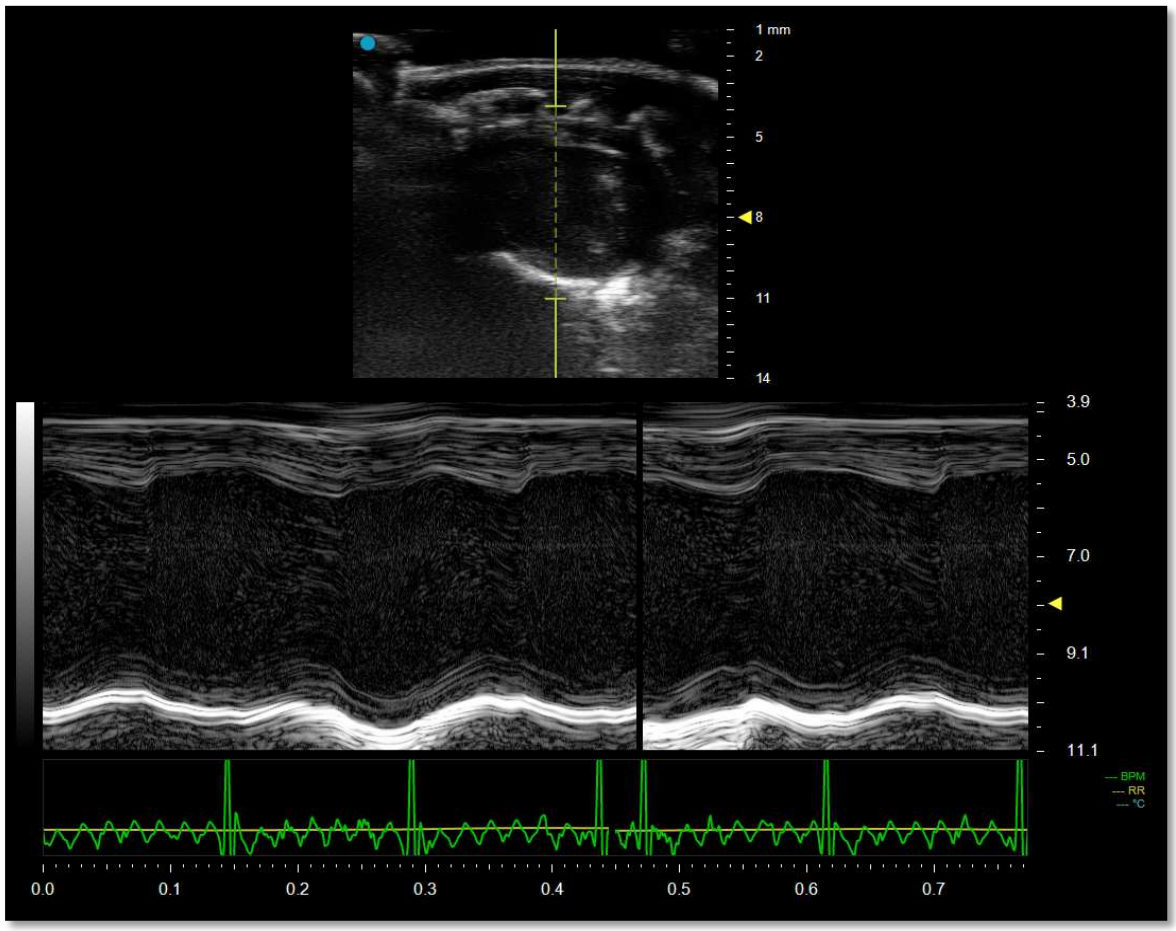

Figure 2.A : In the present figure on the upper part there is shown the echocardiographic image of the mouse heart, the bottom part shows the thickness of the wall on the short Axis. O% saturation and heart beat are monitored constantly

Measurement of Pulse Wave Velocity (PWV) in the Abdominal Aorta Using High-Frequency Ultrasound

Pulse wave velocity (PWV), a well-established surrogate marker of arterial stiffness, was measured in the abdominal aorta of all mice using high-frequency ultrasound imaging. The aim was to detect early vascular changes in response to proteasome inhibitor treatment. PWV was assessed in each animal at two time points: on Day 1, prior to the administration of any drug, to establish a baseline, and again on Day 3, after two consecutive injections of the assigned treatment. This allowed for the comparison of pre- and post-treatment vascular stiffness within each subject.

Two cohorts of mice were included in the study. The first cohort consisted of hypertensive mice in which mild hypertension was induced by administering L-NAME (Nω-Nitro-L-arginine methyl ester) in the drinking water. The second cohort comprised normotensive wild-type controls. Within each cohort, animals were randomly assigned to receive either bortezomib (BTZ), carfilzomib (CFZ), or vehicle (control treatment), following an identical treatment regimen.

Before each imaging session, mice were anesthetized with 1.5% to 2% isoflurane delivered in 100% oxygen using an induction chamber. Once adequate anesthesia was confirmed by the absence of reflexes, each animal was gently positioned in the supine position on a temperature-controlled platform designed for small animal imaging. The platform-maintained core body temperature between 36.5 °C and 38.5 °C. Anesthesia was maintained throughout the imaging procedure via a nose cone delivering 1% to 1.5% isoflurane. To ensure physiological stability and minimize motion artifacts, ECG electrodes embedded in the platform were connected to the forelimbs and hindlimbs using conductive gel, allowing for continuous monitoring of heart rate and respiratory function.

The abdominal fur was removed using electric clippers followed by a depilatory cream to ensure optimal acoustic contact. Pre-warmed ultrasound gel was then applied to the abdominal region. Imaging was performed using a Vevo2100 high-frequency ultrasound system (VisualSonics) equipped with a 24-MHz linear-array. The aorta was first located in B-mode using a transverse orientation, then the transducer was rotated to obtain a longitudinal view of the abdominal aorta, particularly focusing on the suprarenal segment between the renal arteries and the superior mesenteric artery.

To capture the rapid motion of the murine aorta with high temporal precision, imaging was performed in EKV (Electrocardiogram-gated kilohertz visualization) mode. This mode synchronizes data acquisition with both the cardiac and respiratory cycles, generating ultra-high-frame-rate cine loops with frame rates exceeding 3000 frames per second. Within the long-axis view of the abdominal aorta, a region of interest (ROI) approximately 4 mm in length was placed along the anterior aortic wall. The software automatically extracted wall displacement waveforms at two distinct sites along the ROI. The transit time of the pulse wave between these two points was calculated either automatically or with manual correction based on the displacement inflection points, and the PWV was derived using the formula:

PWV = Distance / Time delay

Where:

- **PWV** is the pulse wave velocity (measured in meters per second, m/s),
- **Distance** is the length between the two measurement points along the aortic wall (in meters),
- **Time delay** is the time taken by the pulse wave to travel between those two points (in seconds).

To ensure consistency, the same operator performed all imaging procedures, and each animal was scanned under the same environmental and anesthetic conditions at both time points. The resulting PWV values provided a direct quantitative measure of aortic stiffness, enabling comparison between treatment groups and time points.

Figure 2.B: this figure illustrates the correct placement of the ultrasound probe on the abdominal region of a mouse positioned in a supine orientation on a heating pad. The animal's paw pads are equipped with sensors for pulse oximetry and temperature monitoring. Prior to imaging, the abdominal area must be shaved to ensure optimal ultrasound wave transmission through the abdominal cavity. Continuous monitoring of the mouse's heart rate is essential, especially under anesthesia with 1.2% isoflurane, to maintain physiological stability during the procedure.

Blood Pressure Measurement

To evaluate hemodynamic status, **systolic, diastolic, and mean arterial blood pressure (BP)** were measured using a **non-invasive tail-cuff plethysmography system** (CODA, Kent Scientific Corporation, Torrington, USA), which allows accurate BP monitoring in **conscious, unanaesthetized mice**.

To minimize stress-induced variability and ensure reliable readings, all animals underwent a **habituation session** one day prior to the actual measurements. During this training, mice were gently restrained in plastic holders, and the **inflatable tail cuff and volume-pressure recording (VPR) sensor** were positioned on the tail exactly as they would be during the experimental procedure. This 30-minute session served to familiarize the animals with the setup and reduce stress responses that could confound BP readings.

During the experimental session, the same restraint and tail-cuff protocol was applied. **Multiple consecutive BP measurements** were taken over a 30-minute period to account for any motion artifacts and to derive accurate mean values. The system automatically recorded systolic BP, diastolic BP, and calculated mean arterial pressure (MAP) by analyzing the pulsatile blood flow through the tail.

These measurements were specifically performed in the **L-NAME-treated hypertensive cohort**, and were taken at two critical time points:

- **Baseline (prior to any treatment)**
- **Following the third intraperitoneal injection** of the assigned therapeutic or vehicle control, to assess treatment-related changes in systemic blood pressure.

This non-invasive methodology provided valuable insights into the vascular effects of L-NAME-induced hypertension and the hemodynamic impact of proteasome inhibitor treatment in a physiologically relevant, conscious animal model.

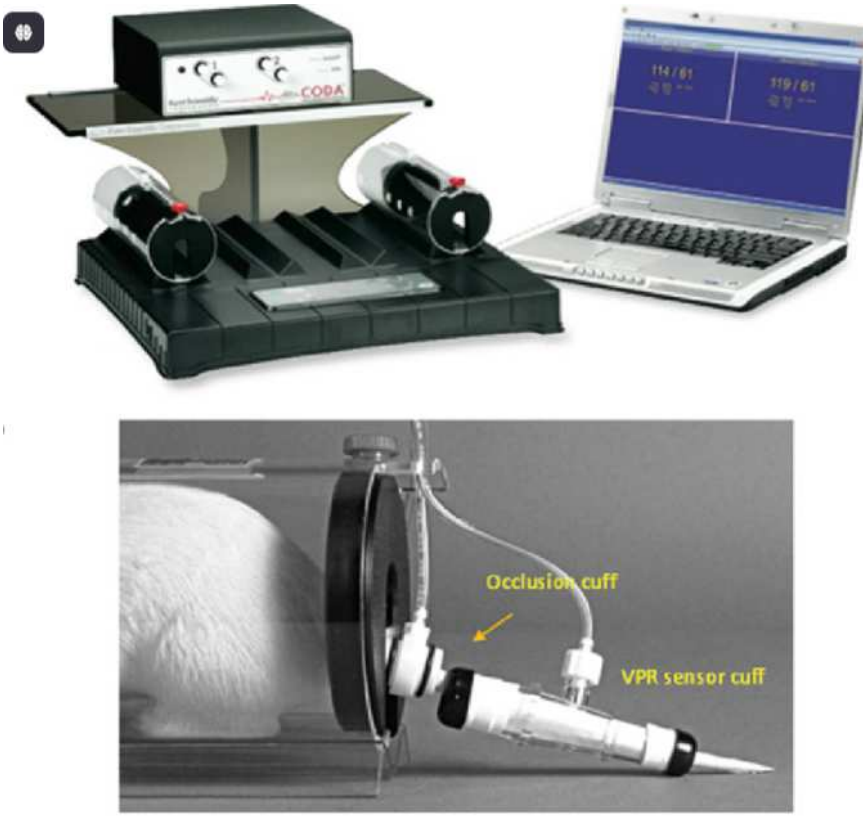

Figure 2.C:

- CODA 2-Channel High Throughput Noninvasive Blood Pressure System, as described in the CODA High-Throughput Manual by Kent Scientific Corporation.
- Proper positioning of the occlusion cuff and the Volume Pressure Recording (VPR) sensor cuff on the rat tail, as outlined in the same manual.

Ex Vivo Assessment of Aortic Stiffness Using ROTSAC (Rodent Oscillatory Tension Setup to Study Arterial Compliance)

To evaluate the biomechanical properties of the aortic wall, particularly arterial stiffness, thoracic aortic segments were subjected to functional testing using the Rodent Oscillatory Tension Setup to Study Arterial Compliance (ROTSAC) system, in accordance with the methodology described by Leloup et al. [60].

In this setup, freshly isolated 2 mm segments of the thoracic aorta were carefully mounted between two precision-aligned parallel stainless-steel hooks in a 10 mL organ bath system. The segments were completely submerged in physiologically buffered Krebs-Ringer (KR) solution, continuously oxygenated with a 95% O_2 and 5% CO_2 gas mixture to maintain pH at 7.4 and kept at a constant temperature of 37°C to mimic in vivo conditions. The composition of the KR solution (in mM) was as follows: NaCl 118, KCl 4.7, $CaCl_2$ 2.5, KH_2PO_4 1.2, $MgSO_4$ 1.2, $NaHCO_3$ 25, CaEDTA 0.025, and glucose 11.1.

A force-length transducer was integrated into the upper hook to precisely monitor changes in force and segment displacement in real time. To simulate the pulsatile nature of blood pressure, aortic rings were subjected to cyclic mechanical stretching. These oscillatory forces alternated

between two defined preload values corresponding to diastolic and systolic pressures, simulating a mouse heart rate of approximately 600 beats per minute (10 Hz frequency).

Transmural pressures exerted on the vessel wall were calculated using the Laplace relationship, which relates internal pressure, vessel radius, and wall tension. The cyclic expansion and recoil of the aorta allowed for the determination of arterial distensibility and elastic recoil capacity.

A key outcome measure derived from this assay was the Peterson's pressure-strain elastic modulus (Ep), a widely accepted indicator of arterial stiffness. Ep was computed using the following formula:

$Ep = D_0 \times (\Delta P / \Delta D)$

Where:

- Ep is the Peterson's elastic modulus
- D_0 is the diastolic diameter of the vessel
- ΔP is the pulse pressure (systolic pressure – diastolic pressure)
- ΔD is the change in diameter during the cardiac cycle (systolic diameter – diastolic diameter)

This procedure was conducted across a range of transmural pressures (from 60–100 mmHg up to 180–220 mmHg, in 20 mmHg increments), enabling the generation of a detailed pressure-stiffness relationship curve under normal physiological buffer conditions.

The ROTSAC platform provides a dynamic and physiologically relevant means of quantifying arterial compliance and stiffness, allowing researchers to dissect changes in vascular wall mechanics that occur in response to disease states, pharmacological interventions, or genetic modifications.

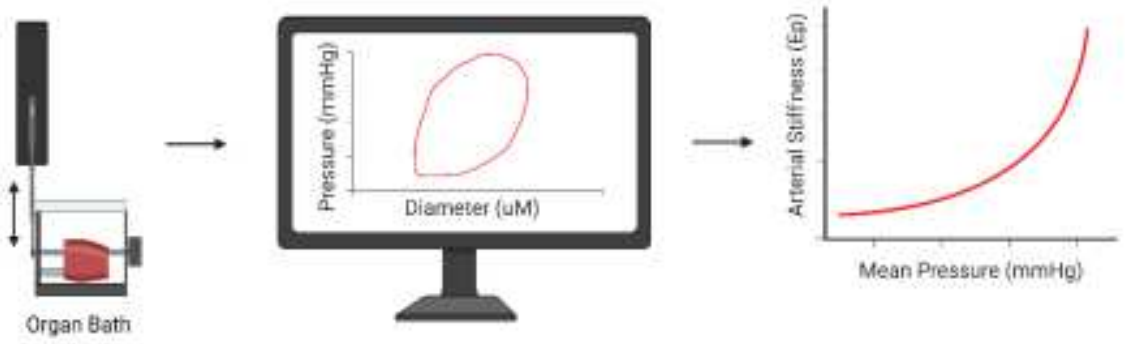

This figure was created by Callan Wesley into his Doctorate thesis "*Measuring Arterial Stiffness At Different Scales: A New Toolbox For Safety Pharmacology"* It does recall the experimental set up of ROTSAC

Evaluation of Vascular Reactivity

Segments of thoracic aorta (2 mm) were mounted under a fixed preload tension of 20 mN, approximating a mean arterial pressure of 100 mmHg. Vascular smooth muscle cell (VSMC) contractility was assessed using cumulative concentrations of phenylephrine (PE; 3 nM–3 μM), an α1-adrenergic agonist. Endothelium-dependent relaxation was then measured by applying increasing doses of acetylcholine (ACh; 3 nM–10 μM), which acts on muscarinic receptors. To block endogenous nitric oxide (NO) activity, L-NAME (300 μM), a non-selective NO synthase inhibitor, was used. The sensitivity of VSMCs to NO, independent of endothelial influence, was determined using the exogenous NO donor 2-(N,N-diethylamino)-diazenolate-2-oxide sodium salt hydrate (DEANO; 0.03 nM–10 μM). Furthermore, a 50 mM potassium solution was added to provoke depolarization-induced contraction that is independent of NO signaling.

3.5 In Vitro Studies

General consideration of Cultured cells in this study

Murine Vascular Smooth Muscle Cells (mVSMC) are isolated from 6-week-old female mice. They remain stable up to passage 10, after which they begin to switch phenotype and enter a hypo proliferative state, requiring less frequent splitting. As they age, these cells become longer shaped and stop growing. The culture medium used is DMEM/F-12 (Gibco) containing phenol red, supplemented with 10% FBS and 1% penicillin/streptomycin mix.

Human Aortic Smooth Muscle Cells (HAoSMC) have a longer shape compared to the murine version. After passage 8, their growth slows down and the phenotype becomes more prolonged. They require a specific medium without phenol red, supplemented with 10% FBS and 1% penicillin/streptomycin mix.

Murine Endothelial Cells (mEC) are fragile and age rapidly, making them unsuitable for use beyond passage 4. They require a specific endothelial cell growth medium that contains phenol red and is supplemented with 10% FBS and 1% penicillin/streptomycin. These cells are difficult to culture due to their fast phenotype switching.

Human Aortic Endothelial Cells (HAoEC) are larger than their murine counterparts and are also fragile in culture. They require a medium containing phenol red, supplemented with 10% FBS and 1% penicillin/streptomycin. They tend to be inactive in specific assays such as the Neutral Red Uptake assay.

Mesenchymal Progenitor Cardiac Endothelial Cells (MPCEC) need to be highly adherent to culture flasks, so it is recommended to coat flasks with a 0.1% gelatin solution to promote attachment. These cells require a higher concentration of fetal bovine serum compared to other cell types to support their growth.

Cell Type	Passage Limit	Morphology/Growth Notes	Medium Composition	Special Notes
mVSMC	≤ 10 stable	Phenotype switch, hypoproliferative	DMEM/F-12 + Phenol red + 10% FBS	More frequent splitting post-P5
HAoSMC	≤ 8	Slows growth, longer shape post-P8	Phenol red-free + 10% FBS	Monitor phenotype/proliferation
mEC	≤ 4	Fragile, fast phenotype switch	Endothelial medium + Phenol red + 10% FBS	Hard to culture, sensitive cells
HAoEC	Not specified	Larger size, fragile	Medium + Phenol red + 10% FBS	Inactive in Neutral Red assay
MPCEC	Not specified	Highly adherent	Medium + higher % FBS + gelatin coating	Use gelatin 0.1% coated flasks

General Cell Culturing and Splitting

Cells were subcultured when they reached approximately 85% confluence. The culture medium was replaced every three days with the respective medium optimized for each cell type.

Cell Washing and Detachment: Prior to passaging, culture medium was aspirated, and cells were gently washed with 2 ml of phosphate-buffered saline (PBS, Gibco), pre-warmed to 37°C. PBS was then removed, and 1 ml of 0.25% trypsin-EDTA (Gibco) was added to detach the cells. The flask was incubated at 37°C for 1 minute to activate enzymatic dissociation. After incubation, the flask was gently tapped to facilitate detachment of the cells.

Trypsin Neutralization and Collection: Trypsin activity was quenched by adding culture medium at a volume three times that of the trypsin used (3 ml medium per 1 ml trypsin). The medium formulations used were as follows:

- **mVSMC:** DMEM/F-12 (Gibco) with phenol red, supplemented with 10% fetal bovine serum (FBS) and 1% penicillin/streptomycin.
- **HAoSMC:** Phenol red-free medium supplemented with 10% FBS and 1% penicillin/streptomycin.
- **mEC:** Endothelial cell growth medium containing phenol red, supplemented with 10% FBS and 1% penicillin/streptomycin.
- **HAoEC:** Medium with phenol red, supplemented with 10% FBS and 1% penicillin/streptomycin.
- **MPCEC:** Medium supplemented with a higher percentage of FBS than other cell types, cultured on flasks coated with 0.1% gelatin solution to promote adherence.

The cell suspensions were transferred to 15 ml centrifuge tubes and centrifuged at **300 × g for 5 minutes** (parameters optimized for maintaining cell viability across all cell types). After

centrifugation, the supernatant was carefully aspirated, and the cell pellet was resuspended in 1 ml of fresh culture medium by gentle pipetting.

Cell Counting and Viability: An aliquot of the cell suspension was mixed 1:1 with 0.4% trypan blue solution and loaded onto an automated cell counter (e.g., Countess II FL, Thermo Fisher Scientific) for quantification of viable cells.

Cell suspensions were then diluted to the desired concentration using fresh culture medium and plated according to the requirements of subsequent experiments.

3.6 Murine Vascular Smooth Muscle Cell Isolation

The isolation protocol was applied to wild-type mice aged 6 weeks as well as GFP/RFP-LC3 transgenic mice for the collection of aortic vascular smooth muscle cells (mVSMCs). It's highly important to choose a mouse that is less than 10 weeks old.

Two culture media formulations were used during the isolation process. The first medium consisted of DMEM/F-12 supplemented with 20% fetal bovine serum (FBS), 1% penicillin/streptomycin, and 1 ml polymyxin B. The second medium was identical but contained 10% FBS instead of 20%. Additionally, a serum-free DMEM/F-12 medium without FBS, supplemented with 125 µl polymyxin B and 1% penicillin/streptomycin, was prepared for enzyme neutralization steps.

Two 6-well plates were prepared for the isolation procedure. The first plate contained Hank's Balanced Salt Solution (HBSS) in two wells, the enzymatic digestion solution in two wells, and serum-free DMEM/F-12 in the remaining two wells. The enzymatic digestion solution comprised elastase, 1% penicillin/streptomycin, 1 mg/ml collagenase, and 1 mg/ml soybean trypsin inhibitor. The inclusion of soybean trypsin inhibitor allowed for the inactivation of trypsin in serum-free conditions, which is typically achieved using FBS-containing media. The second 6-well plate contained the enzyme solution in two wells for subsequent incubation steps.

The aorta was harvested from the mouse following cardiac perfusion with HBSS to flush the vasculature and ensure clearance of blood from the aortic lumen. Surrounding adipose tissue was carefully removed. The thoracic aorta was excised by cutting at the ascending aorta proximally and at the infrarenal abdominal aorta distally. The isolated aortic tissue was placed in cold HBSS on ice for a few minutes.

Subsequently, the aorta was rinsed with sterile HBSS and transferred to the enzyme solution for incubation at 37°C for several minutes to initiate tissue digestion. After enzymatic treatment, the aorta was washed in culture medium to remove residual enzyme. Under a dissecting microscope in a non-sterile environment, the adventitia was gently stripped using fine forceps. The aorta was then opened longitudinally and cut into approximately six smaller segments.

These small aortic segments were transferred to fresh enzyme solution under sterile conditions and incubated until the tissue was fully digested and a cell suspension was obtained. The cell suspension was centrifuged, and the pellet was resuspended in 20% FBS-containing medium.

Remaining tissue fragments were plated in a 48-well plate and incubated for one week to allow cell outgrowth. Once confluent, cells were passaged and expanded in medium containing 10% FBS and transferred to larger culture flasks for continued growth.

3.7 Neutral Red Uptake Assay for the Estimation of Cell Viability and Toxicity

The Neutral Red Uptake (NRU) assay was used to assess cell viability and cytotoxicity by quantifying the ability of viable cells to incorporate and retain the supravital dye Neutral Red (NR). This assay relies on the active uptake and accumulation of the weakly cationic dye into the lysosomes of viable cells. Neutral Red penetrates the cell membrane via passive diffusion and accumulates within lysosomes by binding electrostatically and hydrophobically to anionic and phosphate groups in the lysosomal matrix. Following incubation, the retained dye is extracted using an acidified ethanol solution, and the absorbance is measured spectrophotometrically as an indirect measure of viable cell count.

The assay was performed on **murine vascular smooth muscle cells (mVSMC)**, **human aortic smooth muscle cells (HAoSMC)**, and **murine progenitor cardiac endothelial cells (mPCEC)** after 24-hour treatment with progressive concentrations of the proteasome inhibitors **carfilzomib** (3 nM, 30 nM, 300 nM, 3 μM, 30 μM) and **bortezomib** (3 nM, 30 nM, 300 nM, 3 μM, 10 μM). Each treatment condition was performed in **technical triplicates** for each cell type.

The assay was initially tested on **human endothelial cells**, but these cells failed to take up the Neutral Red dye effectively, rendering them incompatible with this assay under the current protocol.

Seeding Conditions:

- **mVSMC** (passages 3, 4, 5): 6×10^4 cells per well in a 24-well plate
- **HAoSMC** (passages 4, 5, 6): 7×10^4 cells per well in a 24-well plate
- **mPCEC** (passages 2, 3, 4): 6×10^4 cells per well in a 24-well plate

After 24 hours of drug treatment, the culture medium was aspirated and replaced with medium containing **Neutral Red dye (final concentration: 40 µg/ml)**. Cells were incubated with the dye for **3 hours at 37°C** in a humidified atmosphere containing 5% CO_2.

Following incubation, the dye-containing medium was removed, and cells were gently rinsed with **PBS (pre-warmed to 37°C)** to eliminate unincorporated dye. The retained dye was extracted by adding **acidified ethanol solution** (composed of 50% ethanol, 49% distilled water, and 1% glacial acetic acid). The plates were agitated gently at room temperature for 10–15 minutes to ensure complete solubilization of the dye.

Absorbance was measured at **540 nm** using a microplate spectrophotometer. The optical density (OD) values were normalized against untreated controls, and results were expressed as a percentage of viable cells relative to control conditions.

3.8 F-actin and DAPI staining for cytoskeletal imaging

F-actin cytoskeletal organization and nuclear morphology were assessed using phalloidin and DAPI staining in HAoVSMCs and mVSMCs following 24- and 48-hour treatments with Carfilzomib and Bortezomib. Cells were seeded in black-wall, clear-bottom 96-well plates at a density of 5×10^4 cells per well and incubated overnight to allow proper adhesion. After attachment, cells were treated with carfilzomib at concentrations of 3 nM and 3 μM, and bortezomib at 30 nM and 300 nM. Doxorubicin at 1 μM was used as a cytotoxic positive control, and untreated cells served as negative controls.

At the end of the treatment period, the medium was carefully removed, and the cells were fixed with 4% paraformaldehyde in PBS for 15 minutes at room temperature. After fixation, cells were gently washed with PBS and permeabilized with 0.1% Triton X-100 in PBS for 10 minutes. Blocking was performed using 10% normal goat serum in PBS with 0.1% Tween-20 for 1 hour at room temperature in order to minimize non-specific binding. Staining was carried out by incubating the cells for 1 hour at room temperature in the dark with a solution containing Alexa Fluor 488-conjugated phalloidin (1:250) and DAPI (1 μg/mL), both diluted in PBS supplemented with 2% normal goat serum and 0.1% Tween-20. Phalloidin is a bicyclic peptide that binds selectively and with high affinity to filamentous actin (F-actin), stabilizing the filaments and preventing their depolymerization. Due to this strong and specific interaction, fluorescently labeled phalloidin is widely used to visualize the actin cytoskeleton in fixed cells. DAPI (4′,6-diamidino-2-phenylindole) is a fluorescent stain that binds strongly to A-T rich regions in DNA, making it an effective nuclear counterstain that allows visualization of cell nuclei under ultraviolet illumination.

Following staining, cells were washed three times with PBS containing 0.1% Tween-20 and maintained in PBS before imaging. Fluorescent images were captured using the Celena S Digital Imaging System (Logos Biosystems), with all imaging parameters maintained constant across all samples to ensure comparability. For each experimental condition, two images per well were acquired at random fields using the fluorescence objective. The resulting images were then overlayed to qualitatively assess differences in cytoskeletal structure and nuclear morphology between treatment groups.

3.9 Assessment of Autophagic Flux in mVSMCs Using GFP-RFP-LC3 Transgenic Mouse Model Under Proteasome Inhibition

To investigate autophagic flux in response to proteasome inhibition, **mVSMCs were isolated from a transgenic GFP-RFP-LC3 mouse**, which expresses a tandem fluorescent LC3 reporter construct that enables real-time visualization and quantification of autophagy via fluorescence microscopy. This model is based on a transgene in which **LC3 is fused to both green fluorescent protein (GFP) and red fluorescent protein (RFP)**, allowing distinction between early autophagosomes (yellow, due to GFP+RFP colocalization) and mature autolysosomes (red-only, due to GFP quenching in acidic lysosomal environments). Both fluorophores are expressed in a 1:1 stoichiometry from a single construct, enabling accurate assessment of autophagic flux.

The **GFP-RFP-LC3 transgenic mouse line** is generated by introducing the tandem fluorescent LC3 fusion gene into the mouse genome via pronuclear injection. Expression of the transgene is driven by a ubiquitous promoter to ensure widespread expression across tissues, including vascular smooth muscle. Mice carrying the transgene are identified and validated through **genetic testing by PCR-based genotyping**, using primers specific for the RFP and LC3 sequences. Homozygous and heterozygous mice are viable, fertile, and phenotypically normal, with widespread expression of the reporter in most organs, except the brain where it is present at lower levels.

Following confirmation of the transgene, mVSMCs were isolated from a single GFP-RFP-LC3 mouse and cultured in vitro. The cells were then treated for 24 hours with the proteasome inhibitors **carfilzomib** (3 nM and 3 μM) and **bortezomib** (30 nM and 300 nM), alongside untreated vehicle-only controls. To establish reference points for autophagic induction and inhibition, additional wells were treated with **Torin1** (autophagy inducer) and **Bafilomycin A1** (autophagy inhibitor) as positive and negative controls, respectively. Fluorescence microscopy was used to monitor autophagic activity, with yellow puncta indicating accumulation of autophagosomes and red-only puncta representing successful flux to autolysosomes.This study provides a **preliminary assessment of autophagy dynamics** in mVSMCs under proteasome inhibition. Data are derived from **two biological replicates (two 96-well plates)**, using mVSMCs isolated from **a single transgenic mouse**. While the initial observations are informative, additional biological replicates will be required to confirm reproducibility and assess variability across animals.

Data interpretation of Autophagic Flux

To assess autophagic flux in response to proteasome inhibition, we employed fluorescence microscopy in primary mVSMCs isolated from a GFP-RFP-LC3 transgenic mouse. This reporter system enables visualization of autophagosomes and autolysosomes based on the pH sensitivity of GFP. Autophagosomes are identified by yellow puncta, resulting from the co-localization of GFP and RFP signals, while red-only puncta represent autolysosomes, where the acidic environment quenches GFP fluorescence but preserves RFP. Quantification of the relative abundance and distribution of yellow and red puncta across treatment groups provides a readout of autophagic activity and flux.

To calibrate the system and interpret the effects of proteasome inhibitors, we included pharmacological controls that modulate distinct stages of the autophagy pathway. Torin1, an mTORC1 inhibitor, was used to induce autophagy by activating the ULK1 complex and initiating

autophagosome formation. An increase in both yellow and red puncta under Torin1 treatment indicates successful autophagy induction and flux through the lysosomal degradation pathway. Conversely, Bafilomycin A1, a known inhibitor of the vacuolar H^+-ATPase, blocks lysosomal acidification and autophagosome-lysosome fusion, resulting in an accumulation of undegraded autophagosomes. In this case, an increase in yellow puncta with a reduction in red-only signal reflects impaired autophagic flux.

Treatment with the proteasome inhibitors bortezomib and carfilzomib, at both low and high concentrations, was used to investigate how proteasomal stress influences autophagy. Data interpretation will focus on changes in the ratio of yellow to red puncta to distinguish between **enhanced autophagic induction with maintained flux (increased yellow and red puncta)** versus **impaired flux due to lysosomal dysfunction (accumulation of yellow puncta with fewer red**). All quantifications are performed on fixed cells using automated image analysis software to ensure consistency. These measurements enable an integrated assessment of how proteasome inhibition impacts the dynamics of autophagy in mVSMCs.

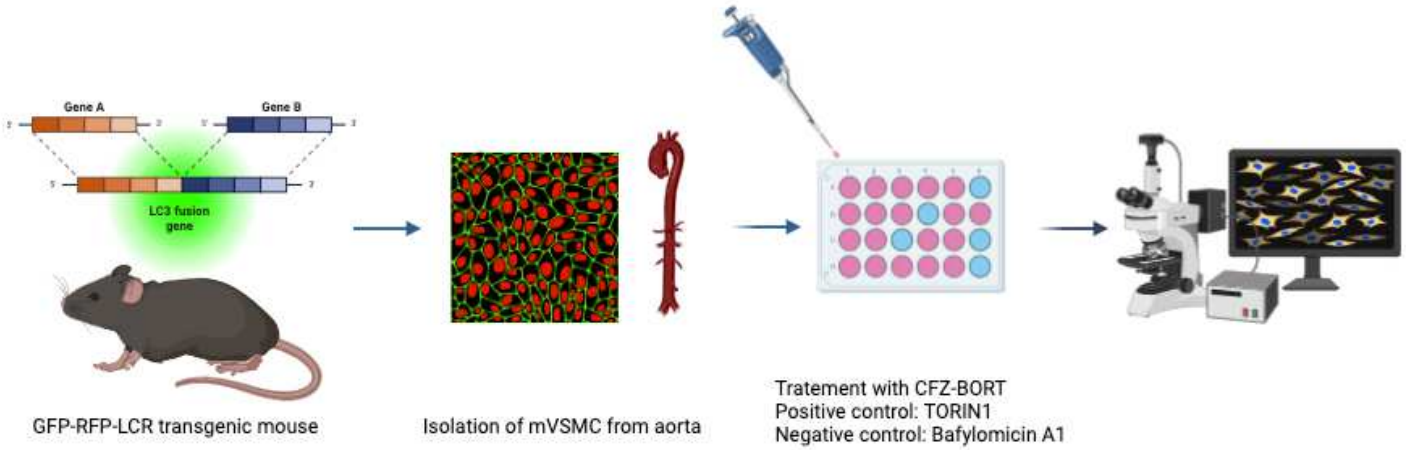

Chapter 4

RESULTS

4.1 Ex vivo Tissue culturing

Bortezomib Vascular reactivity Assessment

Thoracic aortic segments (2 mm in length, T0–T5), harvested from 6 male mice (n = 4 per group), were randomly selected and incubated for 24 hours at 37 °C with Bortezomib at concentrations of 1 nM, 10 nM, or 30 nM. Following incubation, vascular reactivity was assessed under different experimental conditions to evaluate the contractile integrity of medial vascular smooth muscle cells (mVSMCs).

The segments were fully submerged in Krebs-Ringer solution and maintained under CO_2 to mantian Physyological PH conditions. Each was mounted on a force transducer to measure contractile responses to increasing concentrations of the α1-adrenergic receptor agonist Phenylephrine (PE; 3 nM–3 μM). In segments treated with 1 nM and 3 nM Bortezomib, contractile responses to PE were not significantly different from controls. However, beginning at a PE concentration of 10^{-9} M, segments exposed to 10 nM and 30 nM Bortezomib exhibited a statistically significant ($p < 0.0001$) hypocontractile phenotype. The effect was dose-dependent, suggesting that Bortezomib impairs vascular contractility, potentially through dysregulation of adrenergic signaling or direct cytotoxicity to mVSMCs.

To determine whether this hypocontractility was mediated by nitric oxide (NO), additional experiments were performed in the presence of the endothelial nitric oxide synthase (eNOS) inhibitor L-NAME (300 μM). Even when NO production was inhibited, segments previously incubated with 10 nM and 30 nM Bortezomib continued to exhibit significant hypocontractility, with a more pronounced effect at 10 nM than at 30 nM.

To further explore the contribution of endogenous NO, we estimated basal NO levels by comparing contraction under PE stimulation alone to contraction under co-treatment with PE and L-NAME. While there was a tendency for increased NO production in the 30 nM group, the difference was not statistically significant, likely due to intrinsic variability in NO production across different aortic regions and among individual mice. These observations suggest that Bortezomib at higher doses induces a hypocontractile phenotype that is independent of NO signaling and more likely related to direct impairment of mVSMC function.Statistical analysis for the first two figures (from the left) was performed using two-way ANOVA with Sidak post hoc test. The third figure (rightmost) was analyzed using one-way ANOVA with Sidak post hoc test.

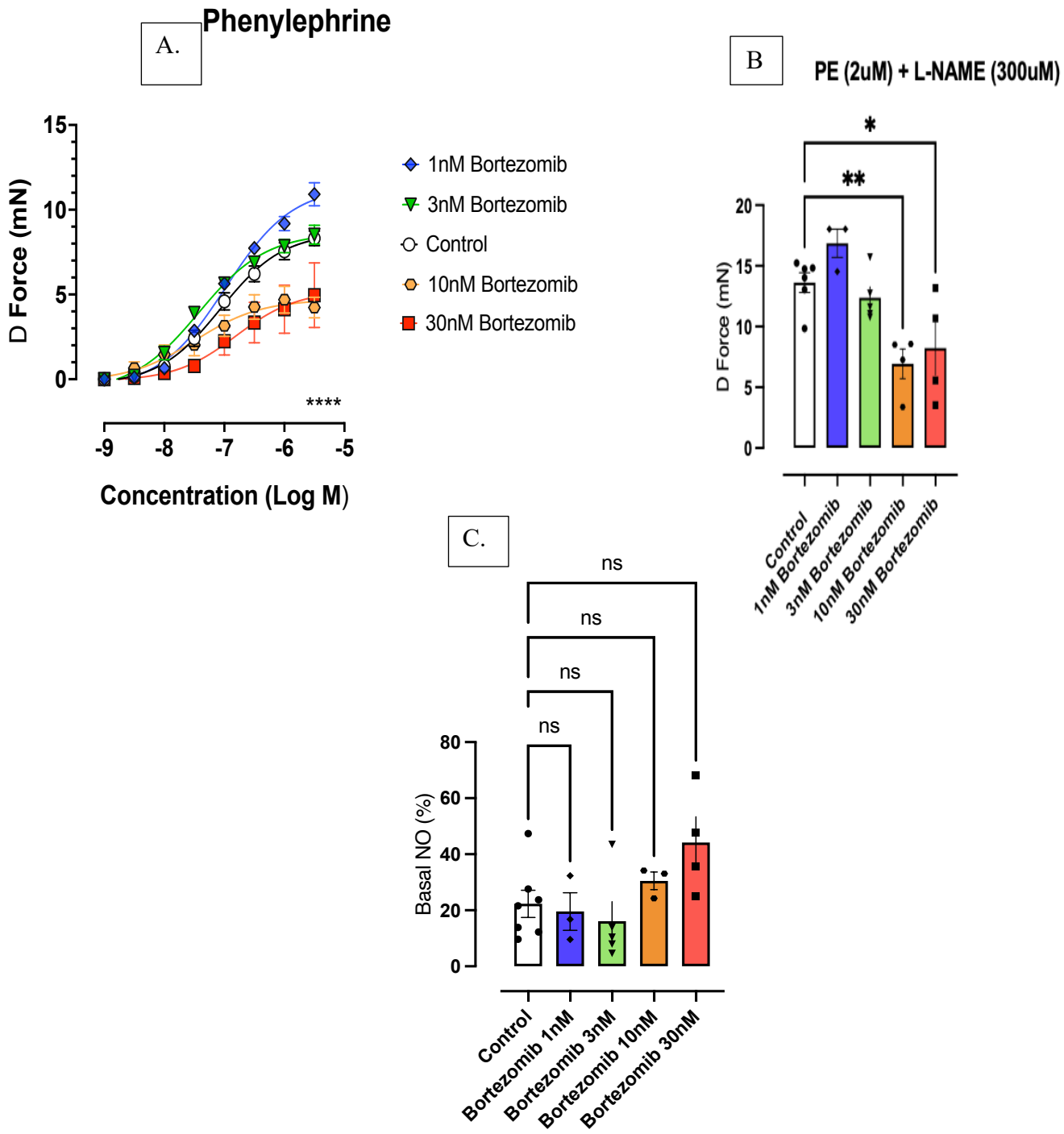

Figure 3.1: This is the contraction Panel of Ex Vivo Assessment of incubated with Bortezomib (1-3-10-30 nM) Thoracic aorta segments. Starting from the **A** the Phenylephrine dose response, **B.** Phenylephrine+ 300µM L-name (e-NOSinhibitor) **C**. the % of NO released by each segment

The relaxation profile of aortic segments incubated with Bortezomib was evaluated under the same experimental conditions using Acetylcholine (ACh; 3 nM–3 µM), a muscarinic receptor agonist that activates endothelial nitric oxide synthase (eNOS), promoting smooth muscle relaxation through cyclic GMP signaling. Additionally, responsiveness to nitric oxide was directly assessed using DEANO, an exogenous nitric oxide donor, was administered to assess VSMC sensitivity to NO independent of endothelial function
,. As shown in the figure, no significant differences in relaxation responses were observed, indicating that Bortezomib does not impair endothelial function under these conditions.

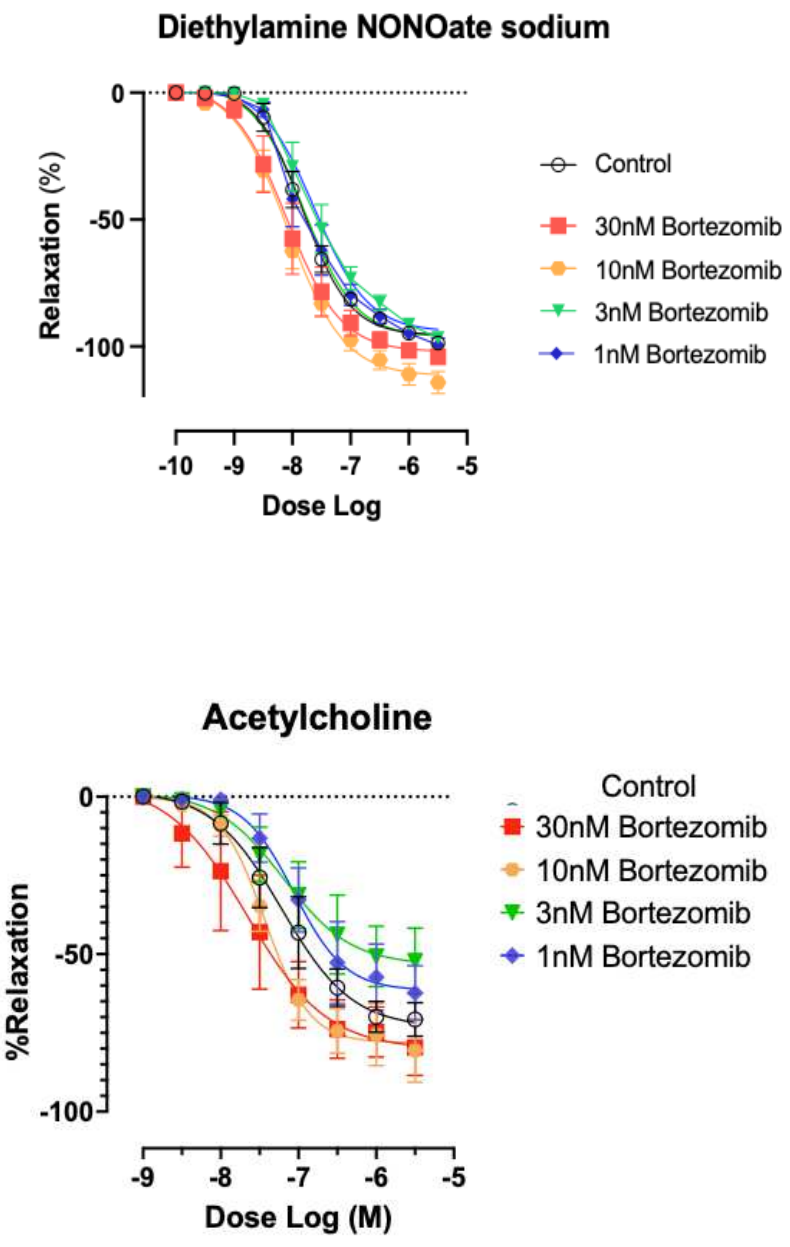

Figure 1.2 Relaxation response of thoracic aortic segments incubated for 24 hours with Bortezomib. Segments were subjected to a dose–response curve with Acetylcholine (Left), followed by stimulation with DEANO (NO donor).

Carfilzomib Vascular Assessment

The same protocol described previously was applied to Carfilzomib. Aortic segments were incubated for 24 hours with Carfilzomib at concentrations of 1, 3, 10, and 30 nM, and both contraction and relaxation responses were assessed. Unlike Bortezomib, Carfilzomib did not induce a hypocontractile phenotype, and no evidence of endothelial dysfunction was observed.

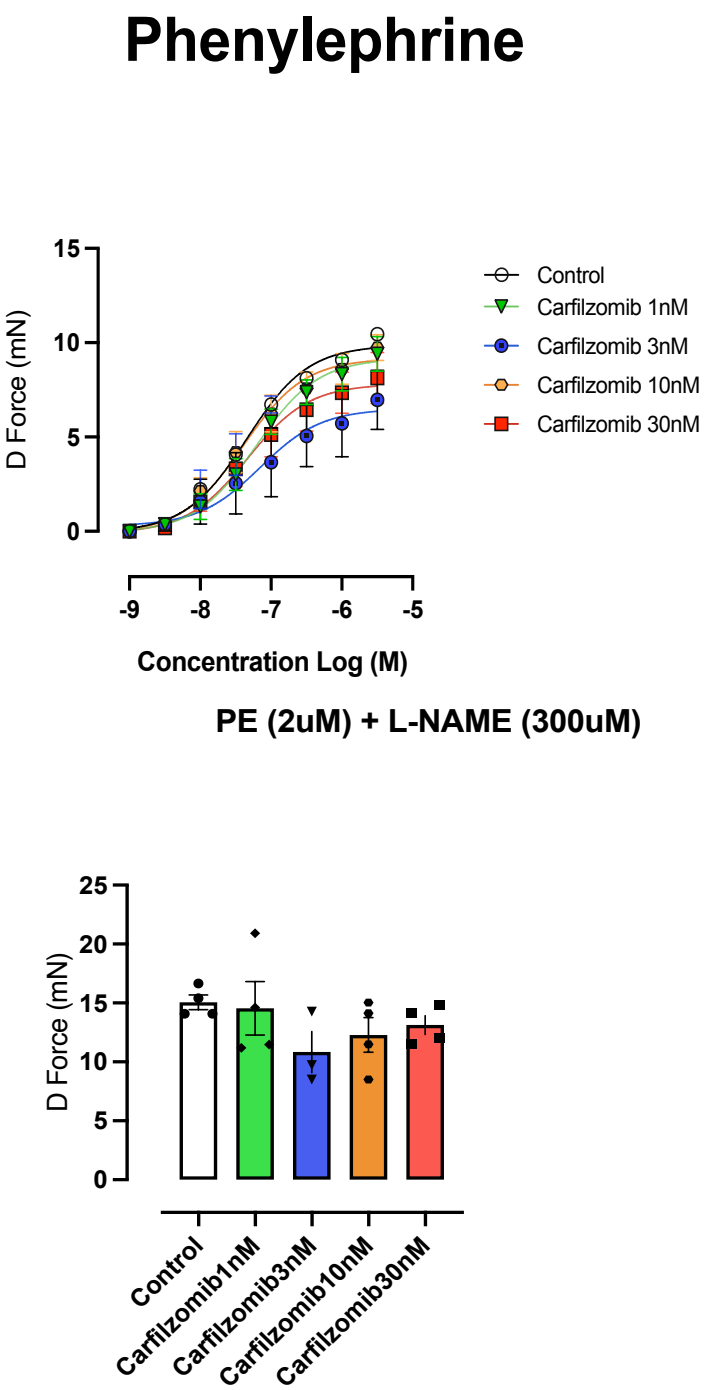

Figure 3 Under PE stimulation or under e-Nos inhibition there is no statistical difference in the behavior of Thoracic aorta under Increasing Carfilzomib concentration

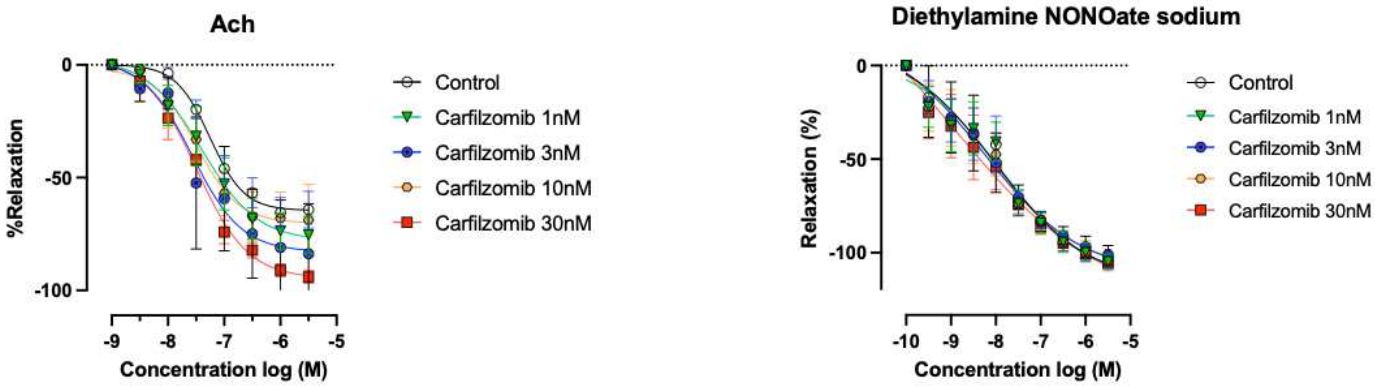

Figure 2 This figure shoes the relaxation panel under Acetocholyne and No donor DEANO to assess endothelial functionality. There are no evident differences between Carfilzomib treated group and Control segments

4.2 Short protocol in Vivo

Vascular reactivity Assessment

Following a short dosing protocol consisting of two injections over 48 hours, we assessed vascular reactivity in Carfilzomib- and Bortezomib-treated mice using the same pharmacological modulation protocol applied in the ex vivo experiments. Additionally, 50 mM KCl was used to induce contraction through an alternative, endothelium-independent pathway driven by membrane depolarization.

Figure 3 Thoracic aortic segments from mice (n = 5 per group) treated with Carfilzomib or Bortezomib were analyzed for vascular reactivity. Contraction was assessed in response to 50 mM KCl **C** (membrane depolarization), a dose–response curve to Phenylephrine (α_1-adrenergic stimulation) **A**, and NO-independent contraction following eNOS inhibition with L-NAME in combination with Phenylephrine **B**

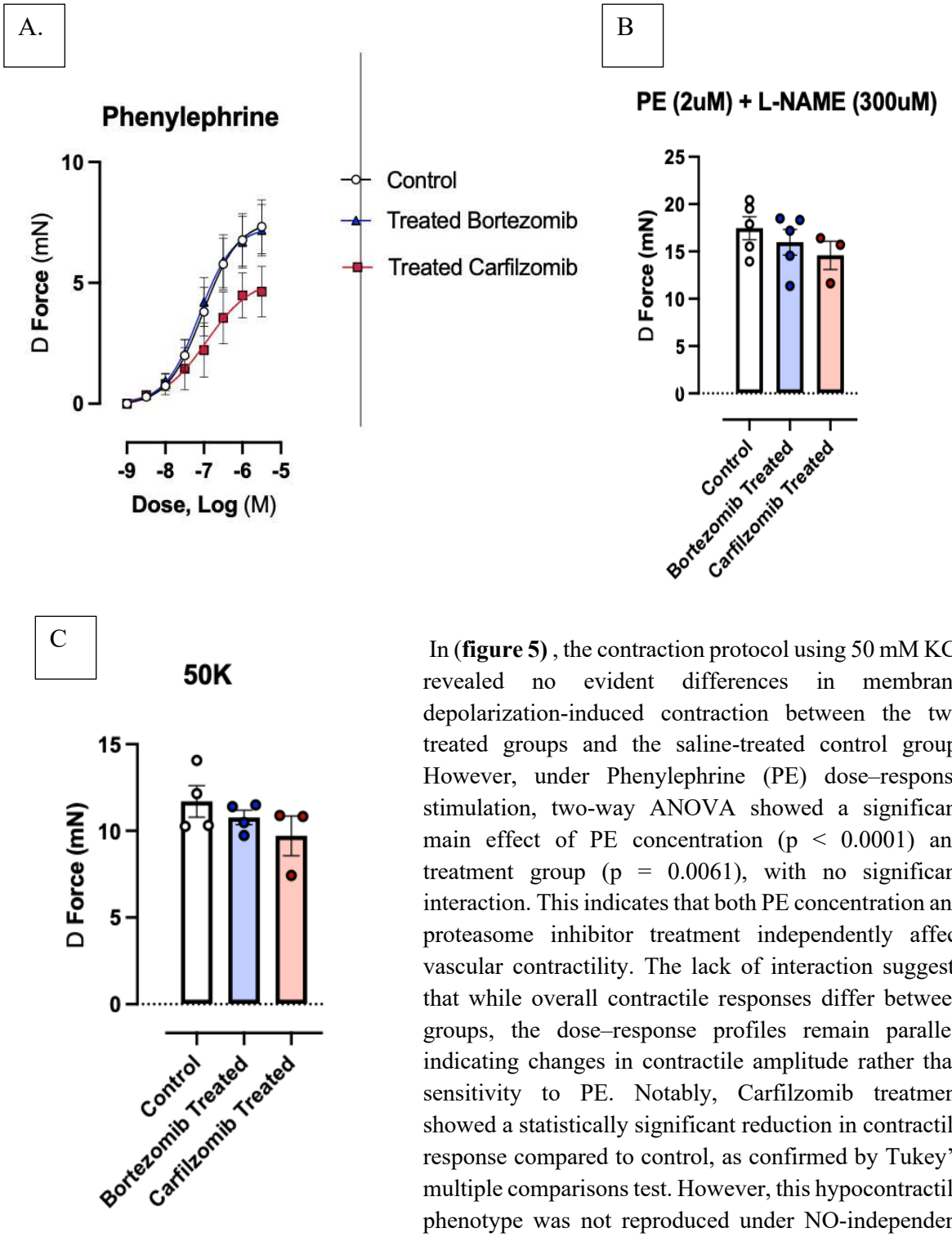

In (**figure 5)** , the contraction protocol using 50 mM KCl revealed no evident differences in membrane depolarization-induced contraction between the two treated groups and the saline-treated control group. However, under Phenylephrine (PE) dose–response stimulation, two-way ANOVA showed a significant main effect of PE concentration ($p < 0.0001$) and treatment group ($p = 0.0061$), with no significant interaction. This indicates that both PE concentration and proteasome inhibitor treatment independently affect vascular contractility. The lack of interaction suggests that while overall contractile responses differ between groups, the dose–response profiles remain parallel, indicating changes in contractile amplitude rather than sensitivity to PE. Notably, Carfilzomib treatment showed a statistically significant reduction in contractile response compared to control, as confirmed by Tukey's multiple comparisons test. However, this hypocontractile phenotype was not reproduced under NO-independent conditions during eNOS inhibition, suggesting that the effect is not sustained in the absence of endothelial-derived nitric oxide.

The relaxation profile was also evaluated under the same conditions. No statistically significant differences were observed between the Carfilzomib and Bortezomib groups in response to Acetylcholine (Ach), which assesses endothelial function. Although there was a slight trend toward higher contractility in the Carfilzomib group, this was not significant and is likely attributable to biological variability. Similarly, no differences were detected among the groups following stimulation with the exogenous NO donor DEANO. **(figure 7)**

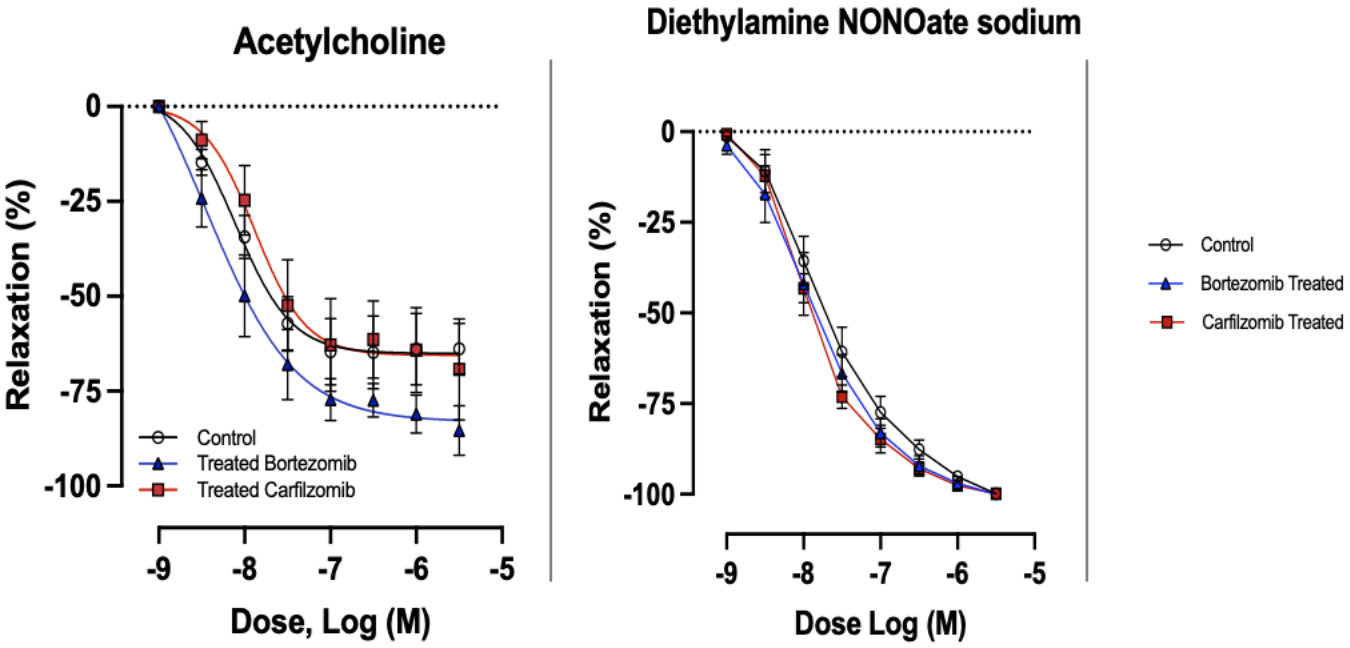

Figure 6 Relaxation Panel of Bortezomib, carfilzomib and Control, showing no difference on overall relaxation and NO sensitivity

Arterial stiffness in vivo short term protocol

Using the Rodent Oscillatory setup, we assessed ex vivo arterial stiffness in thoracic aortic segments from mice treated for two days with Carfilzomib, Bortezomib, or saline (n = 4 per group). Stiffness was measured under physiological conditions and following stimulation with an exogenous NO donor (DEANO) to evaluate the contribution of NO-mediated relaxation to arterial wall compliance.

The figure below **(Figure 8) compares** Peterson modulus (EP) values and shows that within the physiological pressure range (80–120 mmHg), there were no significant differences in arterial stiffness among treatment groups, under both Krebs and DEANO conditions. However, at higher pressures, Bortezomib-treated vessels exhibited a significant increase in stiffness compared to control and Carfilzomib-treated groups.

Two-way ANOVA revealed a significant main effect of pressure ($p < 0.0001$) and treatment ($p = 0.0456$), along with a significant pressure × treatment interaction ($p < 0.0001$). This interaction suggests that the pressure–stiffness relationship is altered by treatment. Specifically, Bortezomib induces a disproportionate increase in stiffness at elevated pressures.

Importantly, this pattern was consistent under both baseline and DEANO-treated conditions, indicating that the increased stiffness is unlikely due to changes in vascular tone or smooth muscle contractility. Instead, these findings point toward a passive structural alteration of the vascular wall—likely involving extracellular matrix remodeling—as a key contributor to the observed mechanical behavior in Bortezomib-treated vessels.

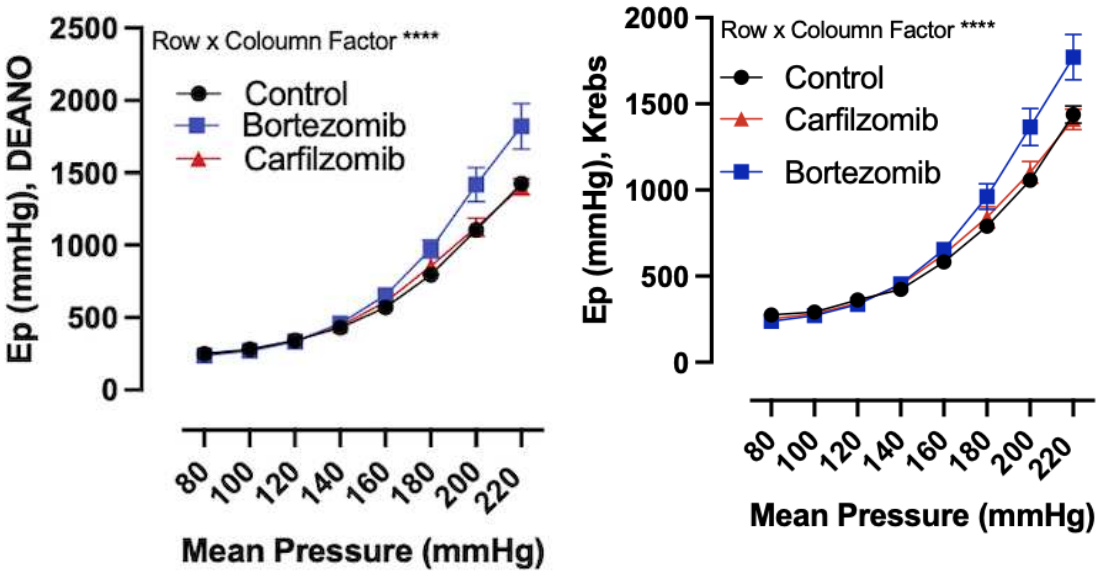

Figure 4 Comparison between Ep modulus (parameter of arterial stiffness) under Bortezomib, Carfilzomib and vehicle treatment in two conditions: Krebs (Physiological-right) and DEANO NO donor (left). This represent vascular compliance under exogen NO increase

4.3 In Vivo Results: Cardiovascular Effects of Proteasome Inhibition in Normotensive and Hypertensive Mice

Cardiac parameters in vivo

Echocardiographic assessments revealed that systemic proteasome inhibition induced subtle yet functionally relevant changes in cardiac performance, particularly under hypertensive conditions. Fractional shortening (FS), a surrogate marker of left ventricular (LV) systolic function, was significantly attenuated in hypertensive mice treated with carfilzomib ($p<0.05$), suggesting an early impairment in myocardial contractility.

Although bortezomib-treated hypertensive mice did not reach statistical significance, a downward trend in FS was observed, indicating a potential for mild systolic dysfunction. This pattern was mirrored in measurements of left ventricular ejection fraction (LVEF), which showed a non-significant trend toward reduction in hypertensive mice following treatment with both carfilzomib and bortezomib ($p=0.06$ for both), suggesting a vulnerability of the hypertensive myocardium to proteasome inhibitor-induced functional stress. Conversely, LVEF remained stable in control mice following treatment with either agent, reinforcing the notion that proteasome inhibitor-induced systolic dysfunction is potentiated under conditions of pre-existing cardiovascular stress hypertension. Further analysis of echocardiographic parameters revealed no significant changes in cardiac structural metrics—such as LV anterior and posterior wall thickness (both in systole and diastole), chamber diameters (LVID;d and LVID;s), or calculated LV mass—across treatment groups in either control or hypertensive mice. These findings imply that the observed reductions in FS and trends in LVEF were not secondary to gross morphological remodeling, but instead indicative of functional alterations in myocardial performance. (table 5.1)

Table 5.1. Echocardiographic parameters of control and hypertensive male (C57BL6/J) mice treated with saline, carfilzomib or bortezomib.

Group	Control			Hypertensive		
Treatment	**Saline**	**Carfilzomib**	**Bortezomib**	**Saline**	**Carfilzomib**	**Bortezomib**
	Mean	Mean	Mean	Mean	Mean	Mean
LVAW;d (mm)	0.8±0.1	0.9±0.1	0.8±0.1	0.8±0.1	0.8±0.1	0.9±0.1
LVAW;s (mm)	1.1±0.1	1.2±0.1	1.1±0.1	1.1±0.1	1.1±0.1	1.1±0.1
LVID;d (mm)	3.9±0.2	3.6±0.1	3.8±0.1	3.7±0.2	4.1±0.2	3.9±0.2
LVID;s (mm)	3.0±0.2	2.5±0.2	2.8±0.1	2.7±0.2	3.2±0.2	3.1±0.2
LVPW;d (mm)	0.9±0.1	0.8±0.1	0.8±0.1	0.9±0.1	0.9±0.1	0.9±0.1
LVPW;s (mm)	1.1±0.1	1.2±0.1	1.1±0.1	1.2±0.1	1.1±0.1	1.2±0.1
FS (%)	23.2±2.6	30.9±2.5	27.7±2.2	28.2±1.7	20.2±2.2*	22.1±2.5
LV Mass AW (mg)	122.2±12.8	101.9±5.7	110.7±6.0	116.2±7.7	126.3±14.6	148.1±21.2
LV Vol;d (uL)	67.2±6.4	55.5±4.6	62.9±3.0	58.4±5.8	71.5±7.1	70.6±6.7
LV Vol;s (uL)	37.6±5.1	23.9±3.9	29.3±2.9	27.1±3.9	42.7±6.2	40.4±6.4

Data are represented as mean ± SEM. Statistical analysis using a One-way ANOVA with Sidak's post hoc test for multiple comparisons, (comparisons were made between the saline, bortezomib and carfilzomib group of either control of hypertensive mice for each parameter. ***p<0.05**. **LVAW;d** = Left Ventricular Anterior Wall thickness in diastole; **LVAW;s** = Left Ventricular Anterior Wall thickness in systole; **LVID;d** = Left Ventricular Internal Diameter in diastole; **LVID;s** = Left Ventricular Internal Diameter in systole; **LVPW;d** = Left Ventricular Posterior Wall thickness in diastole; **LVPW;s** = Left Ventricular Posterior Wall thickness in systole; **FS (%)** = Fractional Shortening; LV Mass AW = Left Ventricular Mass of Anterior Wall; **LV Mass AW (Corrected)** = Corrected Left Ventricular Mass of Anterior Wall; **LV Vol;d** = Left Ventricular Volume in diastole; **LV Vol;s** = Left Ventricular Volume in systole. n= 8 per group.

Hemodynamic parameters were next evaluated to determine whether proteasome inhibition influenced arterial stiffness or blood pressure. In vivo pulse wave velocity (PWV), a validated marker of arterial stiffness, remained unchanged across treatment groups in both control and hypertensive mice, suggesting that short-term administration of carfilzomib or bortezomib does not exacerbate arterial stiffness. Additionally, mean arterial pressure (MAP) and pulse pressure, both surrogate indicators of vascular compliance, were unaffected by treatment, although—as expected—L-NAME-treated hypertensive cohorts exhibited significantly elevated blood pressure compared to their normotensive counterparts. **(figure 9)**

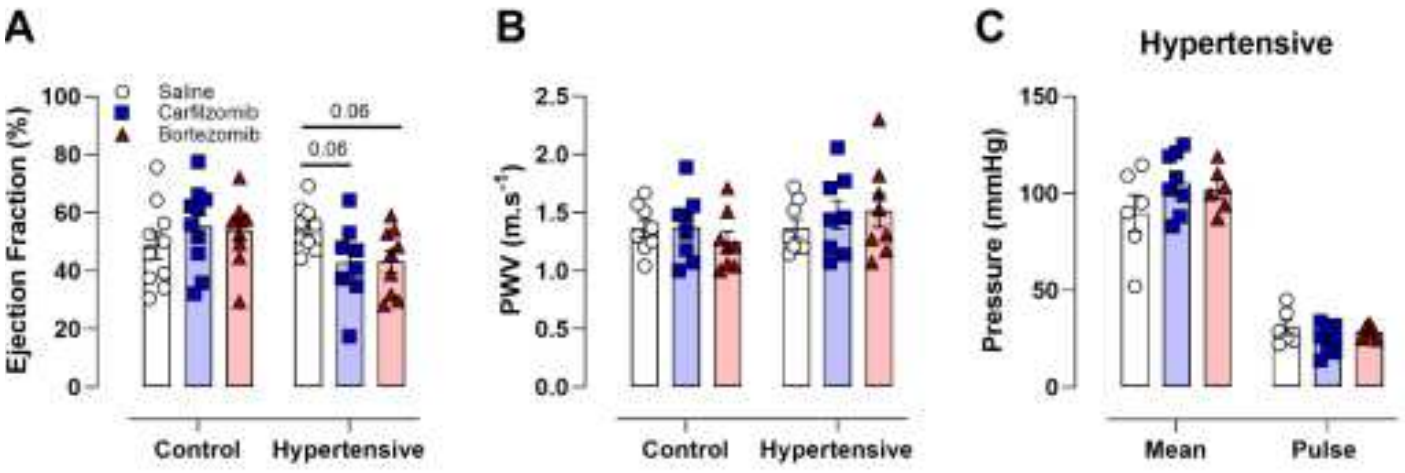

Figure 5: The L-NAME-induced hypertensive group shows a trend toward reduced left ventricular ejection fraction; however, no significant changes in arterial stiffness (as measured by pulse wave velocity, PWV) were observed following Carfilzomib or Bortezomib treatment in either the hypertensive or wild-type cohorts. Similarly, no significant differences were detected in blood pressure fluctuations across treatment groups in both hypertensive and normotensive mice.

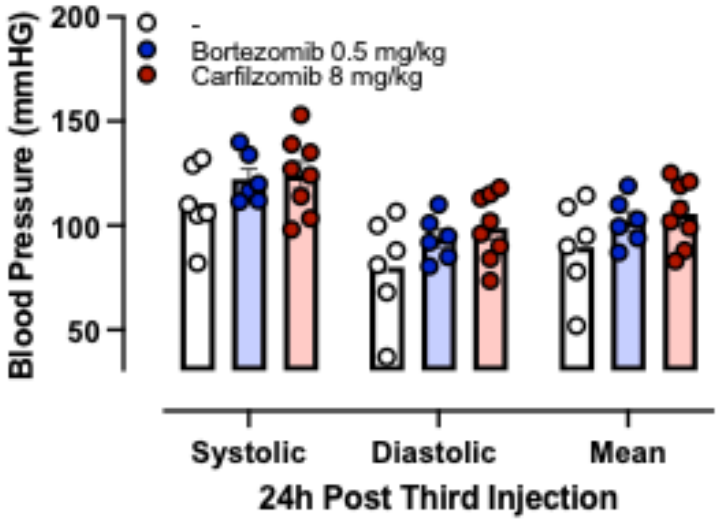

Figure 6: Blood pressure measurements in the wild-type cohort showed no significant alterations in systolic, diastolic, or mean arterial pressure following treatment, indicating preserved hemodynamic parameters.

Carfilzomib Bortezomib effect on Weight loss and cardiac weight

In wild-type mice, treatment with carfilzomib resulted in a notable reduction in body weight, as measured prior to sacrifice. Heart weight, assessed immediately following organ harvesting on the same day, also showed a decreasing trend in the carfilzomib-treated wild-type cohort, as illustrated in **(Figure 11).** Interestingly, this reduction in heart weight was not observed in the L-NAME-induced hypertensive group. This suggests a potential compensatory or restorative mechanism arising from the interaction between hypertension and proteasome inhibition.

Despite these changes, the heart weight-to-body weight (HW:BW) ratio remained unchanged in both wild-type and hypertensive mice, indicating proportional cardiac atrophy rather than pathological hypertrophy or edema. In hypertensive mice specifically, neither body weight nor HW:BW ratios were affected by carfilzomib treatment. This may imply that hypertension mitigates the weight-reducing effects of proteasome inhibition, possibly through systemic compensatory mechanisms or altered metabolic responses under hypertensive stress.

Figure 7 The **A** group (upper line) shows body weight, heart weight and Heart weight body weight ratio in the **normotensive** group, **B** (bottom line) shows the same parameters in L-name induce **Hypertensive** group

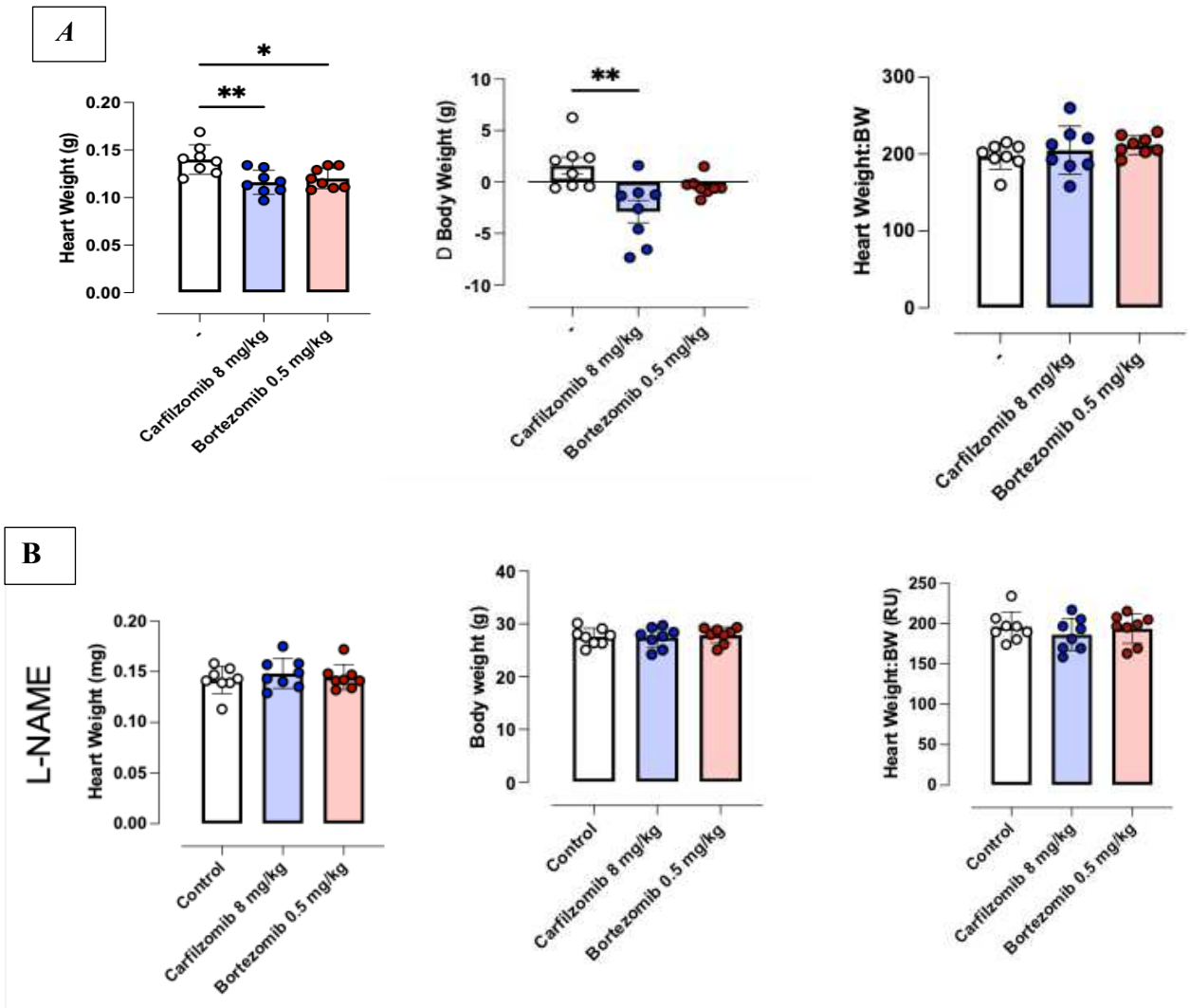

Assessment ex vivo of arterial stiffness

To complement in vivo measures, ex vivo assessments of vascular mechanics were performed to more sensitively detect changes in arterial stiffness **(figure 12).** At baseline physiological pressures (80–120 mmHg), neither diastolic diameters nor Peterson's elastic modulus (Ep) showed any treatment-related changes in control or hypertensive mice, indicating preserved basal arterial mechanical properties. However, under elevated mean pressure conditions (180–200 mmHg), significant interaction effects were noted in pressure-stiffness relationships. In particular, carfilzomib-treated hypertensive mice demonstrated increased arterial stiffness ($p<0.01$) at higher pressure thresholds, suggesting that proteasome inhibition may unmask latent vascular stiffness under conditions of mechanical stress in a hypertensive milieu. This was further supported by the overall rightward shift in the pressure-stiffness curve in treated groups, highlighting altered aortic compliance in response to proteasome inhibition under increased hemodynamic load.

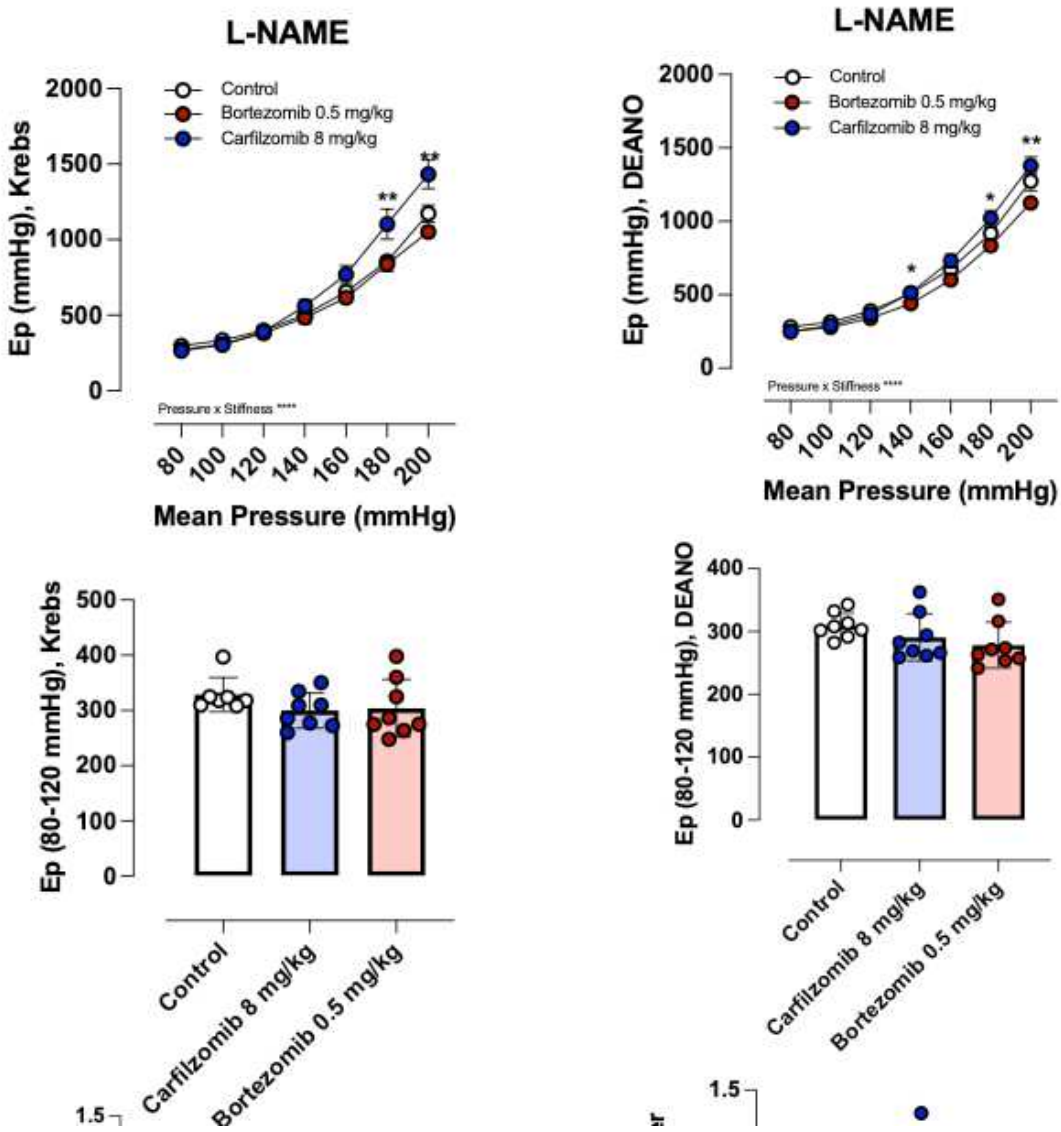

Figure 8 Stiffness Parameters under Krebs and DEANO conditions (upper part). EP modulus under physiological pressures under Krebs and DEANO(bottom part) in Hypertensive l-name induced group

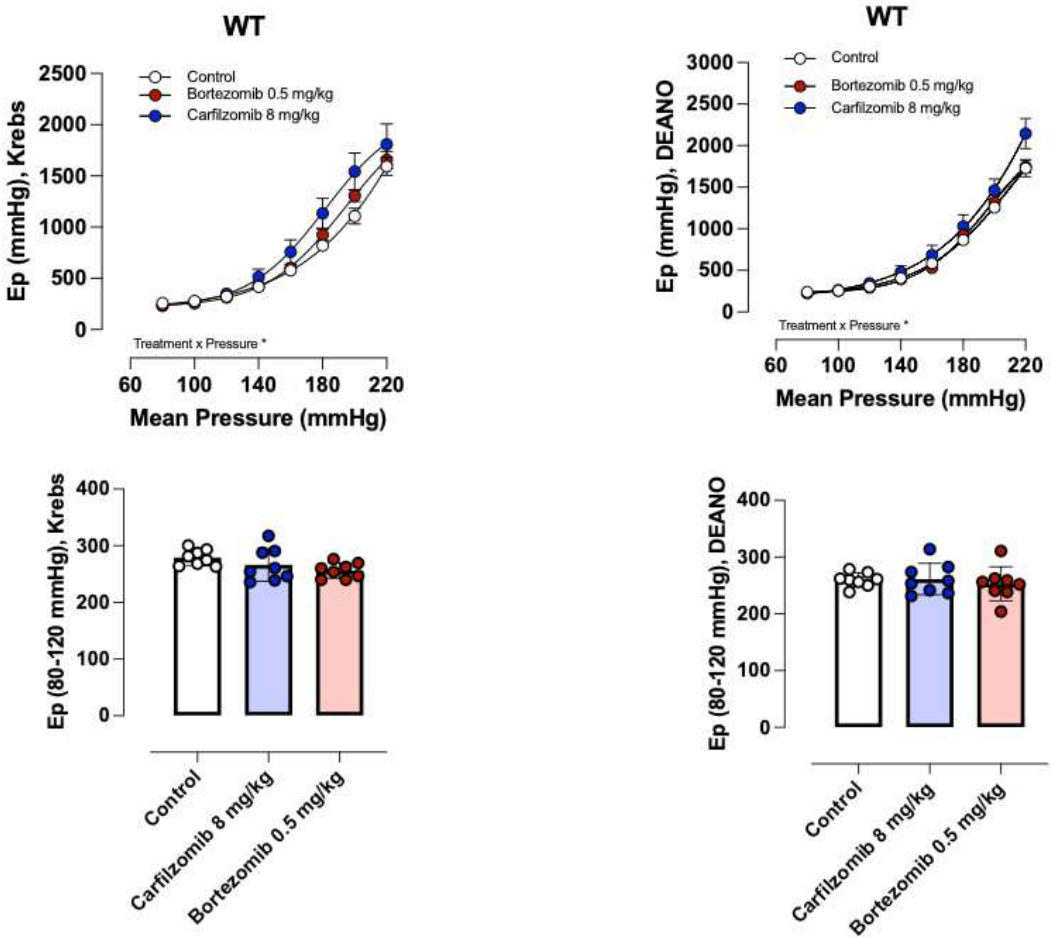

Figure 12 Stiffness Parameters under Krebs and DEANO conditions (upper part). EP modulus under physiological pressures under Krebs and DEANO (bottom part) in **wild type group**

In the wild-type (normotensive) group, Peterson's elastic modulus (Ep), an indicator of arterial stiffness, remained unchanged across the pressure spectrum, both at lower physiological pressures (80–120 mmHg) and at elevated pressures (up to 200 mmHg). This suggests that, under baseline conditions, treatment with proteasome inhibitors—namely Carfilzomib and Bortezomib—does not significantly affect vascular stiffness in healthy mice. However, when nitric oxide (NO) production is pharmacologically inhibited using L-NAME, which creates a hypertensive and NO-deficient environment, the interpretation shifts. In this NO-independent context, a trend toward increased arterial stiffness was observed in the Carfilzomib-treated group at higher pressures (above 160 mmHg), though this trend did not reach statistical significance. This may reflect an emerging mechanical impairment of the vascular wall under conditions of compromised endothelial function when proteasome activity is inhibited.

More compellingly, when comparing across physiological conditions, namely between the normotensive control group and the L-NAME-treated hypertensive group, a consistent elevation in Ep values is evident in the latter. This confirms that L-NAME-induced hypertension is associated with increased arterial stiffness, aligning with known pathophysiological mechanisms

whereby chronic NO deficiency promotes vascular remodeling and loss of compliance. Importantly, despite this overall increase in stiffness in the hypertensive cohort, treatment with Carfilzomib or Bortezomib did not further exacerbate arterial rigidity within the L-NAME-treated group. This suggests that, although proteasome inhibition may influence vascular function under NO-deprived conditions, it does not significantly worsen mechanical stiffness compared to saline-treated hypertensive controls—at least within the timeframe and dosing regimen employed in this study., these findings highlight that while L-NAME-induced hypertension robustly increases arterial stiffness, proteasome inhibitors do not independently or synergistically amplify this effect in a measurable way, pointing to a potentially selective vascular impact under altered endothelial signaling rather than overt mechanical compromise

Finally, vascular reactivity was assessed to determine the functional implications of proteasome inhibition on vascular smooth muscle and endothelial function. For the contraction part In both control and hypertensive mice, no significant changes were observed in contractile responses to phenylephrine (PE), either in the presence or absence of nitric oxide (NO), as modulated by L-NAME. (third graph from the right) Similarly, endothelium-independent contractile responses to potassium chloride (50 mM K+) were unchanged in control mice. However, a notable exception emerged in hypertensive mice, where bortezomib treatment significantly augmented potassium-induced contractions ($p<0.01$ vs control; $p<0.05$ vs carfilzomib), indicating an increase in smooth muscle cell excitability or contractile responsiveness under conditions of hypertension. In the wild type cohort there were no changes in the contraction panel induced by Phenilephrine, Phenileprrine and L-name to stimulate production and and under 50 K

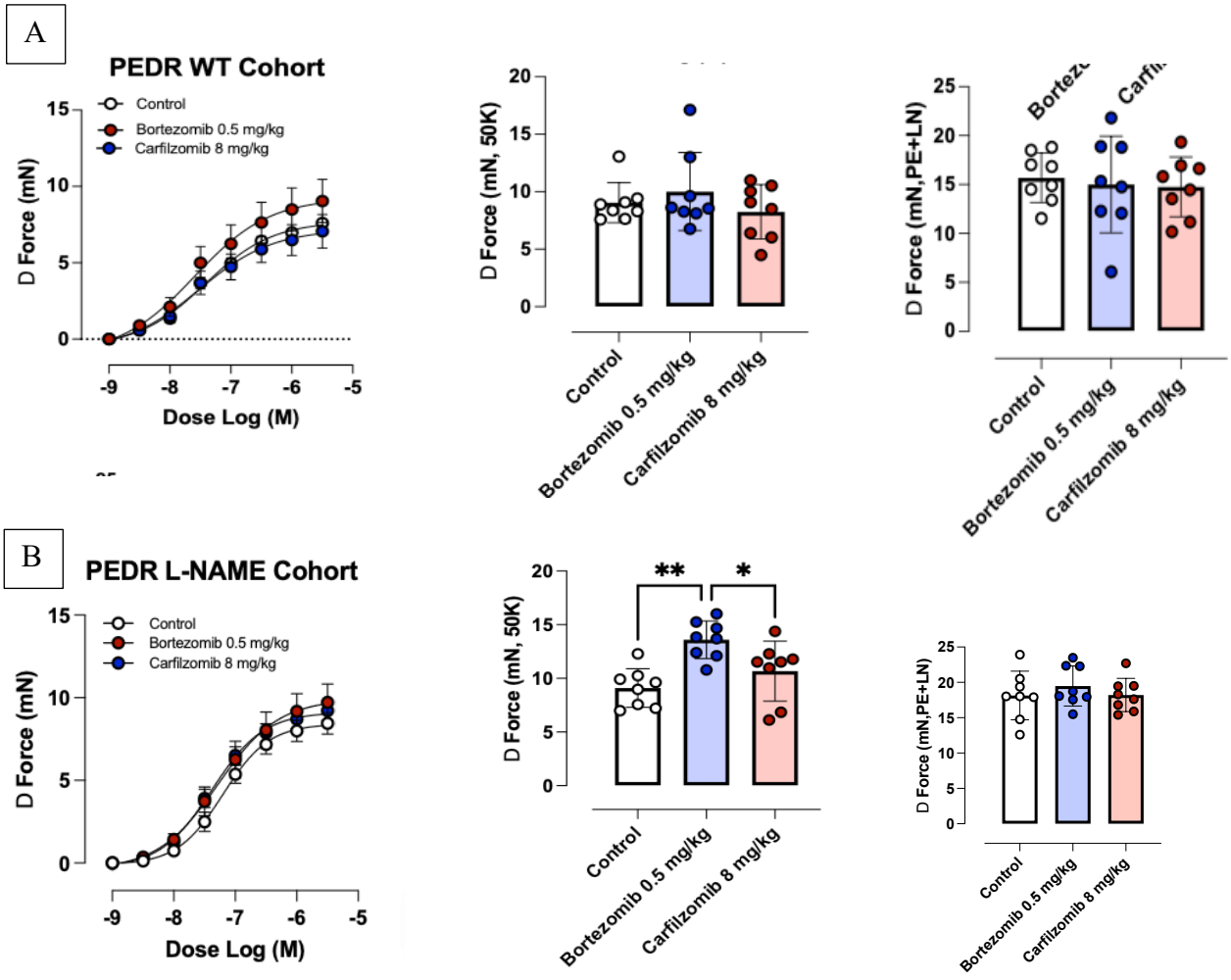

Figure 9 . Vascular reactivity contraction panel under PE dose response for Wild type cohort (**A** line) and Hypertensive cohort under the same conditions (**B** line) .PE dose response, PE+ e-nos inhibitor and potassium induced contraction. Statistical analyses: Two-way ANOVA with Sidak post-hoc test for multiple comparisons (PEDR—phenylephrine dose response). One-way ANOVA with Sidak post hoc test for multiple comparisons all the other graphs (. n=8 per group,)

Endothelium-dependent relaxation responses to acetylcholine (ACh) were preserved in control (normotensive) mice, with no significant differences observed among the treatment groups (Bortezomib-carfilzomib), indicating that proteasome inhibition did not impair basal endothelial function under physiological conditions.

In the **L-NAME-induced hypertensive cohort**, ACh-induced vasorelaxation responses displayed a trend toward enhancement in mice treated with **bortezomib** compared to both control and carfilzomib-treated animals.

While the increase in relaxation did not reach statistical significance at individual concentrations, a **significant interaction effect** was detected ($p < 0.0001$), suggesting that bortezomib may modulate endothelial function or receptor-mediated signaling pathways under hypertensive conditions.

Endothelium-independent vasorelaxation, assessed through cumulative concentration-response curves to the NO donor **DEANO**, revealed a **non-significant leftward shift** in both wild-type and hypertensive groups treated with bortezomib and carfilzomib. Although these shifts did not reach statistical significance, they suggest a potential increase in vascular smooth muscle sensitivity to exogenous NO, potentially reflecting alterations in downstream NO signaling or cGMP responsiveness following proteasome inhibition.

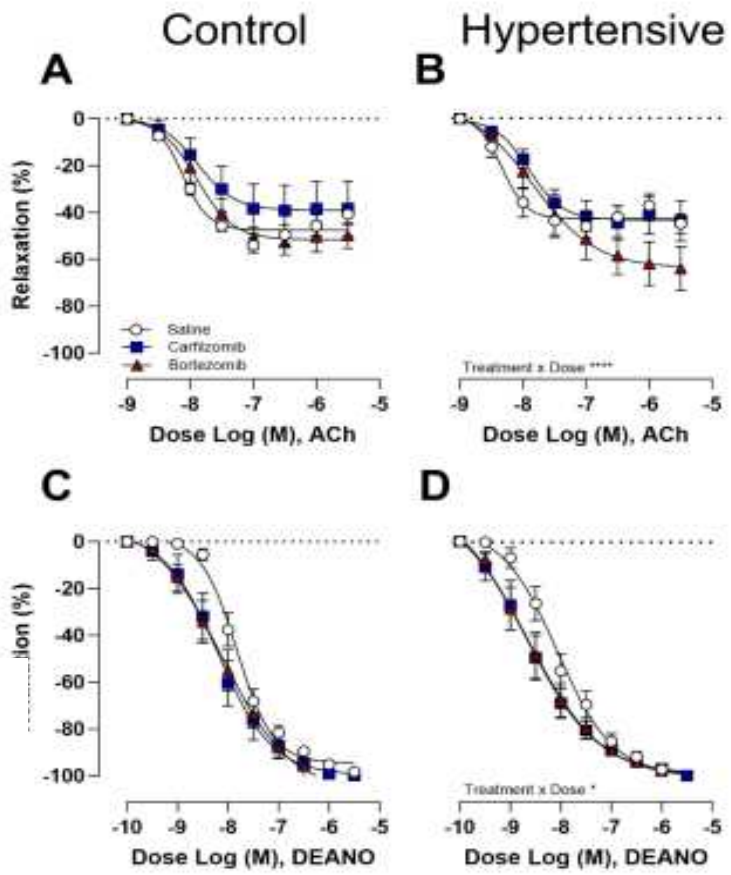

Figure 10 Wild Type and hypertensive group under Ach (acetocholine dose response (**A-B)** and DEANO dose response **(C-D)**

These findings suggest that while proteasome inhibitors do not compromise endothelium-dependent relaxation in normotensive mice, they may subtly modulate endothelial and smooth muscle function under hypertensive conditions, particularly in response to bortezomib.

Collectively, these in vivo findings highlight that carfilzomib and bortezomib, at doses that do not elicit overt cytotoxicity, can induce mild but functionally relevant cardiac and vascular changes, particularly in the context of pre-existing hypertension. These effects include early signs of systolic dysfunction, altered vascular stiffness under mechanical load, and modulated vasoreactivity, underscoring the need for cautious use of proteasome inhibitors in patients with underlying cardiovascular risk.

4.4 Cytotoxicity Assay: Neutral red Assay

To determine whether the hypocontractility observed in Bortezomib-treated aortic segments could be attributed to direct cytotoxicity, we performed a Neutral Red Uptake viability assay across a 24-hour exposure window. This assay enables quantification of viable cells by measuring the accumulation of neutral red dye within lysosomes, serving as a proxy for intact cell membrane function and active metabolic activity.

Given the structural and functional diversity of the aortic wall, we selected three relevant cell populations: Human Aortic Smooth Muscle Cells (HAoSMCs), murine primary cardiac endothelial cells (mpcECs), and murine vascular smooth muscle cells (mVSMCs). These were treated with increasing concentrations of **Bortezomib** (3 nM to 10 µM) or **Carfilzomib** (3 nM to 30 µM), with vehicle-only controls included for baseline normalization.

Bortezomib Exposure

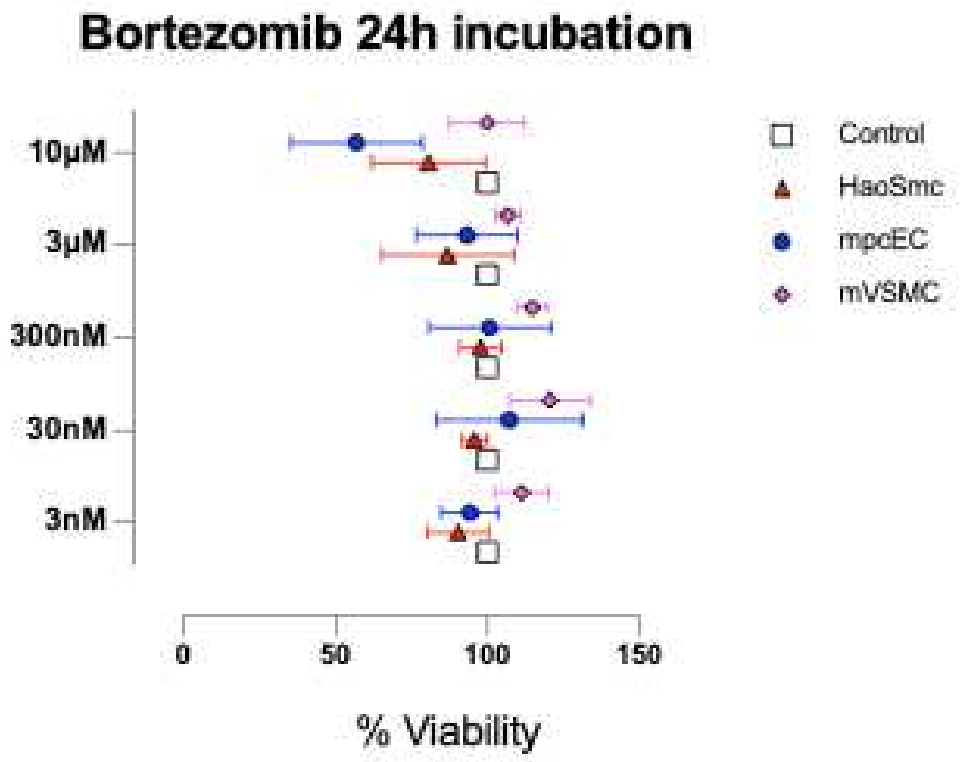

Figure 11 Bortezomib 24h exposition of different cell lines.

As shown in **Figure 15**, all three cell types maintained high viability across a wide range of Bortezomib concentrations. Up to 300 nM, no substantial viability reduction was detected in any cell line, indicating that at the concentrations used in ex vivo vascular experiments (especially 30 nM), Bortezomib does not induce overt cytotoxicity.

At the highest concentration tested (10 µM), a modest but observable decrease in viability occurred, particularly in mpcECs. This may reflect heightened sensitivity due to the unique metabolic demands of endothelial progenitors and their susceptibility to oxidative stress generated through proteasome inhibition and subsequent protein aggregation. Nonetheless, overall viability remained above 80% even at this concentration, reinforcing that cytotoxicity is unlikely to explain the vascular hypocontractility observed at lower doses.

Minor fluctuations in viability across groups were noted and are likely attributable to natural biological variability—such as differences in well confluency, plating density, or growth phase at the time of treatment—rather than compound toxicity.

Carfilzomib Exposure

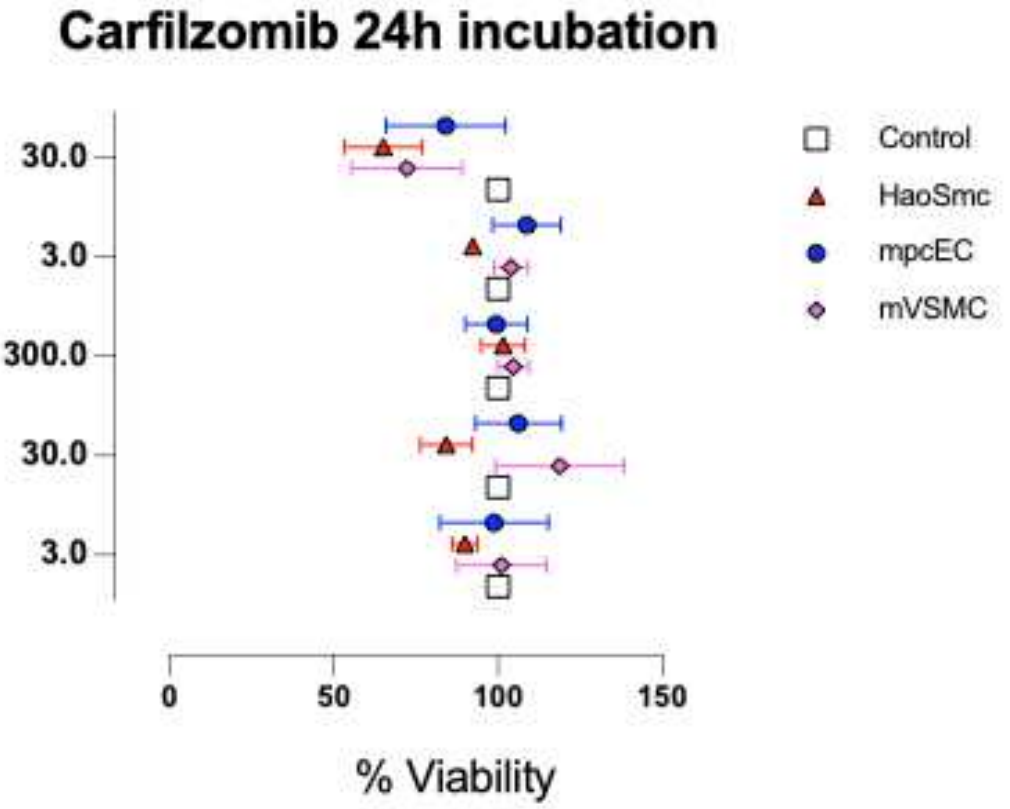

Figure 12 Carfilzomib 24h cell exposure

Similarly, Carfilzomib treatment **(figure 16)** did not result in significant cytotoxicity at concentrations up to 3 µM. Only at 30 µM—a supraphysiological dose beyond the range used for vascular incubation—was a notable reduction in cell viability observed. This effect was most pronounced in HAoSMCs, suggesting that these cells may be particularly vulnerable to high-dose proteasome inhibition. Interestingly, despite being an irreversible proteasome inhibitor, Carfilzomib displayed a more favorable cytotoxic profile at comparable concentrations to Bortezomib, with no sharp viability decline in mpcECs or mVSMCs. This might be related to differences in cellular uptake, proteasome subunit binding affinity, or ROS generation between the two inhibitors.

These findings confirm that at the concentrations used in our ex vivo aortic segment protocols (≤ 30 nM), neither Bortezomib nor Carfilzomib induces measurable cytotoxicity in relevant vascular cell types. Therefore, the hypocontractility observed in the Bortezomib-treated group cannot be explained by a loss of cell viability but rather points toward more subtle, non-lethal effects such as altered calcium handling, impaired contractile machinery, or disruption of endothelial signaling pathways. The differences in cell sensitivity at higher concentrations underscore the importance of selecting physiologically relevant dosing and may also reflect differential stress responses and proteasomal dependencies among vascular cell types.

4.5 F-actin Identification

To explore the mechanism behind the ex vivo Bortezomib-induced hypocontractility, we aimed to determine whether this effect was due to impaired cytoskeletal protein formation or the disassembly of existing cytoskeletal structures in mouse vascular smooth muscle cells (mVSMCs). Among the key structural components of the cytoskeleton, filamentous actin (F-actin) plays a fundamental role in numerous cellular processes. In this experiment, we sought to visually assess the organization and assembly of F-actin in mVSMCs following 24-hour and 48-hour exposures to the proteasome inhibitors Bortezomib and Carfilzomib.

Following stained imaging, cells were analyzed visually and assigned to one of four classes based on a morphological rubric describing F-actin organization:

1 Thick stress fibers traversing the central nuclear region

2 Mixed fibers; some thick filaments entering the perinuclear zone

3 Only thin, peripheral cortical fibers

4 Diffuse or no visible F-actin structure (disassembly)

This classification aimed to provide a semi-quantitative understanding of cytoskeletal remodeling under different conditions. As previously stated in the neutral red cytotoxicity assay, Bortezomib at 300 nM and Carfilzomib at 3 μM did not induce cytotoxicity. This was further evaluated by visual inspection of F-actin architecture and image acquisition. Compared to the positive control (Doxorubicin), where very few intact nuclei were detectable due to pronounced cytotoxicity, Bortezomib-treated mVSMCs appeared enlarged, and a higher number of cells displayed bright and thick central F-actin structures. These stress fibers, traversing the perinuclear region, are typical markers of cytoskeletal remodeling associated with altered permeability and mechanotransduction.

A similar F-actin phenotype was observed in the few remaining viable cells under Doxorubicin treatment, supporting the interpretation that Bortezomib induces comparable cytoskeletal stress despite the lack of overt cytotoxicity.

In contrast, Carfilzomib-treated cells were phenotypically indistinguishable from vehicle-treated controls. F-actin distribution in these groups predominantly fell into Class 2 of the applied visual classification system—representing a balanced actin cytoskeleton with mixed fiber organization and peripheral localization.

Cells treated with Bortezomib were more frequently assigned to Class 1, characterized by thick, continuous F-actin bundles traversing the nuclear region. Cells were classified blindly based on morphology and actin fiber organization. Although no statistical analysis was performed, simple frequency counting of class assignment highlighted a shift in cytoskeletal phenotype under Bortezomib exposure.

Treatment	Phalloidin Class	Fiber Description	Interpretation
Control	2	Mixed fibers, some entering central area	Baseline structure, mild organization
Carfilzomib (3 μM)	2	Mixed fibers, some entering central area	No major disruption; similar to control
Bortezomib (300 nM)	1	Thick central fibers across nucleus	Cytoskeletal stress; Rho/ROCK activation likely
Doxorubicin (ref.)	1	Thick central fibers across nucleus	Known cytotoxic; stress fiber formation

Figure 13 *ALEXA fluor-88 and DAPI fluorescent stain: In red F-actin fibers and in blue cell nucleus on mVSMCs 24h incubation. Starting from the Left* ***A*** *is Bortezomib 300nM treated cells,* ***B*** *is Doxorubicin 1 μM,* ***C*** *is control and* ***D*** *are Carfilzomib 3μM treated cells*

A

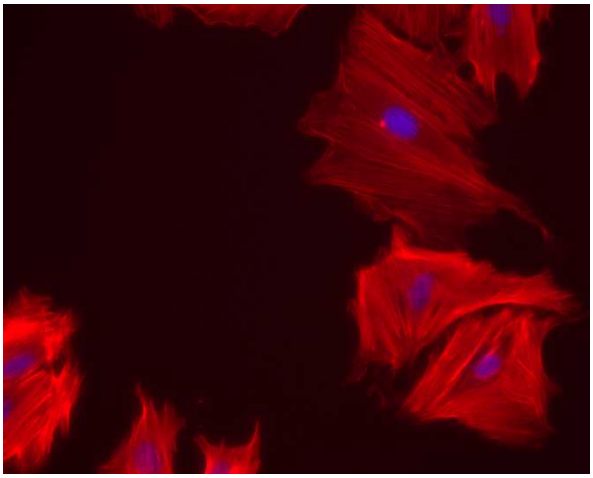

B

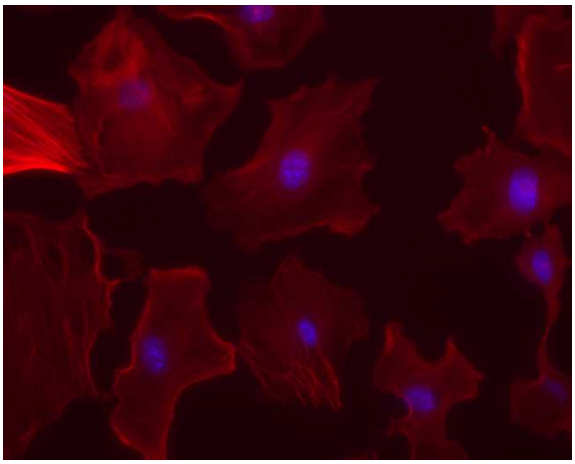

C

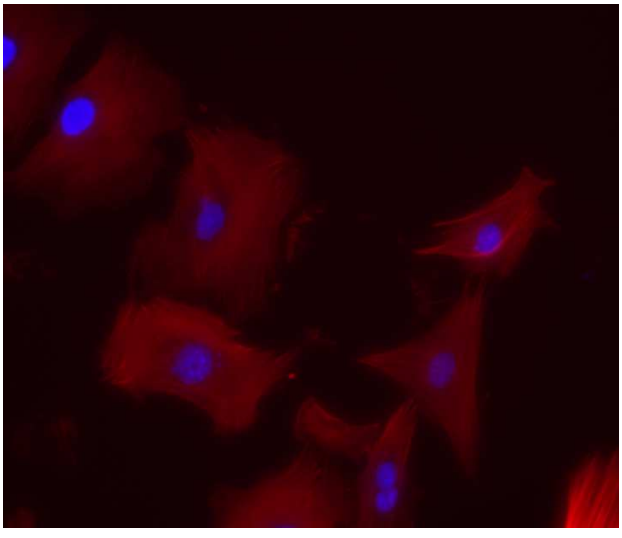

D

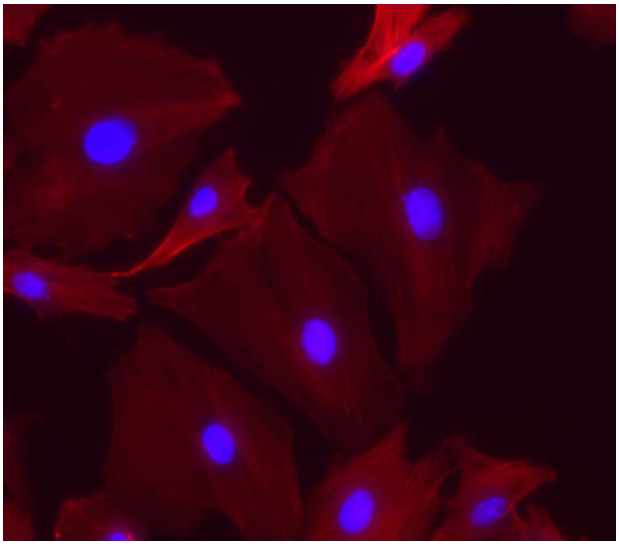

Chapter 5

5.1 Discussion of in vitro and in vivo short protocol (2 injections)

Bortezomib

In this study, ex vivo incubation of thoracic aortic segments with Bortezomib (30 nM, 24 hours) resulted in a significant hypocontractile phenotype, as demonstrated through vascular reactivity assays. Interestingly, this effect was not observed in the in vivo two-dose injection protocol, in which Bortezomib administration did not reduce vasoconstriction in response to phenylephrine (PE). This discrepancy highlights the potential divergence between direct drug effects on isolated vascular tissue and systemic compensatory mechanisms present in a living organism.

A recent study has shown that Bortezomib increases vascular permeability by disrupting endothelial junction proteins like VE-cadherin, without inducing overt cytotoxicity （72）. Our own Neutral Red viability assay confirmed the absence of cytotoxicity in vascular smooth muscle cells (VSMCs) under the tested conditions. Therefore, the observed hypocontractility is likely not attributable to cell death, but rather to functional and structural adaptations of the vessel wall under proteasome inhibition.

One plausible explanation is that increased vascular permeability alters endothelial–VSMC cross-talk, impairing the transmission of contractile signals. This appears to be nitric oxide (NO)-independent, as the hypocontractile response was also observed in the presence of NOS inhibition during isometric stimulation with L-NAME. Thus, the blunted contraction likely stems from intrinsic alterations in VSMC contractile pathways or cytoskeletal organization.

Support for this comes from F-actin phalloidin staining, which revealed increased formation of central, thick stress fibers in Bortezomib-treated mVSMCs—hallmarks of a hypercontractile or stiffened cytoskeletal phenotype. These findings suggest that the VSMCs shift to a mechanically rigid state, losing their plasticity and responsiveness to stimuli despite maintaining structural viability.

A key molecule implicated in this process is α-actinin, an actin crosslinking protein critical for organizing stress fibers and focal adhesions. While α-actinin phosphorylation has been associated with Carfilzomib exposure in some studies, no data yet link its phosphorylation directly to Bortezomib. However, stress fiber assembly in our study may result from upstream activation of the RhoA/ROCK pathway or tension-mediated recruitment of α-actinin to focal adhesions. Indeed, a recent study (Dec 2024) demonstrated that Bortezomib significantly increases RhoA and RhoC levels in endothelial cells, leading to stress fiber formation and heightened endothelial permeability （72）. Although this pathway has not yet been confirmed in mVSMCs, it represents a critical knowledge gap that warrants further investigation, especially considering its potential to drive cytoskeletal stiffening and hypocontractility.

The absence of hypocontractility in vivo after two injections of Bortezomib may reflect early compensatory responses. These include reinforcement of the actin cytoskeleton, upregulation of adhesion proteins, and phenotypic switching of VSMCs to a non-migratory, mechanically rigid state. Such adaptations may serve to seal the vessel and preserve structural integrity in response

to increased permeability. While beneficial in the short term, these changes may eventually reduce VSMC contractility, a phenomenon that likely requires longer drug exposure or pathological priming to be detected in vivo.

On the endothelial side, ex vivo Bortezomib exposure did not induce endothelial dysfunction, nor did it reduce the viability of primary human aortic endothelial cells (HAECs) or murine cardiac mesenchymal progenitor endothelial cells (mpcECs) at physiologically relevant doses. At the highest tested dose (10 μM), however, a modest viability reduction was observed, particularly in mpcECs—possibly due to their greater sensitivity to oxidative stress and protein aggregation triggered by proteasome inhibition on cardiac cells.

In the ROTSAC-based ex vivo aortic stiffness analysis, the two-dose Bortezomib regimen did not alter arterial stiffness under physiological pressures (in both Krebs and NO-donor conditions). However, under supraphysiological pressures (~200 mmHg), Bortezomib-treated aortas exhibited increased stiffness, suggesting that structural vessel changes become apparent only under high mechanical strain. This pressure-dependent stiffening occurred in both Krebs and DEA-NONOate conditions, implying a mechanical, NO-independent remodeling process.

Despite this, existing literature suggests that Bortezomib does not promote collagen deposition. For example, in an Angiotensin II-induced hypertension model, Bortezomib attenuated vascular remodeling, reduced wall-to-lumen ratio, and decreased collagen accumulation【73】. This suggests that collagen might not to be the primary driver of this higher pressure augmented stiffness. Instead, stiffness might result from changes in other ECM components, such as fibronectin, proteoglycans, or elastin cross-linking. While Bortezomib may exacerbate stiffness under higher pressure in a healthy vessel, it may paradoxically exert protective or restorative effects in disease models with existing fibrosis or collagen burden.

Thus, we cannot exclude the recruitment or modification of other ECM components—such as fibronectin, hyaluronan, or perivascular matrix proteins—that could contribute to pressure-dependent stiffening in Bortezomib-treated vessels in non-cancerogenic health animals. Further studies assessing ECM composition and post-translational modifications (e.g., cross-linking, glycation) are needed to elucidate the exact nature of these changes. However, the main focus of this study was to assess under physiological state Arterial stiffness where Bortezomib doesn't affect the arterial elasticity compliance.

Carfilzomib

In the ex vivo vascular assessment of cultured thoracic aortic segments, Carfilzomib did not induce any observable changes in endothelial-dependent relaxation. Similarly, in the in vivo setting following a short-term two-injection protocol, no significant hypocontractile effects were detected under phenylephrine (PE) stimulation. Although there was a statistical trend suggesting a mild hypocontractile response under the PE dose-response curve, this did not extend to differences in maximal PE-induced contraction between Carfilzomib-treated animals and controls. Moreover, the inclusion of eNOS inhibition did not reveal any significant differences in contractile behavior, suggesting that the observed variation may not be attributed to vascular smooth muscle cell (VSMC) dysfunction, but rather to random or non-specific vascular variability.

By contrast, Efentakis et al. (2021) reported that Carfilzomib administration using a similar 48-hour subacute protocol induced a significant reduction in initial contractile responses to prostaglandin F2α and impaired endothelial-dependent vasorelaxation. These effects were mechanistically linked to an increase in leukocyte-derived reactive oxygen species (ROS), highlighting a pathway of endothelial dysfunction mediated by oxidative stress. However, in our study, these findings were not replicated under the same two-injection timeframe. Even when extending the evaluation to four injections over one week, vascular reactivity in Carfilzomib-treated animals remained comparable to that of vehicle-treated controls.

This discrepancy suggests that a more distributed administration schedule may enable the development of compensatory mechanisms, thereby blunting the acute vascular effects observed in the more compressed 48-hour protocol. The lack of observable effects in our in vivo and ex vivo settings reinforce the notion that Carfilzomib's vascular influence is limited, especially when administered under subacute conditions.

Across all conditions—cultured aortic tissue, short-term in vivo exposure, and biochemical assessments—Carfilzomib treatment did not result in significant differences in NO production, VSMC contractility, or endothelial cell-mediated vasorelaxation. These results are consistent with our in vitro findings, where Carfilzomib did not induce cytotoxicity in human aortic vascular smooth muscle cells (HAVSMCs), murine VSMCs (mVSMCs), or murine primary mesenchymal endothelial cells (mpmECs) during a 24-hour incubation period.

At supraphysiological concentrations (30 μM), Carfilzomib reduced HAVSMC viability by approximately 50%, demonstrating some degree of sensitivity in cardiac-derived smooth muscle cells; however, this effect was not observed in mVSMCs, which remained unaffected. Notably, this contrasts with Bortezomib, which exhibited more prominent cytoskeletal stress and cellular sensitivity.

Phalloidin-based F-actin staining confirmed this distinction: while Bortezomib-treated mVSMCs developed prominent thick spindle-shaped stress fibers (indicative of a hypercontractile, rigid phenotype), Carfilzomib-treated cells did not display such changes. Instead, the cytoskeletal organization remained largely similar to that of vehicle-treated controls, suggesting preservation of cytoskeletal integrity.

These observations collectively point to a highly favorable vascular safety profile for Carfilzomib at the cellular, tissue, and whole-animal levels. Furthermore, ex vivo evaluation of arterial stiffness using the ROTSAC platform during the two-day, two-injection protocol revealed no alterations in Peterson modulus (Ep), either under physiological pressures or under supraphysiological mechanical loading. This absence of stiffness alteration was consistent across both Krebs buffer and DEA-NONOate–stimulated conditions, further supporting the conclusion that Carfilzomib does not significantly influence aortic mechanical properties.

Taken together, our data demonstrate that Carfilzomib maintains vascular integrity across in vitro, ex vivo, and in vivo platforms. Its lack of impact on VSMC contractility, endothelial function, cytoskeletal architecture, and arterial stiffness—even under stress—positions Carfilzomib as a proteasome inhibitor with a high vascular safety margin.

5.2 Discussion results of 4 doses regimen protocol in Hypertensive and Normotensive cohort

Across the four-dose, one-week regimen, both carfilzomib and bortezomib demonstrated limited overt cardiac toxicity. Functional cardiac assessments via echocardiography revealed only subtle alterations, with a trend toward reduced systolic function, particularly in hypertensive mice. Importantly, neither agent significantly impaired cardiac performance in normotensive animals, indicating that hypertensive background conditions may amplify cardiac sensitivity to proteasome inhibitors.

Regarding vascular stiffness, in vivo pulse wave velocity (PWV) measurements revealed no significant differences between treatment and control groups in either normotensive or hypertensive mice. However, ex vivo analysis using pressure–diameter curves uncovered pressure-dependent increases in stiffness, particularly in carfilzomib-treated hypertensive mice. This effect was more pronounced at the higher end of the pressure–stiffness spectrum and may reflect earlier recruitment of collagen fibers due to geometrical remodeling, possibly associated with increased baseline vessel diameter. These findings indicate that in vivo PWV may underestimate subtle, pressure-sensitive changes in vascular compliance that are only revealed under controlled ex vivo conditions.

Notably, bortezomib-treated mice (hypertensive and not) did not demonstrate increased stiffness under normal physiological pressure ranges. Surprisingly these results are different from the two days injection protocol that was showing a significant bortezomib increased stiffness at higher pressures. All of this underlines the changed behavior of bortezomib under two different doses regimens shifting from acute to more subacute administration. The absence of significant changes in PWV also in vivo and endothelial function, as measured by acetylcholine-induced relaxation, indicates that short-term proteasome inhibitor exposure does not grossly impair vascular performance. Nevertheless, subtle alterations in biomechanical behavior may have longer-term implications for vascular integrity, particularly under stress or comorbid conditions.

Vascular reactivity was largely preserved across both treatment arms, with minor shifts observed in the sensitivity of vascular smooth muscle cells (VSMCs) to exogenous nitric oxide (NO), as evidenced by leftward shifts in DEANO dose-response curves. This heightened sensitivity could be a downstream effect of altered soluble guanylate cyclase (sGC) pathway protein turnover, a hypothesis supported by literature linking proteasome inhibition to sGC destabilization.

In our L-NAME-treated hypertensive model, we did not observe the anticipated increase in PWV following one week of treatment, consistent with previous findings from our lab that highlight the time-dependent nature of arterial remodeling. Despite the hypertensive background, endothelial-dependent relaxation remained intact in both treatment groups. The lack of dysfunction may reflect rapid resynthesis or preservation of eNOS activity following drug washout in the ex vivo setting.

Bortezomib-treated hypertensive mice exhibited increased contractile responses to potassium chloride (KCl), unlike their carfilzomib-treated counterparts. The disparity between KCl- and phenylephrine-induced contractions under L-NAME suggests divergent pathways of VSMC activation may be differentially affected by proteasome inhibition. While speculative, it is plausible that proteasome inhibitors modulate calcium-handling proteins or ion channel turnover, influencing depolarization-induced responses more than receptor-mediated signaling.

Overall, the four-dose, one-week protocol enabled a nuanced evaluation of proteasome inhibitor effects across both normotensive and hypertensive conditions. While neither carfilzomib nor bortezomib induced pronounced in vivo cardiovascular toxicity, ex vivo assessments revealed important mechanistic insights. Carfilzomib appeared to induce a modest increase in arterial stiffness at high pressures, which was not visualized in the two-injection regimen underlying that repetitive carfilzomib exposition leads to a trend towards increased stiffness at higher pressures. For Bortezomib the results are equal in 2 doses regimen and 4 doses regimen on ex vivo stiffness profile particularly in hypertensive mice. However, Bortezomib demonstrated enhanced contractility in response to 50 mM KCl and increased sensitivity to acetylcholine-mediated endothelial relaxation, suggesting a favorable hyperadaptive response in models of vascular disease. This aligns with previous findings indicating that Bortezomib reduces collagen deposition in severe pathological contexts, such as Angiotensin II–induced hypertension, while its effects in normotensive models may be less beneficial. For instance, the stiffness increases observed in wild-type mice following acute two-dose Bortezomib treatment were not reproduced in either L-NAME-treated or wild-type groups subjected to the prolonged four-dose regimen. This suggests that Bortezomib exerts more favorable vascular effects in the context of pre-existing vascular dysfunction, while its impact appears less beneficial in short-term protocols involving healthy, non-diseased models. The adaptive effects of Bortezomib under pathological conditions may reflect a more complex interplay between vascular remodeling and cellular stress responses.

These outcomes could be linked to the distinct cytoskeletal organization seen in Bortezomib-treated mVSMCs, characterized by stress fiber accumulation. Such architecture may initially enhance sensitivity to mechanical and pharmacological stimuli. However, with extended exposure, compensatory mechanisms may develop that dampen or obscure the early effects observed under acute treatment.

In contrast, Carfilzomib maintained a high safety profile during the two-dose regimen, showing no adverse effects on VSMC function or endothelial integrity. However, under extended exposure, it led to a modest increase in arterial stiffness in both hypertensive and normotensive models, despite the absence of detectable cytotoxicity or cytoskeletal alterations.

These findings emphasize the value of multi-level vascular assessment and suggest that while both proteasome inhibitors are safe under physiological conditions, their effects differ significantly in the presence of cardiovascular comorbidities. These differences likely reflect distinct underlying biochemical pathways and variations in VSMC phenotypic regulation.

This integrated approach effectively captures the complex clinical scenarios associated with proteasome inhibitor therapy and illustrates the importance of combining in vivo cardiovascular imaging, ex vivo biomechanical testing, and molecular-level analysis. Together, these methods can reveal subtle yet meaningful vascular effects that would otherwise go undetected.

Further long-term studies are essential to evaluate the cumulative effects of proteasome inhibitors on vascular remodeling and overall cardiovascular health, particularly in individuals with existing cardiovascular risk factors. Such investigations should maintain a comparative approach between reversible (e.g., Bortezomib) and irreversible (e.g., Carfilzomib) proteasome inhibitors to determine whether the observed effects are drug-specific or represent broader class-related mechanisms.

From a safety pharmacology perspective, both agents appear safe under physiological conditions. Although Carfilzomib is clinically more effective in reducing multiple myeloma burden, Bortezomib may offer distinct vascular benefits in the presence of comorbidities—possibly through compensatory mechanisms involving unique cellular or biochemical adaptations that have yet to be fully characterized.

To better understand these differences, future research should focus on prolonged exposure within a single disease model, ideally incorporating various dosing regimens. Such studies could provide deeper insight into the dynamic shifts in vascular behavior, VSMC phenotype switching, and extracellular matrix (ECM) remodeling driven by proteasome inhibition over time.

5.3 Strength of the study

To our knowledge, this is the first study to directly compare two structurally and functionally distinct proteasome inhibitors—bortezomib and carfilzomib—in a preclinical setting, with a key focus on their vascular effects and particularly on arterial stiffness as a translational biomarker of cardiovascular toxicity. Most prior research has focused on cardiotoxicity, with limited attention given to vascular dysfunction, and even less on arterial stiffness as a physiological outcome. Our study addresses this gap by evaluating vascular effects using an integrated approach combining in vitro, ex vivo, and in vivo methodologies.

Importantly, we utilized both an acute (two-dose, 48-hour) and a subacute (four-dose, one-week) administration protocol for each drug. This design was inspired by the dosing framework applied by Efentakis et al. (2021], who investigated the impact of carfilzomib on cardiac function using similar timeframes. However, unlike Efentakis, who focused primarily on echocardiographic cardiac output and strain parameters, our work extends the evaluation of arterial stiffness, highlighting distinct vascular profiles.

Another major strength lies in our use of the L-NAME-induced mild hypertension model, a validated and translationally relevant rodent model. Unlike the commonly used angiotensin II-induced hypertension model, which causes extensive hypertension, fibrotic arterial stiffening and endothelial dysfunction. L-NAME model, induces mild progressive hypertension and subtler vascular remodeling — making Ang II ideal for fibrosis and aneurysm studies, while L-NAME is better for modeling early diseases.

(1–4 weeks) L-name therapy in drinking water leads to transient endothelial dysfunction, as evidenced by reduced acetylcholine-mediated vasodilation, which is subsequently compensated by increased eNOS phosphorylation. Over time and more administration, the model evolves toward VSMC dysfunction, characterized by altered calcium dynamics, enhanced basal calcium influx, and sarcoplasmic reticulum contractile responses. (71) In the present study L-name administration was one week long.

Our study combines in vivo PWV (arterial stiffness methodologies used in clinical settings) with ex vivo biomechanical analysis of aortic segments using the Rodent Oscillatory Tension Set-up for Arterial Compliance (ROTSAC). This ex vivo tool allows aortic rings to be dynamically stretched and analyzed under pressure, enabling real-time calculation of stiffness via Peterson modulus, derived from diameter-pressure relationships. This approach complements traditional isometric myograph testing by offering a pressure-responsive mechanical readout.

Integrating ex vivo, in vitro and in vivo functional metrics, our framework offers a robust, scalable, and time-efficient preclinical template for vascular safety pharmacology. It not only allows drug comparison under both physiological and pathological conditions but also facilitates pathway discovery on pressure-dependent stiffening and vascular reactivity.

Our methodological strategy is highly adaptable and cost-effective. The combined data offer rich mechanistic insights into drug-induced vascular remodeling, particularly because arterial stiffness is now a recognized surrogate marker for cardiovascular risk and toxicity.

This 1-year project involved cell-based assays, rodent experiments, all aligned toward a comprehensive characterization of proteasome inhibitor vascular implication. The study design can serve as a template for vascular safety profiling of other pharmacological agents, filling a current gap in drug development pipelines where vascular effects are often overlooked.

5.4 Study Limitations

A key limitation of this study is the relatively short exposure duration and the absence of long-term follow-up. Extended observation periods would be valuable in assessing the sustained impact of proteasome inhibitors on vascular remodeling and cardiovascular function. Additionally, while the ex vivo setup allowed for controlled mechanistic investigation, it may not fully replicate the acute pharmacodynamic responses seen in vivo, partly due to potential drug washout during tissue incubation. However, the observed increase in basal arterial stiffness in L-NAME-treated mice serves as an internal validation of the ex vivo model's sensitivity.

Another limitation lies in the route of drug administration. In this study, both carfilzomib and bortezomib were delivered intraperitoneally, whereas their clinical use typically involves intravenous (carfilzomib) or intravenous/subcutaneous (bortezomib) delivery. While previous studies (e.g., Efentakis et al.) have demonstrated that intraperitoneal administration in mice can reach clinically relevant plasma concentrations, variations in pharmacokinetics may contribute to the absence of certain drug effects observed in this protocol.

Moreover, multiple myeloma patients are predominantly older than 70 years. In retrospect, it would have been highly relevant to evaluate proteasome inhibition in aged mice, as aging is associated with endothelial dysfunction and a higher susceptibility to vascular damage. While our study utilized a hypertension model (L-NAME) to simulate a key cardiovascular comorbidity common in the elderly, future studies should include aged animals to better reflect the clinical patient population.

From a methodological standpoint, the evaluation of F-actin distribution in this study was performed using a morphological classification into four phenotypic classes based on the appearance and distribution of F-actin filaments. Although this approach is biologically relevant, it remains inherently subjective and dependent on variables such as cell density, confluence, morphology, and cell cycle stage. This introduces variability and reduces comparability across datasets.

To overcome these limitations, future studies could employ the automated F-actin analysis developed by Zonderland et al. (2019) (74). This method uses a custom macro in Fiji (ImageJ) combined with an **R script** to automatically measure F-actin intensity across the cell and

quantifies F-actin organization by analyzing the distribution and intensity of actin filaments across the entire cell body, with particular attention to central versus peripheral regions.

The macro draws a line perpendicular or parallel to the major cell axis and divides intensity values into uniform bins, ensuring consistency regardless of cell size or shape. This pipeline significantly reduces operator bias and enables standardized quantification across large datasets. Although its implementation was not feasible within the timeframe of this thesis due to the technical programming and optimization required, it presents a promising direction for standardizing cytoskeletal analysis in vascular pharmacology.

The application of such high-throughput and automated imaging tools will be crucial in enhancing reproducibility, statistical power, and cross-laboratory comparability in actin-based mechanistic research. Standardized tools are particularly beneficial in scenarios involving subtle or transient phenotypic differences, such as those observed in proteasome inhibitor-treated cells.

5.5 General Conclusion

This thesis provides a comprehensive comparison between two widely used proteasome inhibitors—Bortezomib (reversible) and Carfilzomib (irreversible)—with a particular focus on their vascular and cardiovascular impact under physiological and hypertensive conditions. The experimental framework integrated in vitro, ex vivo, and in vivo assessments, offering a translational perspective rooted in both cellular mechanisms and functional outcomes.

Bortezomib exhibited a complex and context-dependent vascular profile. Ex vivo incubation with thoracic aortic segments led to hypocontractility. These effects were not observed in vivo following a short-term two-dose protocol, suggesting that systemic compensatory mechanisms may mask direct vascular effects. However, bortezomib on short term exposition induced stiffer behavior under higher pressure on healthy animal. F-actin imaging revealed enhanced stress fiber formation in Bortezomib-treated VSMCs, consistent with increased cytoskeletal rigidity and mechanosensitivity. Interestingly, Bortezomib enhanced vascular reactivity to KCl and acetylcholine in hypertensive models and did not promote collagen deposition, aligning with previous findings that support a protective role in diseased vessels, such as in Angiotensin II-induced hypertension. However, in healthy wild-type mice, acute Bortezomib treatment transiently increased stiffness, indicating that its effects may be less favorable under non-pathological conditions.

Carfilzomib, by contrast, presented a slightly more negative vascular profile, especially under extended dosing conditions. Although no cytotoxicity or direct cytoskeletal disruption was observed, a modest increase in ex vivo arterial stiffness at higher pressures was recorded following the four-dose regimen in both normotensive and hypertensive mice. This effect was not seen in the two-dose protocol. Nevertheless, in the short term, Carfilzomib did not induce arterial stiffness under physiological pressures, and vascular reactivity, NO sensitivity, and endothelial function remained largely intact, indicating an overall high vascular safety margin when administered acutely.

Together, these findings highlight the importance of pressure-dependent stiffness analysis, which captured vascular responses not evident through traditional in vivo measures such as PWV. The results suggest that neither Bortezomib nor Carfilzomib induces arterial stiffness under normal

physiological conditions in the short term, but that their effects diverge in the context of hypertension and prolonged exposure. This distinction emphasizes the need to consider disease state, exposure time, and mechanical load when evaluating vascular safety.

From a safety pharmacology standpoint, both proteasome inhibitors were well tolerated in the short term. However, Bortezomib appears to engage adaptive remodeling pathways in diseased vascular environments, whereas Carfilzomib may contribute to progressive stiffness under prolonged use, albeit without acute toxicity or direct cellular disruption. These drug-specific vascular signatures suggest that not all proteasome inhibitors share the same risk profile, and their use should be tailored based on patient comorbidities and treatment duration.

Future studies should expand on these findings by evaluating long-term exposure, particularly within models of established cardiovascular disease. Further exploration of ECM composition, cytoskeletal adaptations will be essential in distinguishing drug-specific effects from class-wide consequences, guiding safer and more personalized therapeutic strategies in cardio-oncology and b

Crucially, this entire evaluation was conducted within the scope of one year, demonstrating that our methodology is not only comprehensive and mechanistically informative, but also time-efficient and scalable. This pipeline can be adapted to assess vascular safety for any pharmacological compound, making it a powerful tool for preclinical cardiovascular risk screening through evaluation of arterial stiffness.

5.6 Preliminary data on autophagy induced by carfilzomib and bortezomib and hypothesis for future perspectives

To explore whether autophagy functions as a compensatory mechanism during proteasome inhibition in vascular smooth muscle cells (mVSMCs), we conducted a preliminary autophagy assay using an RFP-GFP-LC3 tandem reporter system. This dual-fluorescence construct enables real-time differentiation between autophagosomes (yellow puncta: GFP+RFP) and autolysosomes (red-only puncta: RFP only), based on the acid-sensitive nature of GFP.

Cells were treated with vehicle (DMSO), Torin (mTOR inhibitor, positive control), Bafilomycin A1 (lysosomal fusion inhibitor), Carfilzomib, and Bortezomib. As expected, Torin induced strong red-only puncta, indicating autophagic flux, while Bafilomycin caused an accumulation of yellow puncta due to blocked lysosomal fusion. The Torin + Bafilomycin group showed enhanced yellow accumulation, confirming dual effects of induction and flux blockade. **(figure A)**

Among proteasome inhibitor-treated cells:

- Bortezomib induced both red and yellow puncta, suggesting active autophagic flux—with successful autophagosome formation and lysosomal fusion.
- Carfilzomib, by contrast, showed predominantly yellow puncta with sparse red-only signal, indicating flux impairment or incomplete autophagic progression. **(figure B)**

These results—based on two biological replicates without statistical validation—are preliminary but indicate divergent effects on the autophagy pathway. Given the known interdependence between the ubiquitin-proteasome system (UPS) and autophagy, it is plausible that:

1. Bortezomib acts as a mild autophagy inducer, either directly or via proteostasis stress responses (e.g., ER stress), offering compensatory protection in vascular cells, specifically in the diseased where basal autophagy should already be enanched.
2. Carfilzomib, through irreversible proteasome inhibition, may suppress autophagic flux, particularly under sustained or high-pressure conditions.

This may help explain why Carfilzomib induced a dose- and pressure-dependent increase in aortic stiffness, despite showing no overt cytotoxicity or cytoskeletal disruption. The inability to clear accumulating misfolded proteins due to blocked autophagy could contribute to increased mechanical rigidity and impaired vascular plasticity over time.

In contrast, the attenuation of Bortezomib-induced stiffness in prolonged regimens and its preservation of F-actin architecture may reflect a protective adaptation mediated by autophagy engagement. Whether this is sustainable or ultimately maladaptive requires further investigation

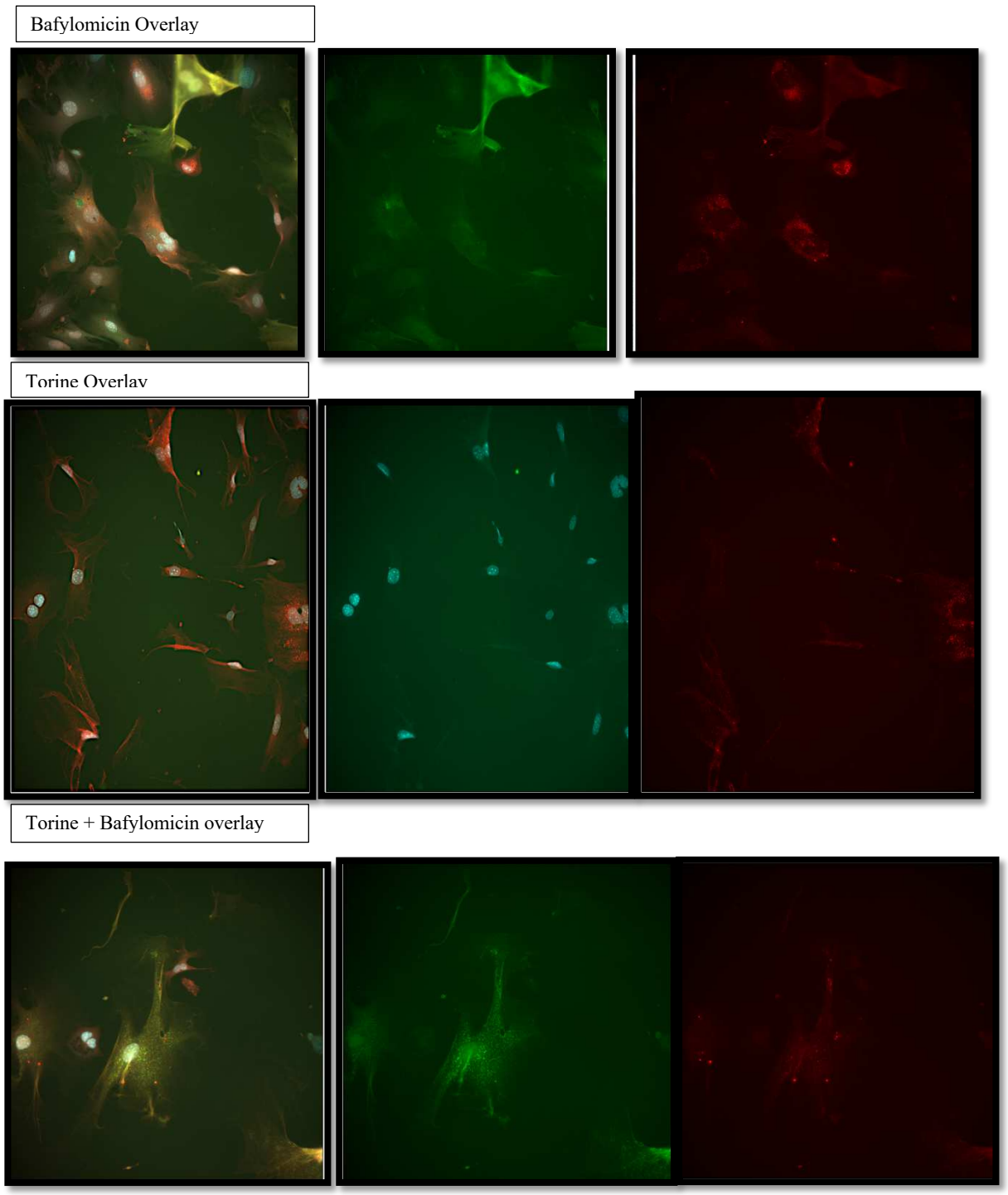

Figure A: RFP-GFP-LC3 fluorescence in mVSMCs treated with Bafilomycin A1, Torin, or their combination.

- **Torin** induces autophagy, shown by increased red-only puncta (autolysosomes), indicating active flux.
- **Bafilomycin A1** blocks autophagosome-lysosome fusion, leading to accumulation of yellow puncta (autophagosomes).
- **Torin + Bafilomycin** causes a buildup of yellow puncta, reflecting strong induction of autophagy with impaired degradation.

Dmso

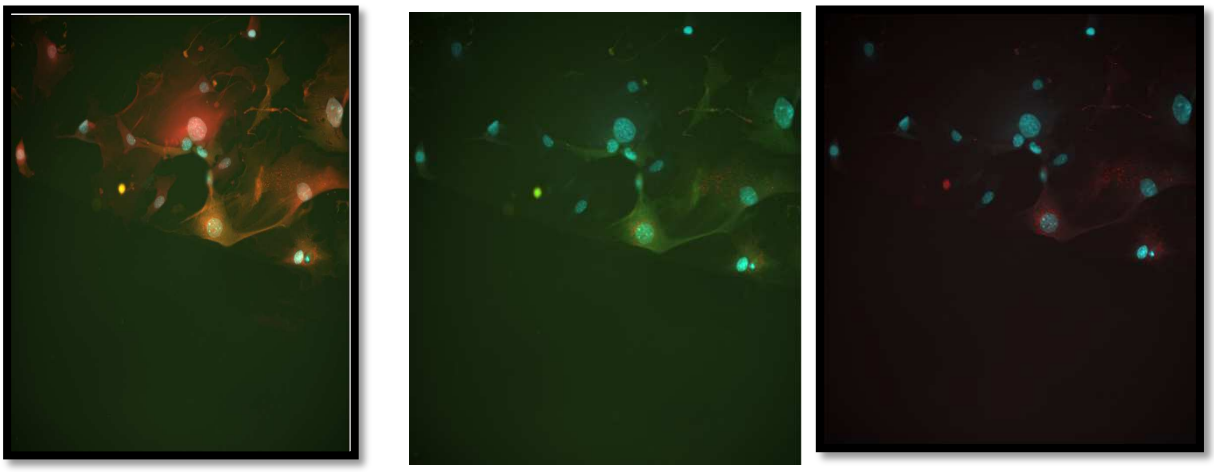

Bortezomib

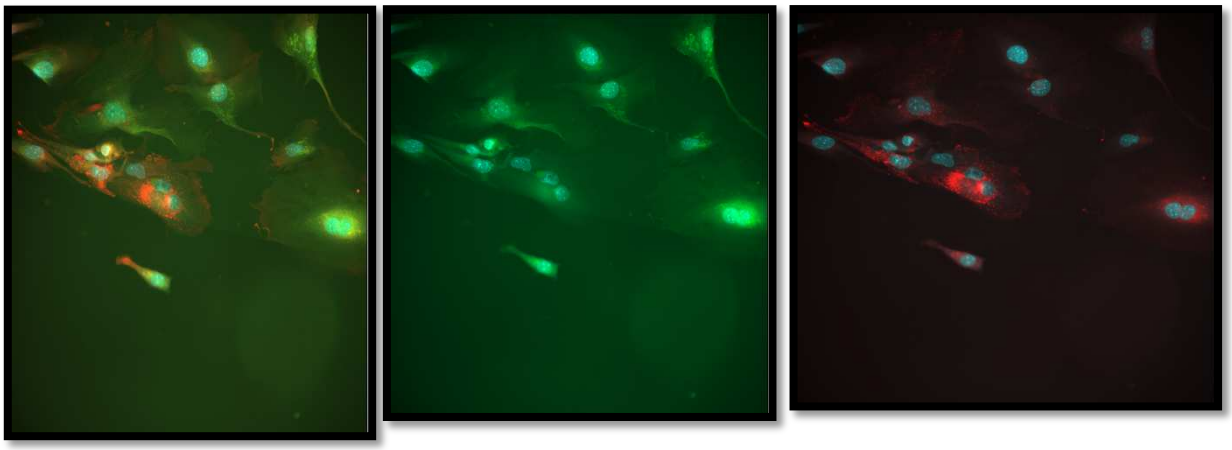

Carfilzomib

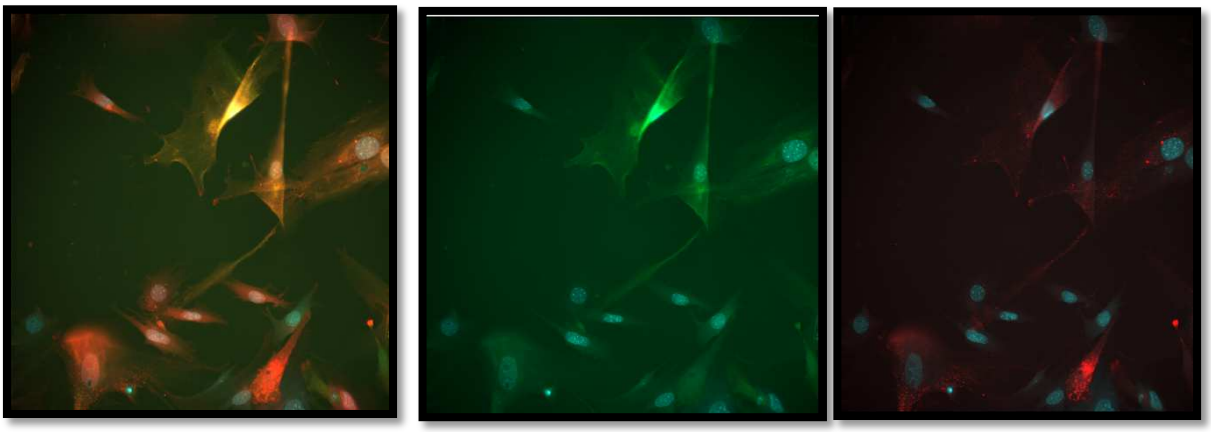

Figure B: RFP-GFP-LC3 fluorescence in mVSMCs treated with vehicle (dmso), Bortezomib, Carfilzomib

- **Dmso** minimal puncta, indicating low basal autophagic activity
- **Carfilzomib** leads to accumulation of yellow puncta, suggesting autophagosome buildup with possible impairment of autophagic flux
- **Bortezomib** shows both yellow and red puncta, indicating active autophagy with successful lysosomal fusion.

However, these speculations arise from a sense of scientific curiosity that defines me as a future Pharmacist/researcher/activist and individual. They extend beyond the primary aim of this thesis, which was to demonstrate the short-term vascular safety of proteasome inhibitors—specifically their lack of adverse effects on arterial stiffness. Nevertheless, such hypotheses and forward-looking reflections are driven by the hope that one day they will contribute to improving clinical outcomes for patients, identifying new therapeutic candidates, and ultimately advancing pharmacology's dual mission: to combat disease effectively while minimizing harm. The ultimate goal remains to maintain the delicate balance between risk and benefit, always striving to tip the scale in favor of patient well-being in the most efficient and meaningful way possible. I reckon this being the Burden and the Blessing of Pharmacology.

BIBLIOGRAPHY

1. Wanchoo, R., et al. (2024, December 1). Bortezomib in cancer therapy: Mechanisms, side effects, and future directions. ScienceDirect.
2. HealthTree. (2024, June 19). How proteasome inhibitors work – HealthTree for Multiple Myeloma.
3. Nature. (2024, March 4). NF-κB in biology and targeted therapy: New insights and directions.
4. BioMed Central. (2024, February 8). Interplay between proteasome inhibitors and NF-κB pathway in inflammation and cancer.
5. Nature. (2023, September 15). Endoplasmic reticulum stress: Molecular mechanism and therapeutic targeting.
6. Richardson, P. G., Hideshima, T., & Anderson, K. C. (2003). Bortezomib (PS-341): A novel, first-in-class proteasome inhibitor for the treatment of multiple myeloma and other cancers. Cancer Control, 10(5), 361–369.
7. Merin, N. M., & Kelly, K. R. (2014). Clinical use of proteasome inhibitors in the treatment of multiple myeloma. Pharmaceuticals, 8(1), 1–20. https://doi.org/10.3390/ph8010001
8. Mikhael, J., et al. (2019). Treatment of multiple myeloma: ASCO and CCO joint clinical practice guideline. Journal of Clinical Oncology, 37(12), 1228–1263. https://doi.org/10.1200/JCO.18.02096
9. Orlowski, R. Z., Moreau, P., Niesvizky, R., et al. (2019). Carfilzomib-dexamethasone versus bortezomib-dexamethasone in relapsed or refractory multiple myeloma. Clinical Lymphoma Myeloma and Leukemia, 19(8).
10. Chari, A., & Hajje, D. (2014). Cardiac and pulmonary complications with carfilzomib: Monitoring and management. Clinical Lymphoma Myeloma Leukemia, 14(3), e117–e120.
11. Efentakis, P., Papachristos, A. I., Varela, A., et al. (2021). Molecular mechanisms of proteasome inhibitors in cardiotoxicity. Heart Failure Reviews, 26(6), 1363–1375.
12. Herrmann, J. (2021). Proteasome inhibition and cardiotoxicity. Circulation Research, 129(6), 757–758.
13. Day, S. M. (2013). The ubiquitin proteasome system in human cardiomyopathies and heart failure. American Journal of Physiology – Heart and Circulatory Physiology, 304(10), H1283–H1293.
14. Doroudgar, S., & Glembotski, C. C. (2013). Endoplasmic reticulum function in the heart: Programmed to conserve. Journal of Molecular and Cellular Cardiology, 55, 85–91.
15. Hwang, J., & Qi, L. (2018). Crosstalk between ER-associated degradation and ER stress response. Trends in Biochemical Sciences, 43(8), 593–605.
16. Wang, X., & Robbins, J. (2006). Heart failure and protein quality control. Circulation Research, 99(12), 1315–1328.
17. McLendon, P. M., & Robbins, J. (2015). Proteotoxicity and cardiac dysfunction. Circulation Research, 116(11), 1863–1882.
18. Goldfarb, L. G., Vicart, P., Goebel, H. H., & Dalakas, M. C. (2004). Desmin myopathy. Brain, 127(4), 723–734.
19. Kumar, S. K., & Rajkumar, S. V. (2018). Minimal residual disease assessment in myeloma. Leukemia, 32(3), 487–496.

20. Hideshima, T., Richardson, P., Chauhan, D., et al. (2002). TNF-α and multiple myeloma pathophysiology. Oncogene, 21(25), 4529–4537.
21. Chen-Scarabelli, C., et al. (2014). Proteasome inhibition and cardiac dysfunction. Circulation Journal, 78(3), 487–494.
22. Powell, S. R., et al. (2012). The ubiquitin-proteasome system and cardiovascular disease. Progress in Molecular Biology and Translational Science, 109, 295–346.
23. Glembotski, C. C. (2007). ER stress in the heart. Circulation Research, 101(10), 975–984.
24. Wang, X., Su, H., & Ranek, M. J. (2008). Protein quality control in cardiac pathogenesis. American Journal of Physiology – Heart and Circulatory Physiology, 295(5), H1729–H1741.
25. Willis, M. S., & Patterson, C. (2013). Proteotoxicity and cardiac dysfunction—Alzheimer's of the heart? New England Journal of Medicine, 368(5), 455–464.
26. McLendon, P. M., & Robbins, J. (2011). Desmin-related cardiomyopathy: An unfolding story. Am J Physiol Heart Circ Physiol, 301(5), H1220–H1222.
27. Madonna, R., Cadeddu, C., Deidda, M., et al. (2015). Improving preclinical models for cardiotoxicity. Heart Failure Reviews, 20, 621–631.
28. Mok, C. C. (2025). Targeting the ubiquitin–proteasome pathway in systemic lupus erythematosus. Expert Review of Clinical Immunology, 21(5), 531–542.

35.OncLive. (2024, May 1). Notable 2024/early 2025 multiple myeloma NCCN guideline updates feature quadruplets and more. h

36. Herrmann, J. (2021). Proteasome inhibition and cardiotoxicity. Circulatio Research,129(6), 757–758. https://doi.org/10.1161/CIRCRESAHA.121.319701

37. Wang, X ., Su, H., & Ranek, M. J. (2008). Protein quality control and ubiquitin–proteasome system in cardiac pathogenesis and therapeutics. American Journal of Physiology - Heart and Circulatory Physiology, 295(5), H1729–H1741. https://doi.org/10.1152/ajpheart.00346.2008

38. Willis,M. S., & Patterson, C. (2013). Proteotoxicity and cardiac dysfunction—Alzheimer's disease of the heart? New England Journal of Medicine, 368(5), 455–464. https://doi.org/10.1056/NEJMcibr1212611

39. Xuereb, R. A., Magri, C. J., & Xuereb, R. G. (2023). Arterial stiffness and its impact on cardiovascular health. Current Cardiology Reports, 25, 1337–1349. https://doi.org/10.1007/s11886-023-01951-1

40. Vlachopoulos, C., Aznaouridis, K., & Stefanadis, C. (2010). Prediction of cardiovascular events and all-cause mortality with arterial stiffness: A systematic review and meta-analysis. Journal of the American College of Cardiology, 55(13), 1318–1327.

41.Boutouyrie, P., Chowienczyk, P., Humphrey, J. D., & Mitchell, G. F. (2021). Arterial stiffness and cardiovascular risk in hypertension. Circulation Research, 128(7), 864–886. https://doi.org/10.1161/CIRCRESAHA.120.316939

42. Laurent, S., Cockcroft, J., Van Bortel, L., et al. (2006). Expert consensus document on arterial stiffness: Methodological issues and clinical applications. European Heart Journal, 27(21), 2588–2605. https://doi.org/10.1093/eurheartj/ehl254

43. Van Bortel, L. M., Laurent, S., Boutouyrie, P., et al. (2012). Expert consensus document on the measurement of aortic stiffness in daily practice using carotid-femoral pulse wave velocity. Journal of Hypertension, 30(3), 445–448. https://doi.org/10.1097/HJH.0b013e32834fa8b0

44.Pilz, N., Heinz, V., Ax, T., Fesseler, L., Patzak, A., & Bothe, T. L. (2024). Pulse wave velocity: Methodology, clinical applications, and interplay with heart rate variability. Reviews in Cardiovascular Medicine, 25(7), 266.

45. Dimopoulos, M. A., Moreau, P., Palumbo, A., Joshua, D., Pour, L., Hájek, R., … Anderson,K.C.(2017).
Impact of prior treatment on patients with relapsed multiple myeloma treated with carfilzomib and dexamethasone vs. bortezomib and dexamethasone in the phase 3 ENDEAVOR study. Leukemia, 31(1), 115–122.

46. Vlachopoulos, C., Aznaouridis, K., & Stefanadis, C. (2010). Prediction of cardiovascular events and all-cause mortality with arterial stiffness: A systematic review and meta-analysis. *Journal of the American College of Cardiology, 55*(13), 1318–1327. https://doi.org/10.1016/j.jacc.2009.10.061

47. Boutouyrie, P., Chowienczyk, P., Humphrey, J. D., & Mitchell, G. F. (2021). Arterial stiffness and cardiovascular risk in hypertension. *Circulation Research, 128*(7), 864–886. https://doi.org/10.1161/CIRCRESAHA.120.316939

48. Laurent, S., Cockcroft, J., Van Bortel, L., et al. (2006). Expert consensus document on arterial stiffness: Methodological issues and clinical applications. *European Heart Journal, 27*(21), 2588–2605. https://doi.org/10.1093/eurheartj/ehl254

49. Van Bortel, L. M., Laurent, S., Boutouyrie, P., et al. (2012). Expert consensus document on the measurement of aortic stiffness in daily practice using carotid-femoral pulse wave velocity. *Journal of Hypertension, 30*(3), 445–448. https://doi.org/10.1097/HJH.0b013e32834fa8b0

50. Pilz, N., Heinz, V., Ax, T., Fesseler, L., Patzak, A., & Bothe, T. L. (2024). Pulse wave velocity: Methodology, clinical applications, and interplay with heart rate variability. *Reviews in Cardiovascular Medicine, 25*(7), 266. https://doi.org/10.31083/j.rcm2507266

51. Ling, Y., Wang, Y., & Sun, Z. (2021). Inhibitors of the ubiquitin–proteasome system block myofibril assembly in cardiomyocytes derived from chick embryos and human pluripotent stem cells. Cell Motility and the Cytoskeleton, 78(12), 355–366.

52. Jaminon A, Reesink K, Kroon A, Schurgers L. The Role of Vascular Smooth Muscle Cells in Arterial Remodeling: Focus on Calcification-Related Processes. Int J Mol Sci. 2019 Nov 14;20(22):5694. doi: 10.3390/ijms20225694. PMID: 31739395; PMCID: PMC6888164.

53.Rombouts KB, van Merrienboer TAR, Ket JCF, Bogunovic N, van der Velden J, Yeung KK. The role of vascular smooth muscle cells in the development of aortic

aneurysms and dissections. Eur J Clin Invest. 2022 Apr;52(4):e13697. doi: 10.1111/eci.13697. Epub 2021 Nov 21. PMID: 34698377; PMCID: PMC9285394.

54. Efentakis P, Doerschmann H, Witzler C, Siemer S, Nikolaou PE, Kastritis E, Stauber R, Dimopoulos MA, Wenzel P, Andreadou I, Terpos E. Investigating the Vascular Toxicity Outcomes of the Irreversible Proteasome Inhibitor Carfilzomib. Int J Mol Sci. 2020 Jul 22;21(15):5185. doi: 10.3390/ijms21155185. PMID: 32707866; PMCID: PMC7432349.

55. Measuring Arterial Stiffness At Different Scales: A New Toolbox For Safety Pharmacology Phd thesis C.Wesley

56. Vlachopoulos C, Aznaouridis K, Stefanadis C. Prediction of cardiovascular events and all-cause mortality with arterial stiffness: a systematic review and meta-analysis. J Am Coll Cardiol. 2010;55(13):1318–27.

57.Hooglugt, Aukiea,b; Klatt, Oliviaa; Huveneers, Stephana. Vascular stiffening and endothelial dysfunction in atherosclerosis. Current Opinion in Lipidology 33(6):p 353-363, December 2022. | DOI: 10.1097/MOL.0000000000000852

58.Hooglugt A, Klatt O, Huveneers S. Vascular stiffening and endothelial dysfunction in atherosclerosis. Curr Opin Lipidol. 2022 Dec 1;33(6):353-363. doi: 10.1097/MOL.0000000000000852. Epub 2022 Oct 21. PMID: 36206080; PMCID: PMC10128901.

59. Zhang, L., Zhou, J. & Kong, W. Extracellular matrix in vascular homeostasis and disease. Nat Rev Cardiol 22, 333–353 (2025).

60.Book: Atherosclerosis, Large arteries and Cariovascular risk M.E Safar, Karger

61. Journal:Inflammation, Endothelial Dysfunction and Arterial Stiffness as Therapeutic Targets in Cardiovascular Medicine
Author(s): Vittoriano Della Corte, Antonino Tuttolomondo, Rosaria Pecoraro, Domenico Di Raimondo, Valerio Vassallo and Antonio Pinto

62. Wesley CD, Neutel CHG, De Meyer GRY, Guns PJ. Unravelling the impact of active and passive contributors to arterial stiffness in male mice and their role in vascular aging. Sci Rep 14, 18337 (2024). doi.org/10.1038/s41598-024-68725-9. Wesley, CD.

63. Pilz N, Heinz V, Ax T, Fesseler L, Patzak A, Bothe TL. Pulse Wave Velocity: Methodology, Clinical Applications, and Interplay with Heart Rate Variability. Rev Cardiovasc Med. 2024 Jul 17;25(7):266. doi: 10.31083/j.rcm2507266. PMID: 39139426; PMCID: PMC11317333.

64.Wilmer, C. V., Nichols, W., & O'Rourke, M. F. (2005). McDonald's blood flow in arteries—Theoretical, experimental and clinical principles. CRC Press: London.

65. Townsend RR, Wilkinson IB, Schiffrin EL, et al. Recommendations for improving and standardizing vascular research on arterial stiffness: a scientific statement from the American Heart Association. Hypertension. 2015;66(3):698–722.

66. Van Bortel LM, Laurent S, Boutouyrie P, et al. Expert consensus document on the measurement of aortic stiffness in daily practice using carotid-femoral pulse wave velocity. J Hypertens. 2012;30(3):445–448.

67. Chari A, Hajje D. Case series discussion of cardiac and pulmonary complications associated with carfilzomib: possible mechanism, monitoring, and management. Clin Lymphoma Myeloma Leuk. 2014;14(3):e117–e120

68. Gosling, R. G., & Budge, M. M. (2003). Terminology for describing the elastic behavior of arteries. Hypertension, 41(6), 1180–1182.

69. Judy Truong, Andrew T. Yan, Gemma Cramarossa, Kelvin K.W. Chan,Chemotherapy-Induced Cardiotoxicity: Detection, Prevention, and Management,Canadian Journal of Cardiology Volume 30, Issue 8,

70. Madonna, R., Cadeddu, C., Deidda, M. et al. Improving the preclinical models for the study of chemotherapy-induced cardiotoxicity: a Position Paper of the Italian Working Group on Drug Cardiotoxicity and Cardioprotection. Heart Fail Rev 20, 621–631 (2015).

71. Vanherck, J. C., Martinet, W., De Meyer, G. R. Y., Fransen, P., & Van Craenenbroeck, E. M. (2022). Short-term and long-term L-NAME exposure differentially affect vascular function and structure in C57BL/6 mice. Frontiers in Physiology, 13, 874015.

72. Nishima, S., Kashiwada, T., Saito, Y., Yuge, S., Ishii, T., Matsuda, K., Kamio, K., Seike, M., Fukuhara, S., & Gemma, A. (2024). Bortezomib induces Rho-dependent hyperpermeability of endothelial cells synergistically with inflammatory mediators. BMC pulmonary medicine, 24(1), 617. https://doi.org/10.1186/s12890-024-03387-x

73. Li, S., Wang, X., Li, Y., Kost, C. K. Jr., & Martin, D. S. (2013). Bortezomib, a proteasome inhibitor, attenuates angiotensin II-induced hypertension and aortic remodeling in rats. PLoS ONE, 8(10), e78564. https://doi.org/10.1371/journal.pone.0078564

74. Zonderland, J., Wieringa, P., & Moroni, L. (2019). A quantitative method to analyse F-actin distribution in cells. MethodsX, 6, 2562–2569. https://doi.org/10.1016/j.mex.2019.10.005